Mitochondrial sequestration of GABA by *Aralar* in *Drosophila Cyfip* haploinsufficiency causes deficits in social group behavior

Alexandros K. Kanellopoulos[1], Vittoria Mariano[1,2], Marco Spinazzi[2,3], Young Jae Woo[4,5], Colin McLean[6], Ulrike Pech[7], Ka Wan Li[8], J. Douglas Armstrong[6], Angela Giangrande[9], Patrick Callaerts[2], August B. Smit[8], Brett S. Abrahams[4,10], Andre Fiala[7], Tilmann Achsel[1] and Claudia Bagni[1,11,*]

[1]University of Lausanne, Department of Fundamental Neurosciences, Lausanne, Switzerland
[2]KU Leuven, Department of Neurosciences, Leuven, 3000, Belgium
[3]VIB Center for Brain & Disease Research, Leuven, 3000, Belgium
[4]Department of Genetics, Albert Einstein College of Medicine, Bronx, New York;
[5]Department of Genetics and Genomic Sciences, Icahn School of Medicine at Mount Sinai, New York, USA
[6]University of Edinburgh, School of Informatics, Edinburgh, UK
[7]Georg-August-University Göttingen, Department of Molecular Neurobiology of Behaviour, Göttingen, Germany
[8]Department of Molecular and Cellular Neurobiology, Center for Neurogenomics and Cognitive Research, VU University Amsterdam, Amsterdam, The Netherlands
[9]Centre National de la Recherche Scientifique, UMR7104, Institut National de la Sante´ et de la Recherche Medicale, Universite´ de Strasbourg, Illkirch, France
[10]Dominick P. Purpura Department of Neuroscience, Albert Einstein College of Medicine, Bronx, USA
[11]University of Rome Tor Vergata, Department of Biomedicine and Prevention, Rome, Italy

***Corresponding author:** Claudia Bagni, Ph.D.
e-mail: claudia.bagni@unil.ch; claudia.bagni@uniroma2.it;
Tel (1): +41-216925120; Tel (2): +39-0672596063

Running title: Mitochondria regulate GABA availability and behavior

Keywords: Mitochondrial activity, mitochondrial membrane potential, GABA, social group behavior, Aralar, Drosophila, CYFIP1, autism, schizophrenia.

SUMMARY

Social impairment is frequently associated with mitochondrial dysfunction and altered neurotransmission. While mitochondrial function is crucial for proper brain homeostasis, it remains unknown whether mitochondrial disruption contributes to social behavioral deficits. Here, we show that *Drosophila* mutants in the homolog of the human *CYFIP1*, which is linked to autism and schizophrenia, exhibit mitochondrial hyperactivity and altered group behavior. We reveal a biologically relevant mechanism, how GABA availability is regulated by mitochondrial activity and its contribution to behavior and brain metabolism. Specifically, increased mitochondrial activity causes a sequestration of GABA in the mitochondria, reducing GABAergic signaling and resulting in social deficits. Pharmacological and genetic manipulation of mitochondrial activity or GABA signaling corrects the observed abnormalities. We identify the mitochondrial transporter Aralar, which explains how increased mitochondrial activity sequesters GABA. This study increases our understanding of how mitochondria activity modulates neuronal homeostasis and social behavior under physiopathological conditions.

INTRODUCTION

Human brains, which account for only 2% of overall body weight, use 20 percent of all mitochondrial energy (Castro et al., 2018; Mergenthaler et al., 2013). To fulfill these energy requirements, mitochondria supply neurons with energy by generating metabolites via the tricarboxylic acid (TCA) cycle and ATP through oxidative phosphorylation (OXPHOS) (Hollis et al., 2017; Vos et al., 2010). Neurons critically depend on mitochondrial function for a variety of processes, including neurogenesis, synaptic plasticity and neurotransmission (Kann and Kovacs, 2007; Khacho and Slack, 2018; Li et al., 2004; Marland et al., 2016; Raefsky and Mattson, 2017; Schwarz, 2013; Vos et al., 2010; Yang et al., 2012). During synapse formation the bi-directional flux of pre-synaptic mitochondria is increased (Badal et al., 2019). Furthermore, mitochondria regulate calcium buffering, controlling the release of neurotransmitters from neurons and ensuring proper synaptic functioning (Williams et al., 2013), emphasizing the importance of mitochondrial function during development and in the adult brain (Khacho and Slack, 2018; Picard, 2015; Son and Han, 2018).

Converging lines of evidence support a role for mitochondria in brain dysfunctions such as autism spectrum disorder (ASD), schizophrenia (SCZ) and other disabilities (Castora, 2019; De Rubeis et al., 2014; Gandal et al., 2018; Garcia-Cazorla et al., 2018; Hollis et al., 2017) featuring synaptic dysfunctions.

Mitochondrial dysfunction has been observed in ASD with a prevalence of approximately 5-8% (Ghanizadeh et al., 2013; Griffiths and Levy, 2017; Legido et al., 2013; Patowary et al., 2017; Rossignol and Frye, 2012; Toker and Agam, 2015; Valenti et al., 2014) and in SCZ (Akarsu et al., 2014; Taurines et al., 2010). Respiratory complex activity deficiencies as well as aberrant over-activity have been observed in ASD children (Fryea, 2011; Goldenthal et al., 2015) and patients with SCZ. A positive correlation between mitochondrial complex I and III mRNA levels has also been reported in SCZ (Akarsu et al., 2014; Taurines et al., 2010) and in individuals with psychotic symptomatology (Bergman and Ben-Shachar, 2016), though other studies have shown the opposite, namely impaired mitochondrial network dynamics associated with reduced cellular respiration and complex I abnormalities in SCZ (Rosenfeld et al., 2011). Furthermore, clinical studies have associated metabolic disturbances, including mitochondrial dysfunction at the levels of mtDNA, activity, atypical redox metabolism and differences in metabolites in patients with ASD and SCZ (Hollis et al., 2017; Konradi and Ongur, 2017; Patowary et al., 2017).

Mitochondrial genes have been reported to be differentially expressed in the cerebral cortex of ASD patients and strongly correlated with genes associated with synaptic transmission (Schwede et al., 2018), and in SCZ, disruptions in mitochondria have been found in different brain regions, cell types and subcellular locations (Konradi and Ongur, 2017). Recently, a human whole genome methylation study revealed that two crucial biological processes, mitochondrial metabolism and protein ubiquitination, associated with ASD brains (Stathopoulos et al., 2018). In agreement, a GWAS study showed a significant enrichment for ASD and SCZ-associated common variants in genes that regulate synapse & mitochondrial homeostasis (Gandal et al., 2018). While these studies suggest a potential association between energetic balance, synaptic transmission, and psychiatric disease, the functional significance of mitochondrial disturbances to neurological disease, and the mechanistic links between these processes, remains unclear.

Copy number variations (CNVs) and single nucleotide variants (SNVs) in the *CYFIP1* gene have been associated with SCZ and ASD (Leblond et al., 2012; Stefansson et al., 2014; Tam et al., 2010; Vanlerberghe et al., 2015; Wang et al., 2015; Zhao et al., 2013). Furthermore, genomic instability at the 15q11.2 BP1-BP2 locus, which encompasses four genes including the Cytoplasmic FMR1 interacting protein 1 (*CYFIP1*), has also recently emerged as a recognized syndrome (Cafferkey et al., 2014; Cox and Butler, 2015; De Wolf et al., 2013; Nevado et al., 2014; Urraca et al., 2013; Williams et al., 2019; Yuen et al., 2017). Among the 4 implicated genes, converging evidence suggest that *CYFIP1* is a key factor mediating risk for the BP1-2-deletion disorders (Das et al., 2015; Nebel et al., 2016; Vanlerberghe et al., 2015; Wang et al., 2015; Woo et al., 2016; Yoon et al., 2014). CYFIP1 has a dual role in the brain, regulating local protein synthesis via binding eIF4E and controlling actin remodeling as part of the hetero-pentameric Wave Regulatory Complex (WRC) (Anitei et al., 2010; Chen et al., 2010b; De Rubeis et al., 2013; Di Marino et al., 2015; Eden et al., 2002; Genheden et al., 2015; Hsiao et al., 2016; Napoli et al., 2008; Oguro-Ando et al., 2015; Panja et al., 2014; Pathania et al., 2014; Schenck et al., 2003; Stradal and Scita, 2006). Moreover, recent studies demonstrated that CYFIP haploinsufficiency in humans, mice and flies confers domain-specific cognitive impairments and behavioral deficits (Bachmann et al., 2019; Bozdagi et al., 2012; Domínguez-Iturza et al., 2019; Silva et al., 2019; Woo et al., 2019). However, the molecular mechanisms linking CYFIP1 deficiency with alterations in behavior and cognition remain unknown.

Here we investigated the molecular mechanism underlying social behaviors in *Drosophila*, demonstrating a mechanistic link between alterations in mitochondrial metabolism, neuronal communication and social behavior. Using *Cyfip* haploinsufficient flies we show that an increase in mitochondrial activity, energy metabolism and membrane potential causes abnormal GABA signaling, leading to deficits in social group interactions in flies. Furthermore, we identify the solute carrier Aralar as the mitochondrial transporter responsible for the uptake of GABA into mitochondria which is activated by mitochondrial membrane polarization. We provide genetic, biochemical, pharmacological and morphological evidence that explains how dysregulation of mitochondria homeostasis regulates GABA signaling and the social component of behavior.

RESULTS

Cyfip$^{85.1}$/+ flies have deficits in social behavior

CYFIP haploinsufficiency in humans and flies has recently been shown to confer domain-specific cognitive impairments (Woo et al., 2019). Because increasing evidence points towards a role of CYFIP1 in ASD- and SCZ like behaviors (Domínguez-Iturza et al., 2019; Silva et al., 2019), and given the prevalence of social deficits in these disorders, we investigated if CYFIP haploinsufficiency affects ASD-like behaviors focusing in well-established paradigms for social group behavior in *Cyfip*$^{85.1}$/+ and control flies (Schenck et al., 2003). First, male flies were tested in a food competition assay (Anholt and Mackay, 2012; Zwarts et al., 2011) where the index of approaches was used to obtain an average of the total number of social events in a 2 minutes time frame. *Cyfip*$^{85.1}$/+ male flies showed a reduced number of social events relative to control flies (Figure 1A and Supplementary movies 1 and 2). This holds also true for female flies (Figure S1A). Second, social performance of the *Cyfip*$^{85.1}$/+ flies was further investigated by observing *Drosophila* courtship, a complex innate social behavior in flies (Ejima and Griffith, 2007; Sokolowski, 2010). *Cyfip*$^{85.1}$/+ male flies showed a decreased courtship index towards a wild type female (Figure 1B and Supplementary movies 3 and 4). Third, we monitored grooming behavior of individual flies in an observation chamber (Tauber et al., 2011). *Cyfip*$^{85.1}$/+ male flies showed an excess of grooming behavior in comparison to control flies (Figure 1C and Supplementary movies 5 and 6) suggesting an increase in repetitive behavior. Moreover, we recorded behavior of flies within a social group, measuring the distance between two flies as social space (Simon et al., 2012). *Cyfip*$^{85.1}$/+ flies, on average, show longer distance to the closest neighbor fly in comparison to control flies within a group (Figure 1D) confirming further the social interaction impairment of *Cyfip*$^{85.1}$/+ flies. In addition, *Cyfip*$^{85.1}$/+ flies stayed further away from the wall of the open field arena (Figure 1D), indicating their natural thigmotactic behavior (attraction to the contact of the wall) (Besson and Martin, 2005) is also disturbed. *Cyfip*$^{85.1}$/+ flies exhibit hyperactivity overs 24 hours when compared to controls (Figure S1B), but no differences in locomotion activity were observed during the day time (ZT0-ZT6) (Figure S1C), the timeframe that the social assays were performed. This indicates that hyperactivity does not interfere with our social behavioral assays and the observed social deficits were not due to impaired motor ability. *Cyfip* mutant flies (males and females) do not differ from the controls (Figure S1D and E) in negative geotaxis as measurement for motor reflex (Sun et al., 2018), anxiety (Garcia and Teets, 2019) or startle response (Zhang et al., 2002). Then, we used the TARGET system to interrogate temporal and regional specific effect of *dCyfip* knock-down by transgenic RNAi (UAS-CYFIP-IR) expression in the adult animal (McGuire et al., 2003). Pan-neuronal attenuation of *Cyfip* mRNA levels in adult flies (Figure S1F) phenocopied the decreased competition for food in *Cyfip*$^{85.1}$/+ mutant animals (Figure S1G). Importantly, the decreased social score in the *Cyfip*$^{85.1}$/+ flies was fully rescued by expression, in adulthood only, of a transgene harboring the wild type *Cyfip* (UAS-CYFIP-WT/genetic rescue) (Figure S1G). These data provide evidence that CYFIP is required to mediate social behavior in adult flies.

Proteomic analysis of *Cyfip*$^{85.1}$/+ mutant reveals deficits in mitochondrial pathways and disease networks

To identify the molecular mechanism underlying the observed behavioral dysfunctions in the *Cyfip*$^{85.1}$/+ flies, we performed tandem mass spectrometry in control and *Cyfip*$^{85.1}$/+ mutant brains. Analysis identified a total of 345 dysregulated proteins, of which 309 were present at greater abundance and 36 at lower abundance in *Cyfip*$^{85.1}$/+ flies compared to controls (Table S1). The identified proteins corresponded to 361 fly genes and mapped with high confidence to 264 human orthologs (i.e. 73%). Fly protein-protein interaction (PPI) and cluster networks were then constructed by mining publicly available databases: FlyBase (Attrill et al., 2016), BioGRID, IntAct, BIND, DIP (Salwinski et al., 2004), and MINT (Salwinski et al., 2004) (Figure 2A). The strongest signal recovered in these network-based analyses was for the community of mitochondrial proteins (Community 3, $p = 2.4 \times 10^{-6}$, permutated p-value<1%). This mitochondrial signal was likewise one of the top hits in the gene ontology analysis, identifying differentially expressed mitochondrial proteins (Figure 2B and Table S2) and highlighting dysregulation of TCA cycle, energy metabolism and mitochondrial electron transport, as well as neurotransmitter release related processes (Figure 2C and Figure S2). Further, disease-related analyses identified a highly significant overrepresentation of gene networks implicated in SCZ, dementia, and syndromic epilepsy (Figure 2D).

Cyfip$^{85.1}$/+ flies show increased brain mitochondrial size and respiration

Given that our proteomic analysis suggested a role for mitochondria and energy metabolism in the *Cyfip*$^{85.1}$/+ flies, we assessed whether the mutant flies showed any alterations in mitochondrial respiration. Using high-resolution respirometry, we observed a striking increase in mitochondrial respiratory capacity through the respiratory chain in *Cyfip*$^{85.1}$/+ brains (Figure 3A), both at the level of coupled respiration through complexes I and II (Complex I (CI) and Complex I+II (CI+II) and at the level of maximal electron transfer capacity (CI+II ETS) (Figure 3B). The respiration differences appear to be driven by complex I and complex IV (COX), because no difference was detected upon specific blockage of complex I (Figure 3B). In contrast, no alterations were observed in the oxygen consumption in *Cyfip*$^{85.1}$*/+* fly body (Figure 3C), suggesting that mitochondrial activity is specifically dysregulated in the CNS. The labeling brains with tetramethylrhodamine ethyl ester (TMRE), an established marker for mitochondrial membrane potential (Perry et al., 2011), revealed an increased signal intensity in the *Cyfip*$^{85.1}$*/+* brains, further suggesting that the flies exhibit increased mitochondrial membrane potential (Figure 3D). This finding was also confirmed by Rhodamine 123 staining (Figure S3A). No differences were observed in mitochondrial DNA (mtDNA) copy number or abundance of mitochondrial proteins between *Cyfip*$^{85.1}$/+ mutants and controls (Figure 3E, Figure S3B-C). To independently validate this finding, we used another widely used marker of mitochondrial activity/mass, the citrate synthase (CS) activity (Spinazzi et al., 2012). CS activity in *Cyfip*$^{85.1}$/+ mutants was not altered in comparison to control brains (Figure S3D). Next, mitochondrial morphology was analyzed by Tandem Electron Microscopy (TEM) in fly brain from both genotypes and a remarkable difference was observed in the mutant flies. Precisely, mitochondria area and perimeter were increased in *Cyfip*$^{85.1}$/+ mutant flies in comparison to controls (Figure 3F), which is indicative of higher mitochondrial activity (see Discussion). The higher metabolic rate of *Cyfip*$^{85.1}$/+ flies is not due to higher food consumption, as feeding behavior during the day time (Figure S3E) and over 24 hours (Figure S3F) was not altered. In conclusion, these data reveal that the mitochondrial activity and size are increased in *Cyfip*$^{85.1}$/+ mutant flies.

Cyfip$^{85.1}$/+ flies have an excessive TCA/Krebs cycle

The high enrichment of proteins relating to mitochondrial function (OXPHOS and TCA cycle) in the mass spectrometry dataset (Figure S2), and the demonstration of increased mitochondrial membrane potential in the *Cyfip$^{85.1}$/+* fly brain, prompted us to investigate whether *Cyfip$^{85.1}$/+* flies have any alterations in the TCA cycle (Krebs or citric cycle), which produces the substrates for oxidative phosphorylation for energy production. First, TCA metabolites (Figure 4A) were determined by stable-isotope-dilution Liquid Chromatography Mass Spectrometry (LC-MS) from *Cyfip$^{85.1}$/+* brains. Of the metabolites that are produced in the TCA cycle itself, isocitrate, 2-oxoglutarate (α-ketoglutarate, α-KG) and succinate levels are increased, indicating that enzymatic activity/ies in this section of the cycle are higher (Figure 4B). Of note, α-ketoglutarate and succinate generate two of the three NADH molecules, which serve as fuel for complex I oxidation, suggesting that upregulation of the TCA cycle is responsible for the increased complex I activity we observe in the *Cyfip$^{85.1}$/+* brain (Figure 3B) (Maguire et al., 2015). Examination of the mass spectrometry data further validated that the levels of NADH-producing enzymes, specifically the NAD-dependent isocitrate dehydrogenase (IDH) (Yoon et al., 2017) and the α-ketoglutarate hydroxylase, are indeed upregulated (Table S2). NAD-IDH activity increased 3-fold in *Cyfip$^{85.1}$/+* brains in comparison to controls (Figure 4C), and the activity of α-KG-dependent hydroxylase was also significantly increased in *Cyfip$^{85.1}$/+* brains (Figure 4D). Interestingly, the total levels of the oxidized and reduced forms of nicotinamide adenine dinucleotide (NADt: NAD$^+$ and NADH) were not altered between *Cyfip$^{85.1}$*/+ and controls in isolated mitochondria (Figure 4E), however the reduced form (NADH), had a significantly higher level (Figure 4F). Tracing of ^{13}C-labelled glucose shows a drastic increase of isotope-labelled succinate in *Cyfip$^{85.1}$*/+ flies, while incorporation of the ^{13}C-label into to malate and citrate/isocitrate does not change in the two genotypes (Figure 4G). This confirms that the biochemical reactions between citrate/isocitrate and succinate, i.e., IDH and αKG, are overactive and shows that the TCA cycle overactivity is fed by glycolysis. Further analysis of the amino acid composition using stable isotope tracing as well as HILIC-MS/MS, revealed higher levels of amino acids related to the TCA cycle in *Cyfip$^{85.1}$/+* brains (Figure S4A, B). These findings confirm that the *Cyfip$^{85.1}$*/+ brain shows an increase in TCA cycle and complex I activity.

The deficit in social behavior in *Cyfip*$^{85.1}$/+ flies is energy-dependent

Given that *Cyfip*$^{85.1}$/+ flies have altered social behaviors and increased mitochondrial respiration we next tested whether the alterations in mitochondrial function were causally involved in mediating the behaviors seen in the *Cyfip*$^{85.1}$/+ flies. At first, we normalized energy production by reducing IDH activity to partially inhibit the TCA cycle. Using *Idh3a* mutant flies, which have decreased IDH activity and reduced α-ketoglutarate levels (Ugur et al., 2017), we found that social behavior in the food competition assay was reduced in *idh3a*/+ flies, and that the double *idh3a*/+*;Cyfip*$^{85.1}$/+ behaved as controls (Figure 5A). Further, pharmacological inhibition of IDH activity using the ML309, a selective inhibitor of IDH that effectively lowers the production of α-ketoglutarate levels (Davis et al., 2014), also ameliorated the abnormal social feeding behavior in *Cyfip*$^{85.1}$/+ flies (Figure 5B). Interestingly, *idh3a* /+ single mutant or overexpression of IDH in fly brain (Figure 5C) showed a reduction in social behavior similar to the *Cyfip*$^{85.1}$/+ flies, suggesting that both too much and too little energy production leads to a social behavioral defect. Importantly, the ML309 compound also restored the increased mitochondrial activity in the *Cyfip*$^{85.1}$/+ flies (Figure 5D). These results demonstrate a novel association of social behavior with the TCA cycle, and highlight the importance of the IDH enzyme as a potential therapeutic target.

We next designed an experiment to test whether dampening mitochondrial activity and mitochondrial membrane potential might also normalize social behavior. Control and *Cyfip*$^{85.1}$*/+* flies were fed with rotenone (an inhibitor of complex I) for 4 days at a concentration of approximately 500 times less than that used to model Parkinson disease in flies. Although this treatment had no effect on the behavior of wild type flies (Figure S5A), we found that it ameliorates social deficits in *Cyfip*$^{85.1}$*/+* mutants (Figure 5E) after 4 days of feeding. The effect of rotenone treatment was reversible (Figure S5B). Of note, the same treatment did not restore the hyperactivity of *Cyfip*$^{85.1}$*/+* mutants (Figure S5C), suggesting that the mitochondrial phenotype is specific to social behavior. Moreover, reducing complex I activity by crossing *Cyfip*$^{85.1}$*/+* flies to flies with a genetic reduction of complex I activity (*Pink1*^{B9}/+ mutants; (Morais et al., 2009) also rescued social behavior to levels that were indistinguishable from controls (Figure 5F). As for the *Idh*3a mutant, *Pink1*^{B9}/+ flies exhibited social deficits similar to those seen in *Cyfip*$^{85.1}$*/+* mutants. Finally, western blotting analysis revealed that *Cyfip*$^{85.1}$*/+* mutants harbored increased levels of the mitochondrial complex I subunit NDUFS3

(Figure S3B), consistent with the mass spectrometry data. Assessments of *ndufs3/+* mutant flies, harboring a mutation affecting mitochondrial complex I, also uncovered abnormal social behavior in these flies, whereas the double *ndufs3*/+;*Cyfip*$^{85.1}$/+ mutants were normal with regard to number of social interactions (Figure 5F). Combined, these results point to a novel, causal, role for mitochondria and energy metabolism in the regulation of a complex social behavior.

Reduction of *Cyfip* in a subset of GABAergic neurons recapitulates the social interaction deficits

Excitation/inhibition balance in micro circuitries plays an essential role in the pathophysiology of psychiatric disorders with shared social deficits (Benke and Mohler, 2017; Boccuto et al., 2013; Brambilla et al., 2003; Cellot and Cherubini, 2014; Coghlan et al., 2012; Edden et al., 2012; Friedman et al., 2003; Kuo and Liu, 2019; Mukherjee et al., 2019; Robinson and Gradinaru, 2018; Zoghbi and Bear, 2012). Additionally, both in ASD and SCZ, there is differential expression of mitochondrial genes in different brain regions, cell types and subcellular locations (Konradi and Ongur, 2017). Therefore, to identify whether there is any cell type sensitive to the identified *Cyfip*$^{85.1}$/+, social behavior, we knocked down *Cyfip* individually in both major excitatory (cholinergic) and inhibitory (GABAergic) neurons (Hsu and Bhandawat, 2016; Kolodziejczyk et al., 2008; Lee et al., 2003), neuronal clusters important for social behavior in fly brain (Koganezawa et al., 2016; Yuan et al., 2014). No effect on social behavior was observed when *Cyfip* levels were reduced in cholinergic neurons (Figure 6A). However, depletion of *Cyfip* in GABAergic neurons recapitulated the feeding-dependent socialization defect seen in the *Cyfip*$^{85.1}$/+ flies (Figure 6B), and this could be rescued by genetic reintroduction of *Cyfip1*. Attenuation of *Cyfip* mRNA levels specifically in GABAergic neurons was confirmed (Figure S6A).

The *Drosophila* brain contains around a thousand well-mapped GABAergic neurons responsible for distinct behavioral functions (Figure S6B). This allowed us to further investigate possible defects in the GABAergic system by assessing subsets of GABAergic neurons sensitive to *Cyfip* dosage. To do so, the GAL4 system was used to deplete *Cyfip* individually in three distinct GABAergic interneuron subtypes: in the anterior paired lateral neurons (APL, a single GABAergic neuron per brain hemisphere that innervates the ipsilateral mushroom bodies (MB) through broad projections (Liu and Davis, 2009; Masuda-Nakagawa et al., 2014; Wu et al., 2011), in the antenna lobe local interneurons (LNs; whose processes are restricted to a local region), and in the dorsal paired medial neurons (DPMs, which project to the MB to stabilize memories). Reducing *Cyfip* levels in the APLs or LNs recapitulated behavioral deficits observed with pan-neuronal or pan-GABAergic knockdown, while no effect was observed for the DPMs (Figure 6C).

Reduction of *Cyfip* causes GABA to accumulate in mitochondria

Given the sensitivity of GABAergic cells to *Cyfip* dosage we investigated vesicular GABA levels in *Cyfip*$^{85.1}$*/+* flies. Immunohistochemistry experiments (Homberg and Muller, 2016; Tochitani and Kondo, 2013) of *Cyfip*$^{85.1}$*/+* whole mount brains showed reduced vesicular GABA levels (Figure 6D). To address whether such a reduction was due to a pre- or post-synaptic phenotype, we monitored synaptic transmission in GABAergic neurons. By expressing the UAS-synaptophysin-pHTomato (Pech et al., 2015) in GABAergic neurons (Figure 6E), we uncovered a surprising increase in synaptic release in GABAergic neurons of *Cyfip*$^{85.1}$*/+* flies in comparison to control flies (Figure 6F). Using *in vivo* Ca^{2+} imaging in the GABAergic neurons (Pech et al., 2015), *Cyfip*$^{85.1}$*/+* flies show no changes in Ca^{2+} presynaptic responses (Figure S6C). Furthermore, the number of GABAergic neurons, as probed by glutamic acid decarboxylase 1 (GAD1) staining, revealed no difference in the brains of *Cyfip*$^{85.1}$*/+* and control flies (Figure S6D). *GAD1* mRNA and protein levels also did not change (Figure S6E, F). These findings prompted us to measure glutamate levels, the metabolic precursor of GABA, by immunohistochemistry (data not shown) and HILIC-MS/MS (Figure S7A). No differences in glutamate levels were observed between *Cyfip*$^{85.1}$*/+* and control flies. Interestingly, the total concentration of GABA in *Cyfip*$^{85.1}$*/+* mutants was not altered compared to controls by HILIC-MS/MS (Figure 6G). Combined, these results suggested that the entire pool of GABA synthetized (metabolic, intracellular, and extracellular) is not altered.

The increased activity of the Krebs/TCA cycle in *Cyfip*$^{85.1}$*/+* lead us to hypothesize that GABA might be driven into the mitochondria, supplying NADH and succinate to Krebs/TCA cycle (Bonnighausen et al., 2015; Carillo, 2018; Maguire et al., 2015; Michaeli et al., 2011). We therefore measured GABA levels by ELISA following a fractionation to enrich mitochondria and synaptic vesicles (Depner et al., 2014). Interestingly, GABA concentration in the mitochondrial fraction of *Cyfip*$^{85.1}$*/+* mutants was markedly higher compared to controls, reduced in the synaptic vesicles, and, as also observed by HILIC-MS/MS, unchanged in the total fraction (Figure 6H). The purity and enrichment of the mitochondria preparation was confirmed by Western blot with the mitochondrial marker ATP5B and the synaptic marker BRP (Figure S7B). Taken together, these data are consistent with the idea that a reduction of *Cyfip* causes a redistribution of GABA from a vesicular/synaptic to a mitochondrial compartment, supporting the elevated mitochondrial activity in *Cyfip*$^{85.1}$*/+* flies and leading to subsequent alterations in social behavior.

GABA augmentation fully normalizes behavioral abnormalities in *Cyfip*$^{85.1}$*/+* flies

Given that *Cyfip*$^{85.1}$*/+* flies show a redistribution of GABA from a synaptic to a mitochondrial compartment, that loss of *Cyfip* in GABArgic interneurons is sufficient to cause behavioral deficits, we next aimed to investigate whether the sequestration of GABA is causally involved in the *Cyfip*-related behavioral abnormalities. To do so, we augmented GABA levels in *Cyfip*$^{85.1}$*/+* flies in three distinct ways; via feeding flies GABA, DL-2,4-diaminobutyric acid (DABA, a GABA-transaminase uptake inhibitor) or the anticonvulsant valproic acid (VPA, induces GABA release) (Chateauvieux et al., 2010; Coghlan et al., 2012; Reynolds et al., 2007). Feeding *Cyfip*$^{85.1}$*/+* flies for 5 days with GABA (Figure 6I), DABA or VPA (Figure S7C, D) ameliorated the social behavior deficit. Interestingly, feeding flies with GABA also rescued behavioral deficits in the adult pan-neuronal *Cyfip*$^{85.1}$*/+* mutants (Figure S7E). Similarly, pan-neuronal abrogation in adult flies of the enzyme glutamic acid decarboxylase (GAD1) for 2 days led to a reduced number of social events (Figure S7F). Separate experiments in adult wild-type flies showed that a high GABA diet actually decreased social interaction (Figure S7G). Furthermore, feeding flies diazepam (valium), a positive allosteric modulator of the GABA-A receptor, was also able to restore the social deficits of the *Cyfip*$^{85.1}$/+ (Figure S7H). These data show that augmentation of GABAergic signaling in adult is sufficient to ameliorate the behavioral deficits in flies resulting from reduced *Cyfip* dosage. Finally, underscoring the centrality of GABAergic signaling to this process, we demonstrate that administration of GABA, DABA, or VPA to the GABAergic-specific *Cyfip* abrogation flies also restores social interactions (Figure S7I). Of note, the effect of GABA administration lasted 2 days post treatment (Figure S7J).

Aralar, a novel GABA transporter, drives the excessive mitochondrial accumulation of GABA in *Cyfip*$^{85.1}$/+ flies

Our findings suggest that reduced available GABA causes the social deficits in *Cyfip*$^{85.1/+}$ flies, and that the reduction in vesicular GABA is due to GABA being transported into mitochondria, where it is catabolized into other intermediates through the GABA shunt and TCA cycle. We therefore set out to determine how GABA is being shunted into mitochondria.

Mitochondrial GABA transporters in eukaryotes have surprisingly not been largely characterized (Bonnighausen et al., 2015). However, using gene ontology analysis for GO:0005741 mitochondrial outer membrane (Table S3), we identified 36 candidate transporters in the fly and performed a genetic screen to test their effects in the *Cyfip*$^{85.1}$/+ flies. Flies with mutations in the 36 putative GABA transporters were individually crossed with the *Cyfip*$^{85.1}$/+ flies and tested in the food competition social interaction paradigm. Of the 36 putative GABA transporters tested, only the *Aralar*^{MI07552} mutant showed a significant effect - completely rescuing the behavioral deficits of *Cyfip*$^{85.1}$/+ flies (Figure 7A, B). Importantly, crossing the *Cyfip*$^{85.1}$ fly with the *Aralar*^{MI0755} mutant resulted in ameliorating the *Cyfip*$^{85.1}$/+ grooming and social space behavior deficits (Figure 7C, D), but not their hyperactivity (Figure S8A), further confirming that the mitochondrial dysregulation and Aralar have a specific effect on social behavior. Of note, the *Aralar*^{MI07552}/+ mutant flies exhibit a decreased competition for food (Figure 7B), decreased grooming (Figure 7C) and hyperactivity (Figure S8A), similar to *Cyfip*$^{85.1}$/+ flies.

Aralar has been so far described for its function as carrier exchanging a glutamate and a proton (H^+) from the cytoplasm for an aspartate inside the mitochondria. Of note, this transport stoichiometry indicates that the proton gradient drives the transport (Palmieri, 2013). Our genetic findings strongly suggest that Aralar is the novel GABA transporter. To assess whether GABA localization was affected by the mutation in Aralar, GABA levels were evaluated by ELISA upon fractionation of mitochondrial and cytosolic components. Importantly, while cytoplasmic GABA levels were increased in *Aralar*^{MI07552}/+ mutant brains, the levels and sequestration profile of GABA across the cytoplasm and mitochondria in the *Aralar*^{MI07552}/*Cyfip*$^{85.1}$ double mutants were indistinguishable from controls (Figure 7E). The combined genetic and localization data strongly suggest that Aralar is a GABA transporter. In support of our model, inhibition of Aralar by pyridoxal 5'-phosphate (PLP) (Amoedo et al., 2016), ameliorated the competition for food of the *Cyfip*$^{85.1}$*/+* flies (Figure S8B).

To address how a reduced dose of Cyfip could change the activity of Aralar, we examined if Cyfip controls Aralar expression. Remakarbly, neither *Aralar* mRNA level (Figure S8C) nor its efficiency of translation, distribution of the mRNA on a polysomes/mRNP gradient, change (Figure S8D) suggesting that the regulation occurs at the level of Aralar activity.

As a final proof of our hypothesis, we aimed at increasing the proton gradient across the mitochondrial membrane, which increases Aralar activity and monitor social behavior in a wild type fly. Flies were treated with a sublethal dose of oligomycin to reduce Complex V activity (Spinazzi et al., 2012) reducing therefore the proton flux and increasing mitochondrial membrane potential, as confirmed by the TMRE staining (Figure 7F). Notably, under these conditions, the competition for food of wild type flies was decreased (Figure 7G) together the level of available GABA in the cytosol (Figure 7H), resembling the *Cyfip*$^{85.1}$*/+* mutant condition**.** These data further support our previous observations that homeostasis of mitochondria GABA levels plays an important role in driving social behavior.

DISCUSSION

Using a Drosophila model of *Cyfip1* haploinsufficiency, a hot spot genetic variant proven to increase risk for SCZ and a candidate risk factor for ASD, we revealed that increased mitochondrial activity and membrane potential (Figure 3) reduces GABA availability (Figure 6) and plays a causal role in mediating social behavioral abnormalities (Figure 1).

Contribution of GABA transmission to brain dysfunctions

It has been suggested that neurodevelopmental disorders may result from an imbalance between the excitatory glutamatergic and the inhibitory GABAergic pathways (Ben-Ari, 2017; Benke and Mohler, 2017; Braat and Kooy, 2015; Cellot and Cherubini, 2014). Changes in inhibitory activity that lead to altered excitatory/inhibitory (E/I) balance in specific brain areas have been reported in patients with ASD, SCZ and epilepsy (Foss-Feig et al., 2017; Sohal and Rubenstein, 2019; Yizhar et al., 2011). Mechanistic studies in mice using optogenetic manipulations in mPFC have demonstrated that increasing the E/I ratio leads to social deficits, while restoration of E/I balance by increasing inhibition in specific GABAergic neurons (PV+) rescues the observed social deficits (Selimbeyoglu et al., 2017; Sohal and Rubenstein, 2019; Yizhar et al., 2011). In addition, treatment with benzodiazepine, which enhances GABA-A receptor activity, ameliorates social behavioral deficits in mouse models of epilepsy and ASD (Han et al., 2014; Han et al., 2012; Sohal and Rubenstein, 2019), consistent with our data in flies (Figure S7). Further, developmental Gabrb3 deletion in mouse somatosensory neurons leads to tactile sensitivity and reduced sociability through loss of GABA-A receptor-mediated presynaptic inhibition, pointing out the importance of somatosensory dysfunction in ASDs (Orefice et al., 2016). It is notable that CYFIP1 is enriched at inhibitory synapses and loss of CYFIP1 in rodents increases the E/I ratio (Davenport et al., 2019). Our work shows that augmentation of GABAergic signaling in adult flies, through either genetic or pharmacological approaches including treatment with the GABA-A receptor positive allosteric modulator diazepam (valium), fully normalizes abnormal social behavior (Figure S7). Combined, these findings suggest a common pathophysiological mechanism in these neurological disorders that starts with GABA impairment and leads to social deficits. However, despite past evidence of abnormal GABA signaling in ASD (Ben-Ari et al., 2012; Cellot and Cherubini, 2014) and indications that cortical inhibitory neurons exhibit an enrichment in ASD risk gene expression (Wang et al., 2018), until now how alterations in GABA and E/I balance occur in these disorders has remained less clear.

Mitochondrial activity modulates GABA availability via Aralar

Here, we demonstrate that an increase in mitochondrial metabolism causes GABA to be sequestered away from the synapses into the mitochondria. The translocation of GABA reduces the amount of GABA available for vesicular uptake (Figure 6), likely affecting neuronal activity. In fact, several of our observations are best explained by an effort of the GABAergic circuit to homeostatically correct low GABA release: the number of released vesicles is increased (Figure 6), and the GABA-A receptor is overexpressed (data not shown, see also (Davenport et al., 2019)). Reduced GABAergic transmission then affects behavior (Figures 1, 7).

To enter the mitochondria, GABA needs to be transported through the mitochondrial membrane. To date, a mitochondrial GABA carrier has not been identified in any organism except in plants (Michaeli et al., 2011). Here, we screened candidate transporters for a rescue of the aberrant social behavior of *Cyfip* mutant flies, leading to the isolation of the protein Aralar, which we went on to show that is responsible for the GABA uptake into the mitochondrial in *Drosophila* (Figure 7). This work strengthens the link between mitochondrial function, GABA transmission, and social behavior.

Aralar belongs to the SLC25 family, the largest family of solute transporters that consists mainly of mitochondrial proteins (Palmieri, 2013; Zorova et al., 2018). Aralar homologs are present in all metazoans (Amoedo et al., 2016), including two human homologs – SLC25A12 (AGC1) and SLC25A13 (AGC2). Aralar transporters have thus far been shown to function by exchanging an aspartate on the mitochondrial matrix for a glutamate plus a proton on the cytosolic side, with the pH gradient across the inner membrane forming the bioenergetic driving force for solute exchange. As the major aspartate exporter from the mitochondrion, the Aralar proteins play a major role in the malate-aspartate shuttle that carries redox equivalents across the mitochondrial membrane and thus aligns the redox potential of the mitochondria and the cytosol (Amoedo et al., 2016; Palmieri, 2013). Our study now indicates that Aralar can also transport GABA, in addition to glutamate, despite the lack of one carboxylic group that seems to be dispensable for binding to the transporter.

Neither *Aralar* mRNA level nor its translational efficiency changes between the two genotypes (Figure S8), indicating that its expression is not altered in *Cyfip* mutant brain. Instead, the activity of the Aralar transporter changes. Since Aralar needs a proton for import of its substrate into mitochondria, the equilibrium distribution of the transport substrates is set by the pH gradient across the mitochondrial membrane, which in turn is a function of fuel availability, oxidative phosphorylation and activity of the TCA cycle. In strong support of this notion, the effect we detected with oligomycin treatment. Oligomycin is a highly specific inhibitor of Complex V and thus selectively drives the pH gradient up. Oligomycin causes an accumulation of GABA in the mitochondria and affects social behavior (Figure 7).

In *Cyfip* mutants, two key enzymes of the TCA cycle, namely IDH and αKG, are upregulated at the protein (Figure S2 and Table1) and activity levels (Figure 4); furthermore the mitochondria in the *Cyfip* mutant brains show a morphology (Figure 3) that is typical of hyperactive mitochondria with a larger perimeter and area (Yao et al., 2019). Interestingly, we show that alterations to the TCA cycle via overexpression of the IDH enzyme causes social aberrations comparable to those of the *Cyfip* mutant flies (Figure 5). Further, pharmacological or genetic inhibition of the IDH enzyme normalizes the increased mitochondrial activity observed in *Cyfip* mutant flies and ameliorates their social deficits (Figure 5). These data serve to further support a link between mitochondrial function, GABA transmission, and social behavior. Additionally, both of the human Aralar homologs have calcium-binding motives in their cytosolic domain, and cytosolic calcium robustly increases transport activity (Napolioni et al., 2011); the calcium-binding motives are conserved in *Drosophila* Aralar. As such, the local calcium rises observed during pre-synaptic vesicle release may well be sufficient to trigger the GABA transport process, with local mitochondria responding to reduce the local GABA availability. Thus, mitochondrial activity and high calcium, both effects of increased neurotransmission, can effectively reduce GABAergic neurotransmission. This suggests that under physiological conditions the Aralar-mediated GABA sequestration process is likely to serve as a homeostatic feed-back inhibition mechanism. In addition, we note that every other physiological mechanism that increases the mitochondrial potential will reduce GABAergic transmission.

Disturbances of mitochondrial GABA control affects social behavior

Our data here demonstrate a pivotal role for mitochondrial metabolism dysregulation, and the associated sequestration of GABA into mitochondria, in causing social behavioral deficits. Restoration of mitochondrial membrane potential by a variety of pharmacological or genetic means rescues the social behavioral deficits due to *Cyfip1* haploinsufficiency (Figure 5). Our data thus might explain in molecular terms the positive effect on patients with ASD and SCZ of some antipsychotic drugs such as haloperidol, chlorpromazine, fluphenazine or risperidone on patients with ASD and SCZ that act by decreasing mitochondrial respiration and membrane potential (Balijepalli et al., 1999).

The Aralar mutation that increases cytosolic GABA levels (Figure 7E) also affects social behavior similar to the *Cyfip* mutation (Figure 7B,C), while the double mutation normalizes cytosolic GABA levels and rescues social behavior. Moreover, GABA administration to wild-type animals reduces social behavior (Figure S7). Taken together, this suggests a precarious equilibrium where too little and too much GABA availability is detrimental. Thus, our findings predicts that disturbances of mitochondrial function would cause pathological alterations in social behavior; and explain the link between mitochondrial dysfunction and ASD is well established (reviewed in (Hollis et al., 2017)). While mitochondrial dysfunction may affect the nervous system in various ways, our model predicts that Aralar should be specifically linked to social disorders. Interestingly, two ASD associated SNPs have been uncovered in AGC1/SLC25A12, the human Aralar isoform that is known to be expressed in neurons (see Aoki and Cortese, 2016, for meta analysis; Pardo et al., 2013), and AGC1 expression is upregulated in the prefrontal cortex of ASD patients (Anitha et al., 2012; Lepagnol-Bestel et al., 2008). Further, disruption of the gene in mice causes hypomyelination and abnormal neurofilament accumulations (Sakurai et al., 2010); more subtle changes in AGC1 activity are thus likely to alter brain development and cause ASD.

This study provides the first causal evidence linking mitochondrial energy production through the TCA cycle to alterations in GABA metabolism, and further uncovers a mechanistic link between these molecular processes and alterations in behavior in social groups (Figure 8). As alterations in mitochondrial metabolism are a hallmark of diverse neurodevelopmental disorders in humans, this mechanism could represent a common mechanism underlying social deficits in these disorders and it has the potential to be relevant for physiological regulation of neurotransmission and also for a wide range of neurodevelopmental and neuropsychiatric disorders. Our study demonstrates that social deficits in our fly model can be rescued by pharmacological dampening of mitochondrial respiration, as this modulates Aralar activity. Therefore, molecules that specifically activate or inhibit human Aralar should be considered as potential therapeutic approaches for treatment of these disorders.

AUTHORS CONTRIBUTION

A.K.K. and C.B. conceived the study; T.A. conceived, designed some experiments and analyzed the data. A.K.K., V.M., M.S., C.M., U.P., K.W.L., A.B.S., A.F. performed the experiments and/or analyzed the data; Y.J.W., J.D.A., A.G., P.C., B.S.A., provided research material; A.K.K. and C.B., wrote the manuscript with input from all authors.

ACKNOWLEDGMENTS

This work was supported by VIB, KUL Funds Opening the Future (OTF), Queen Elisabeth Foundation (Belgium), SNSF 310030-182651, NCCR Synapsy 51NF40-158776 (Switzerland), Novartis (Switzerland) to CB. Additional funds were from HEALTH-2009-2.1.2-1 EU-FP7 “SynSys” to CB, A.B.S. and D.J.A., the German Research Foundation (SFB 889/B04) and the Bernstein Center for Computational Neuroscience Göttingen (grant number 01GQ1005A) to UP and AF. INSERM, CNRS and LABEX to AG. AKK was recipient of the Autism Speaks *Meixner Translational* Postdoctoral Fellowship (Grant No 9728), Greek State Scholarships Foundation IKY and the Fondation *Sophie* Afenduli. M.S. was the recipient of an EMBO long-term fellowship (ALTF 648-2013) and supported by funding to Bart De Strooper. PC was supported by grant from VIB and FWO (G065408.N10 and G078914N). We thank to Efthimios Skoulakis, Ronald Davis, Rob Jackson, Brett H. Graham, Hugo Bellen and Patrik Verstreken for fly stocks and reagents. We acknowledge the Developmental Hybridoma Studies Bank for antibodies, the Bloomington *Drosophila* Stock Center and Vienna Drosophila Resource Center for resources and Flybase for essential information. We thank Annick Crevoisier and Eef Lemmens for administrative and assistance. We are grateful to Vassil Altanov, Elisa Cappuyns and Lysimachos Zografos for preliminary data, Kris Dickson, Richard Benton for critical reading of this manuscript. We thank Ilse Smolders and Ann Van Eeckhaut for their help with initial HPLC analysis. We are particularly grateful to Dr. Julijana Ivanisevic and Dr. Hector Gallart-Ayala at the Metabolomic Unit, University of Lausanne, for the excellent advice, support and analysis of the metabolites and to Federico Caicci at the Electron microscopy facility of the Department of Biology, University of Padova for the excellent TEM analysis of the mitochondria. Graphical model was made through Servier Medical Art (http://www.servier.com).

COMPETING FINANCIAL INTERESTS

The authors declare no competing financial interests

METHODS

***Drosophila* stocks and rearing conditions.** Flies were cultured in vials containing a standard *Drosophila* medium at 25 °C with 60-80% humidity in a 12h light/dark cycle. The fly line used as control was wild-type Canton-S *w^{1118}* (iso1CJ). Heterozygous mutant flies for CYFIP (*$Cyfip^{85.1}$/+*) lacking two-third of the *Cyfip*-coding region were described previously by Schenk *et al.* (Schenck et al., 2003). The *$Cyfip^{85.1}$/+* mutant flies used in this study were first isogenized for 6 generations with a Cantonized *w^{1118}* background. Regulation of CYFIP expression was achieved using the tissue specific GAL4/UAS system (Brand and Perrimon, 1993). In this study, to abrogate the levels of CYFIP we used the UAS-CYFIP-RNAi (UAS-CYFIP-IR) transgene as described before (Galy et al., 2011), which was linked to the Upstream Activation System (UAS). GAL4 in turn will bind the UAS activating transcription of CYFIP-IR. As a result, the RNAi construct is transcribed and endogenous *Cyfip* transcript will be downregulated. GAL4/GAL4 females were crossed en masse to UAS-CYFIP-IR/UAS-CYFIP-IR males to generate GAL4/UAS-CYFIP-IR progeny. GAL4/GAL4 and UAS-CYFIP-IR/UAS-CYFIP-IR females were also crossed with *w^{1118}* males to generate GAL4/+ and UAS-CYFIP-IR/+ progeny respectively that served as controls. Tissue-specific GAL4 expression was achieved using the tissue-specific GAL4 promoters as follows: pan-neuronal (Elav), in cholinergic (Cha-Gla4), and GABAergic (Gad-Gal4). To avoid neurodevelopmental problems and possible lethality, the ElavGal4, was combined with the temporal TubGal80^{ts} system (McGuire et al., 2003; McGuire et al., 2004). At 18°C, TubGal80^{ts} is expressed and binds GAL4, prohibiting its binding to the UAS (i.e., no transcription of UAS-CYFIP-IR). In contrast, at 29-30°C TubGal80^{ts} is degraded and will release GAL4 which in turn will bind the UAS thus activating transcription of UAS-CYFIP-IR. As a result, expression of CYFIP will be downregulated. All flies/progeny for promoter-Gal4;TubGal80^{ts} and their controls were cultured at 18°C and 2-days after eclosion were placed at 29-30°C allowing UAS-CYFIP-IR transcription. For Ca^{2+} imaging, flies were generated that express either synaptophysin-GCaMP (Pech et al., 2015) under control of the specific promoter GAL4 line (Zars et al., 2000). The Ca^{2+} sensors were amplified from pUAST vectors (Pech et al., 2015) using PCR and subcloned into a mb247-pCasPer vector (Pech et al., 2013). The *w pink1^{B9}* flies were kindly provided by Patrik Verstreken (VIB/KULeuven) and described in (Morais et al., 2009). The *ndufs3* flies were kindly provided by Brett Graham (Baylor College of Medicine, Houston) and the *idh3a* flies described in (Ugur et al., 2017) were a gift from Hugo Bellen (Baylor College of Medicine, Houston). All the other transgenic flies used in this study were purchased from the Bloomington stock center.

All the behavioral experiments in flies were performed in a walk-in chamber by Fitoclima Aralab (https://www.aralab.pt/), that offers highly precise and reproducible conditions for climatic and temperature testing.

Drosophila single Pair Mating Assay. Social performance of the *Cyfip$^{85.1}$/+* flies was next investigated by observing courtship, a complex innate *Drosophila* behavior. Briefly, courting *Drosophila* males perform a characteristic sequence of behaviors: orienting toward and following the female, tapping her with their forelegs, vibrating one wing, licking her genitalia, and attempting to copulate (Bastock, 1956; Bastock, 1955; Ejima and Griffith, 2007; Sokolowski, 2001, 2010).

Five to seven days-old virgin males and females were used. Each assay consisted of one *Cyfip$^{85.1}$/+* male and one wild type female introduced into a plexiglass-mating chamber (1 cm diameter × 4 mm height). The courtship activities were video recorded until successful copulation, or longer (6 minutes) in the absence of copulation, using a 65X SD camcorder (Samsung) mounted on a tripod. The assays were done under ambient light at 22 °C temperature and 70% humidity. From the videos recording the courtship index (CI) was calculated for each male. Briefly, CI is the fraction of total recording times the male performed courtship behaviors (orienting, chasing, tapping, licking, singing, copulation attempts) (Ejima and Griffith, 2007; Siegel and Hall, 1979; Sokolowski, 2001, 2010).

Drosophila quantitative assay for social events (competition for food). Assays were performed on socially experienced, 3–7 days-old male flies. Groups of eight males from the same genotype were anesthetized 24 h prior to the assay and placed in vials with food. On the day of the assay, the males were transferred without anesthesia to an empty vial and were deprived of food for 90 minutes, after which they were exposed to a food droplet and given 2 minutes to acclimate to this disturbance. The flies were then observed for an additional 2-minutes, and the total number of social event encounters scored. Behavioral assays were conducted in a behavioral chamber (25 °C, 60-70% humidity) between 8 a.m. and 11 a.m. Statistics were calculated using a one-way fixed effect ANOVA model, Kruskal Wallis test in combination with Dunn's multiple comparison test. A group of male flies were tested simultaneously to obtain an average of the total number of social events in 2 minutes (i.e. number of total approaches, lunges, tussles, wing threat and initiation of courtship scored) (Dankert et al., 2009). The index of approaches in such a complex set up (8 flies) was used to quantify behavior.

Grooming behavior. Flies of 5 days old were collected the day before the assay and kept in vials with fresh food. The day of the experiment they were anesthetized by placing them on ice for 2 min and then placed into a grooming chamber (circular arena of 1cm diameter). Flies were allowed for 20 min to acclimate and then grooming activity was recorded for 3 min, using a 65X SD camcorder (Samsung) mounted on a tripod. To measure grooming behavior, raw videos were analyzed blind to the genotype, calculating the time of grooming over 3 min.

Social space behavior. Flies were separated by gender the day prior to each experiment and kept in vials with fresh food. The analysis of social space behavior was performed using a horizontal circular chamber (a Petri dish of 9 cm diameter) as described before (Simon et al., 2012). Flies were briefly anesthetized by placing them on ice for 2 min and placed into the chamber. Flies let to acclimate for 10 min and then digital images were collected after the flies reached a stable position (up to 25 min). Digital images were imported in Image J and an automated measure of the nearest neighbor to each fly was determined using our own custom R script (available upon request).

Thigmotaxis behavior, flies tend to move closer to the wall of an open arena to avoid the central part (more threatening, centrophobicity) (Besson and Martin, 2005). The distance of a fly from the wall of the chamber was measured using our own custom R script. Graphs and statistical analysis were performed using Prism 4 (GraphPad Software, San Diego, CA, USA).

Negative geotaxis experiment. The negative geotaxis experiment allows to evaluate the reflex motor response in *Drosophila* as previously described (Kosmidis et al., 2011). Briefly, 2-days-old control and *Cyfip*$^{85.1/+}$ flies were transferred individually into polystyrene tubes. The flies were allowed to acclimate for 10 min in a dark environment of 25°C and 70-80% humidity illuminated by red light. Each fly was vortexed for 2 sec and tested twice in for negative geotaxis measuring the time the fly climbs the distance of 6 cm.

Food intake assay. A colorimetric estimation of food intake was performed as previously described (Aditi et al., 2016) with some modifications. Briefly groups of 7-days old mated male flies, entrained for under 12:12 LD (Light-dark cycle), were transferred onto food medium containing 2.5 % (w/v) food dye (Erioglaucine blue disodium salt; Sigma-Aldrich), 2% agar and 5% sucrose, and left for feeding ad libitum for 2 hours. After feeding the flies were washed with PBS 1X, each body was detached from the head and singularly homogenized in 100 µl of chilled PBS 1X and centrifuged at 10.000 rpm for 10 min. 50 µl of supernatant was used for absorbance recording at 620nm using a spectrophotometer.

Drosophila locomotor activity. The *Drosophila* Activity Monitoring (DAM) system from Trikinetics Inc. (Walthman, MA) was used to record the locomotor activity of flies. Male flies (1-week old), anesthetised on ice, were individually loaded into the locomotor activity-monitoring tubes, thin 5 mm diameter polycarbonate tubes containing 5% sucrose and 2% agar food and incubated for at least 4 days under 12:12 LD (light - dark) conditions at 25 °C and 50-60% humidity. Light was turned on at 7:30 am and turned off at 7:30 pm. The DAM system software counts the number of times the single fly walks through an infrared beam aimed at the middle of the tube. Data were recorded as the number of crossings (transitions) per bin of 5-30 minutes. To allow the flies to recover from anaesthesia and to get acclimatized to the new environment from the first day was excluded from the analysis. Two independent experiments were performed and at least 40 flies for each genotype were analysed. Statistical analysis was conducted using GraphPad Prism 6.0 software. Data were evaluated by one-way analysis of variance (ANOVA) with Sidak's post hoc test and by non-parametric Kruskal-Wallis's test with Dunn's correction.

Western Blotting analysis. For Western blot analysis, male fly heads were homogenized in 2x Laemmli buffer containing DTT. They were loaded on 10%

acrylamide gels, transferred to PVDF membranes and probed with primary antibodies. The primary antibodies used: anti-Syntaxin (DSHB) at 1:3000, anti-GAD1 (kind gift of Prof. Job Jackson), anti-ATP5B (Abcam) at 1:4000, anti-NDUFS3 (Abcam) at 1:4000, anti-HSP60 (Santa Cruz) at 1:4000, anti-Tom20 (Santa Cruz Biotech) at 1:1000, anti-VDAC/Porin (Abcam) at 1:2000, anti-Bruchpilot (DSHB) at 1:500, and anti-Tubulin (DSHB) at 1:4000. Detection was obtained using the Odyssey infrared imaging system (LI-COR, Bioscience). The fluorescence secondary antibodies DyLight 800 anti-rabbit and DyLight 800 anti-mouse were used at 1:5000 (Thermo Scientific).

RNA Extraction, RT-PCR and quantitative PCR (qPCR). Total RNA, from 30 male fly heads 1 week old, was extracted using Trizol reagent (Invitrogen, Carlsbad, CA) according to manufacturer's instructions to extract total RNA. Before proceeding with the RT-PCR, RNA quantity and quality were determined with the NanoDrop 2000 UV-Vis Spectrophotometer (Thermo, USA). Four independent samples for each genotype and 2 biological replicates have been collected.

Total RNA was diluted to prepare aliquots of 200 ng/10 µl and used in RT-PCR reaction for 1 h at 37 °C, using random primers, M-MLV enzyme (Invitrogen), buffer 5x M-MLV reaction buffer, RNAase out and dNTPs, according to manufacturer's instructions (Invitrogen). cDNA was diluted 1:20 and 5 µl cDNA was used for each qPCR 15 µl reaction. qPCR was conducted on a Light Cycler 96 (Roche, Switzerland) with SYBR Green PCR mix (Roche, Switzerland) with primers of our genes of interest: *Cyfip, gad,* and ribosomal proteins *L13* and *L32* (encoding for the 60S ribosomal protein L13 and L32 respectively). All primer pairs were designed through the Fly Primer Bank (www.flyrnai.org/flyprimerbank) and were synthesized by IDT (Belgium) and Microsynth AG (Switzerland).

Two technical replicates for each biological replicate were assessed. Statistical analysis was conducted using GraphPad Prism 6.0 software (La Jolla, CA). Data were evaluated by one-way analysis of variance (ANOVA) with Sidak's post hoc test and by Kruskal-Wallis's test with Dunn's correction or Mann-Whitney test.

Quantitative PCR for mtDNA content. Drosophila whole DNA (genomic and mitochondrial) from adult brains was obtained using a method previously described (Yoon et al., 2017). The isolated DNA was used for qPCR as described above. Primers against the mitochondrial ribosomal protein 16S and the ribosomal protein *L13* were used to amplify mtDNA and genomic DNA respectively.

Polysomes/mRNPs gradient

The protocol was slightly modified from (Napoli et al., 2008). Specifically, *Drosophila* heads were homogenized in lysis buffer (100 mM NaCl, 10 mM MgCl2, 10 mM Tris-HCL pH 7.5, 0.5 mM DTT, Protease inhibitor cocktail, 50 µg/mL CHX, RNAse OUT and RNAsin inhibitor 2.5 µl/mL). The lysates were incubated 5 min on ice and then centrifuged 5 min at 1000 g. In the supernatant Triton-X 20% and NaDoc 10% was added. Samples were then centrifuged 8 min at 12000g at 4ºC and the supernatants centrifuged through 15%-50% (w/v) sucrose grandients for 2 hours at 37.000 rpm. Gradients were collected in 12 fractions. Equal volumes from each fraction was used for RNA extraction using Phenol-Chloroform-Isoammilic alcohol (according to manufacturer’s conditions). 2 pg/µl of spike in Firefly Luciferase (FLuc) mRNA, (Promega) was added as loading control. The mRNA was used for RT and quantitative PCR as described in the manuscript. *Aralar* mRNA level (Aralar primer For: TCCTGGGACTCTTTTCCGAAT; Aralar primer Rev: GCCTGGAACTCCGAGAAGG) was normalized to Fluc mRNA level (FLuc Primer For: ATCTGCCTCCTGGCTTCAAC; FLuc Primer Rev: CGGTAGACCCAGAGCTGTTC).

Drosophila drug administration. All compounds were purchased from Sigma-Aldrich and were used as described before (Kanellopoulos et al., 2012; Zwarts et al., 2011). The drugs were dissolved as per the manufacturer's instructions and used at the following concentrations: GABA at 50 µM, DABA 100 µM, Valproic acid (VPA) at 1 mM, Diazepam at 50 µM, Rotenone at 1-10 µM, Pyridoxal 5’ phosphate (PLP) at 50 µM, and Oligomycin at 500 µM. Compounds in solution were mixed with Formula 4-24® Instant *Drosophila* Medium (blue food) in water. Approximately 50–60 adult flies were placed in plastic vials containing 500 µl of each solution on top of an agar matrix and allowed to feed *ad libitum* before behavior. Vehicle treatment consisted of solvent added to blue food alone.

Immunohistochemical analysis. Fly brains were dissected under a stereomicroscope in phosphate-buffered saline 1x (PBS) for no longer than 1 hour and fixed in PBS 1x containing 3,7% formaldehyde for 10-15 minutes at room temperature using a rotator. After 3 washes of 10 minutes in PBT (PBS 1x, 0.3% Triton-X) the brains were blocked in 10% Normal Goat Serum in PBT for 30 minutes. The brains were then incubated with anti-GABA (Sigma-Aldrich) at 1:500, anti-nc82 (DSHB) at

1:500, anti-GAD (DSHB) at 1:250, in 5% NGS in PBT at 4 °C overnight. After the primary antibody incubation, the brains were washed in PBT 3 times for 10 minutes per wash and incubated with secondaries Alexa Fluro 546 or 488 (Life Technologies, USA) at 1:1000 in 5% NGS in PBT for 1-2 hours at room temperature (RT). Then the brains were washed again in PBT for 3 times at RT for 10 minutes and mounted in Mowiol containing DAPI (1:1000) on a glass slide. Pictures were taken on the Olympus FluoView™ FV1000 Confocal Microscope and analyzed with ImageJ software.
For the TMRE (Enzo) and Rhodamine 123 (Sigma-Aldrich) stainings, brains were dissected in HL3 solution (mM): 110 NaCl, 5 KCl, 10 NaHCO3, 5 Hepes, 30 sucrose, 5 trehalose, and 10 MgCl2, pH 7.2. Dissected brains were stained with 10nM TMRE or Rhodamine123 dye for 5 minutes at room temperature. Brains were quickly washed with HL3 solution, mounted on glass slides and immediately imaged with confocal microscope Leica SP8 using the same settings for all the samples.

FACS Analysis. To isolate the GABAergic neuronal population from *Drosophila* brain, the enhancer-trap line Gad-GAL4 was used to drive the expression of GFP in GABAergic neurons of *wild type and Cyfip*$^{85.1}$/+ flies. Brains from adult flies (n = 60) per genotype were dissected in cold 1xPBS. Tissues were dissociated using 0.05% trypsin-EDTA (Life Technologies) for 60 minutes at 37 °C in the dark. The GFP-positive cells were fractionated from the GFP negative population using a BD FACSAria I by BD Biosciences (San Jose) with a 70 µm nozzle tip at 60psi. GFP was excited by a blue laser (488nm) and detected using a 530/30 bandpass (BP) filter. Dead cells were excluded using propidium iodide (PI) at a final concentration of 1 µg/ml and detected using a 610/20 BP filter. Post sort purity check was performed to ensure clean fractionation of both the GFP-positive and -negative populations. Data were analyzed and presented with FlowJo software (Tree Star, Ashland, OR).

Ca^{2+} Imaging. Control and *Cyfip*$^{85.1}$/+ flies were generated to express the synaptically targeted Ca^{2+} sensitive fluorescent protein G-CaMP3 in the GABAergic neurons. Brains of male transgenic flies (seven days old) expressing synaptophysin-GCaMP (Pech et al., 2015) under direct control of the mb247-promoter (Pech et al., 2013) were imaged at a frame rate of 5 Hz and for 100 ms per frame at 488 nm through a window cut into the head capsule using a upright fluorescence microscope (Zeiss Examiner D1) equipped with a xenon lamp (Lambda DG-4, Sutter Instrument), a 14-bit CCD camera (Coolsnap HQ, Photometrics) and a 20 × water-immersion objective (NA =1.0). 50 µl of freshly prepared 1M KCl were injected into the Ringer's solution covering the brain (final concentration at the brain ~0.05M). Image acquisition was controlled using the software Metafluor (Visitron Systems, Puchheim). Image processing and analysis was performed with Fiji software. Circular regions of interest (ROIs, diameter ~20 µm) were placed in the center of the calyx or on the lobes. Background fluorescence outside the neuropils was subtracted from each ROI, "F_0" was determined by the average pixel intensity of five frames directly before stimulus onset, ΔF is the difference between the fluorescence in each frame and F_0, and resulting values were normalized by dividing by F_0. The experimental flies were heterozygous for the sensor in either the *w^{1118}* background only or carrying the C*$yfip^{85.1}$/+* mutation. Both controls and mutant flies were measured alternately on the same days.

Mass Spectrometry. Sample was dissolved in Laemmli buffer and run on a 10% SDS-PAGE gel, which was stopped when the front reached about 1/5 of the gel. The gel was fixed overnight and stained briefly with colloidal coomassie blue. The protein-containing gel piece was chopped into 1 mm by 1 mm pieces, destained, and subjected to trypsin digestion as described previously (Chen et al., 2015). The tryptic peptides were dissolved in 17 µL 0.1M acetic acid, and analyzed by nano-LC MS/MS using an Ultimate 3000 LC system (Dionex, Thermo Scientific) coupled to a TripleTOF 5600 mass spectrometer (Sciex). Peptides were fractionated on a 200 mm Alltima C18 column (100 µm i.d., 3 µm particle size). The acetonitrile concentration in the mobile phase was increased from 5 to 30% in 90 minutes, to 40% in 5 minutes, and to 90% in another 5 minutes, at a flow rate of 400 nL/minutes. The eluted peptides were electro-sprayed into the TripleTOF MS. The nano-spray needle voltage was set to 2500V. The mass spectrometer was operated in a data-dependent mode with a single MS full scan (m/z 350−1200, 250 msec) followed by a top 25 MS/MS (85 msec per MS/MS, precursor ion > 90 counts/s, charge state from +2 to +5) with an exclusion time of 16 sec once the peptide was fragmented. Ions were fragmented in the collision cell using rolling collision energy, and a spread energy of 10eV. The MS raw data were imported into MaxQuant (version 1.5.2.8), and searched against the uniprot-proteome_fruitfly_%3AUP000000803 database, with match between run enabled. Further MaxQuant settings were left at default.

Database analysis. Orthology mapping was obtained using the DRSC DIOPT tool (Hu et al., 2011)-that makes use of the following resources: Ensembl Compara (Vilella et al., 2009), NCBI Homologene, Inparanoid, Isobase, OMA, OrthoDB, OrthoMCL, Phylome, RoundUp and TreeFam.

Disease Enrichment. We investigated disease enrichment of the union dataset (mapped to 278 human genes) using gene-disease annotation data collected from OMIM (Amberger et al., 2015), GeneRIF (Mitchell et al., 2003) and Ensembl variation (Chen et al., 2010a) databases using the topOnto package (https://github.com/statbio/topOnto). The annotation data was standardized using MetaMap (Aronson and Lang, 2010) and NCBO Annotator to recognize terms found in the Human Disease Ontology (HDO) (Schriml et al., 2012). Recognized disease ontology terms were then associated with gene identifiers and stored locally. Disease term enrichment, for the 279 human genes, were then be calculated using the Topology-based Elimination Fisher method (Alexa et al., 2006) found in the topGO package (http://topgo.bioinf-mpi-inf.mpg.de/), together with the standardized OMIM/GeneRIF/Ensembl variation gene-disease annotation data (17731 gene-disease associations), and the full HDO tree (3140 terms). We tested the dataset for functional enrichment using the GO Cellular Component (CC) and Biological Function (BP) ontologies (Ashburner et al., 2000), together with the topGO package and Elimination Fisher method. We found 1078 (1692) CC terms for Fly (Human) and 6479 (14291) BP terms (See Supplemental Tables). Enrichment results are shown in Figure 2, where P-values have been corrected using the Bonferroni correction at the 0.01 (***) and 0.05 (**) significance level, using the number of terms in the GO tree.

Construction of PPI networks from external Databases. The fly PPI network was built using the total 361 genes found, together with interactions extracted from the publicly available databases: FlyBase, BioGRID, IntAct, BIND, DIP, MINT.The fly PPI network was filtered to contain only interactions between the 361 genes found the final largest connected component contains 274 genes and 1014 interactions. The network was found to have overall associative mixing (0.097), driven by main contributors BioGRID (0.187) and FlyBase (0.85). The corresponding human PPI network built from the 278 human orthologs, was found to consist of 234 genes and 1143 interactions.

The fly PPI network consisting of 274 genes and 1014 interactions, using the Vision visualization package (http://visone.info/html/) and clustered using the Modularity based Potts model and simulated annealing algorithm “spinglass” (Reichardt and Bornholdt, 2006; Traag and Bruggeman, 2009) available in R (http://igraph.sourceforge.net) (spin states set to 500, and gamma to 2.0). Genes are highlighted using GO annotation with “mitochondrion” (GO:0005739) related genes in peach, “cytoskeleton” related genes in navy blue, and “synaptic vesicle” related genes in orange. For each cluster in the fly PPI network found, we further tested the significance of enrichment for function and disease, using the Hypergeometric distribution for sampling without replacement:

$$P\left(X = \mu_{fc}; \mu_{fc}, Cn, F, N\right) = \frac{\binom{F}{\mu_{fc}}\binom{N-F}{Cn-\mu_{fc}}}{\binom{N}{Cn}},$$

$$P - value\left(\mu_{fc}\right) = \sum_{i=0}^{\mu_{fc}} \begin{cases} P(X = i) & : \quad P(X = i) \leq P\left(X = \mu_{fc}\right) \\ 0 & : \quad P(X = i) > P\left(X = \mu_{fc}\right). \end{cases} \quad \text{(eqn-1)}$$

Where in eqn-1, N is the total number of genes in the network; Cn the number of genes in the community; F the total number of functional annotated genes in the network, and μ_{fc} the number of functional annotated genes per community. P-values were tested for their strength of significance, by recording the percentage of P-values found from every community/annotation combination, lower than or equal to the observed P-value, when 1000 random permutations of the annotation labels were made. A pseudocount of 1 was added to avoid permutated P-values of zero. P-values found with a strength of significance < 1% were considered statistically significant. Functionally enriched clusters, for GO “mitochondrion”, “cytoskeleton” and “synaptic vesicle” related annotations are also highlighted.

Gene ontology analysis for genetic screening. 178 Drosophila genes were associated to GO “mitochondrial outer membrane” (GO:0005741). Out of 178, 43 genes were selected that were described to be involved in transport (excluding protons, electrons transport and OXPHOS). From the 43 genes, we obtained 36 available mutant fly strains from the Bloomington Drosophila Stock Center (NIH P40OD018537) and used in this study.

Metabolite quantification. Both groups of metabolites, amino acids and TCA cycle intermediates, were quantified using stable-isotope-dilution Liquid Chromatography Mass Spectrometry (LC-MS) as described below. Snap frozen brain samples were pre-extracted and homogenized by the addition of 100 µL of MeOH:H2O (4:1) per 10 fly brains (2 x 20 seconds at 10000 rpm, Cryolys Precellys Homogenizer, Bertin Technologies, Rockville, MD, US). Homogenized extracts were centrifuged (15 minutes at 4000 g at 4°C) and the resulting supernatant was evaporated to dryness in a vacuum concentrator (LabConco, Missouri, US). Total protein content was measured in pellets using the BCA assay. Dried sample extracts were resuspended in 50µL of MeOH:H2O (4:1, v/v) and mixed with 250µL of the ice-cold internal standard solution (in 100% acetonitrile). Samples were then incubated 30 minutes at -80°C in order to promote protein precipitation and centrifuged 15 minutes at 4°C and 2700g. The resulting supernatants were injected for LC-MS analysis.

Quantification of amino acids was performed using Hydrophilic Interaction Liquid Chromatography coupled to high resolution mass spectrometry (HILIC - HRMS) in positive ionization mode using a QExactive™ Hybrid Quadrupole-Orbitrap interfaced with Thermo Accela 1250 UPLC pump and CTC PAL Analytics autosampler. Metabolites were separated using a BEH Amide, 1.7 µm, 100 mm × 2.1 mm I.D. column (Waters, Massachusetts, US). The mobile phase was composed of A = 20 mM ammonium formate and 0.1 % FA in water and B = 0.1 % FA in ACN. The linear gradient elution from 95% B (0-2 minutes) to 65% B (14 minutes) and down to 50% B (16 – 18 minutes) was applied, followed by 4 minutes of column re-equilibration in the initial gradient conditions. The flow rate was 400µL/minutes and the sample injection volume was 10 µL. HESI source conditions were set as follow: sheath gas flow at 60, Aux gas flow rate at 20, Sweep gas flow rate at 0, spray voltage at +3kV, capillary temperature at 300°C, s-lens RF level at 60 and aux gas heater temperature at 300°C. The instrument was set to acquire over the mass range 60−900, with the MS acquisition parameters set as follows: resolution at 70’000 FWHM, 1 microscan, 1e6 AGC and maximum inject time at 100 ms. Amino acids and derivatives were quantified by using a standard calibration curves and isotopic labeled internal standards. LC-MS data was processed using TraceFinder Clinical Research (version 4.1, Thermo Fischer Scientific).

Quantification of TCA cycle intermediates was performed using Hydrophilic Interaction Liquid Chromatography coupled to tandem mass spectrometry (HILIC - MS/MS) in negative ionization mode using a 6495 Triple Quadrupole system (QqQ) interfaced with 1290 UHPLC system (Agilent Technologies). TCA metabolites were separated using a ZIC-pHILIC (100 mm, 2.1 mm I.D. and 5 µm particle size) column. The mobile phase was composed of A = 20 mM ammonium Acetate and 20 mM NH4OH in water at pH 9.35 and B = 100% ACN. The linear gradient elution from 90% B (0-1.5 minutes) to 50% B (8 – 11 minutes) and down to 45% B (12 – 15 minutes) was applied, followed by 9 minutes of column re-equilibration using the initial gradient conditions. The flow rate was 300 µL/minutes, column temperature 30°C and sample injection volume 2µl. ESI source conditions were set as follows: dry gas temperature 290 °C and flow 14 L/minutes, sheath gas temperature 350 °C, nebulizer 45 psi, and flow 12 L/minutes, nozzle voltage 0 V, and capillary voltage -2000 V. Data were acquired in a Dynamic Multiple Reaction Monitoring (DMRM) mode with a total cycle time of 600 msec. Collision energies were optimized for each metabolite. LC-MS/MS data was processed using the Agilent Quantitative analysis software (version B.07.00, MassHunter Agilent technologies). Relative quantification of metabolites was based on EIC (Extracted Ion Chromatogram) areas for the monitored MRM transitions.

For absolute quantification, calibration curves and the stable isotope-labeled internal standards (IS) were used and the concentrations of the compounds were calculated as the ratio of MS response (peak area) between the analyte and the IS, to account for matrix effects. Finally, the concentrations were reported to total protein content in brain tissue.

For isotope tracing, flies were fed with sucrose free food containing [U-13C]-glucose for 6 hours and immediately dissected in cold PBS 1x. For each sample ten drosophila brains were pre-extracted and homogenized as described above. Brain extracts were analyzed by Hydrophilic Interaction Liquid Chromatography coupled to high resolution mass spectrometry (HILIC - HRMS) in negative ionization mode using a 6550 Quadrupole Time-of-Flight (Q-TOF) system interfaced with 1290 UHPLC system (Agilent Technologies) as previously described (Gallart-Ayala et al., 2018). Raw LC-MS files were processed in Profinder B.08.00 software (Agilent Technologies) using the targeted data mining in isotopologue extraction mode. The metabolite identification was based on accurate mass and retention time matching against an *in-house* database containing data on 600 polar metabolite standards (analyzed in the same analytical conditions). The Extracted Ion Chromatogram areas (EICs) of each isotopologue (M+0, M+1, M+2, M+3,…) were corrected for natural isotope abundance

(Midani et al., 2017) and the label incorporation or ^{13}C enrichment was calculated based on relative isotopolgue abundance (in %), in each one of two analyzed conditions (Roci et al., 2016).

Mitochondrial Functional Assays. High resolution respirometry. For measuring mitochondrial respiration in *Drosophila* brains: ten fly heads from 4 days old male were rapidly dissected under a microscope and mechanically homogenized in Miro6 Buffer (20 mM Hepes, 110 mM sucrose, 10 mM KH_2PO4, 20 mM taurine, 60 mM lactobionic acid, 3 mM $MgCl_2$, 0.5 EGTA, pH 7.1, 1 mg/ml fatty acid free BSA, catalase 280 U/ml) (Krumschnabel et al., 2015), then immediately and loaded into an Oroboros 2K oxygraph chamber filled with Miro6 buffer equilibrated at 25 °C.

Drosophila bodies. For mitochondrial respiration in fly bodies, fly heads were rapidly removed and bodies were mechanically permeabilized in Miro6 Buffer. The body homogenates were then spun at 200 g for 5 minutes and the supernatant was immediately loaded into the Oroboros 2K oxygraph. In each of these protocols, the intactness of the mitochondrial outer membrane was checked by addition of exogenous cytochrome c.

Oxygen consumption rates were measured before and after addition of the following sequence of substrates and specific inhibitors: 1) 2.5 mM pyruvate, 1 mM malate in flies, and a mixture of 2.5 mM pyruvate, 10 mM glutamate, and 1 mM malate in human cells (CI leak), followed by 2.5 mM ADP to determine complex I-driven phosphorylating respiration (CI OXPHOS). 2) 5 mM succinate to determine the phosphorylating respiration driven by simultaneous activation of complex I and II (CI+II OXPHOS). 3) Titrating concentrations of the mitochondrial uncoupler CCCP to reach the maximal, uncoupled respiration (CI+II electron transfer system, ETS). 4) 200 nM rotenone to fully inhibit complex I-driven respiration and measure complex II-driven uncoupled respiration (CII electron transfer system, CII ETS). 5) 0.5 µM Antimycin A to block mitochondrial respiration at the level of complex III. Residual oxygen consumption was always negligible. 6) 2 mM ascorbate, 0.5 mM TMPD to measure cytochrome c oxidase (CIV or COX)- driven respiration. 7) 300 µM potassium cyanide to specifically block cytochrome c oxidase activity and measure residual background oxygen consumption caused by chemical interaction between ascorbate and TMPD. Cytochrome c oxidase-driven respiration is the cyanide sensitive oxygen consumption.

NADH and NADt levels were measured from brain lysates using the NAD/NADH Quantitation Colorimetric Kit (Biovision, K337). The enzyme activity of IDH was determined from isolated mitochondria using the BioVision kit (K756-100). Mitochondria were isolated as previously described (Depner et al., 2014; Yoon et al., 2017).

Citrate synthase (CS) activity was measured using the MAK193 assay kit (Sigma-Aldrich). Briefly, isolated mitochondria from 100 fly brains were used for measuring the CS activity. CS activity was calculated using a coupled enzyme reaction, which leads in a colorimetric (412 nm) product proportional to the enzymatic activity present. One unit of CS is the enzyme that generates 1.0 mmole CoA per min at 25°C and pH 7.2. The absorbance was measured in a microplate photometer at 412 nm.

Electron microscopy. Fly brains from 3-5 days old flies were dissected in cold PBS 1x and fixed over-night in 2% paraformaldehyde and 2.5% gluteraldehyde in 0.1 M sodium cacodylate buffer pH 7.4. After rinsing in 0.1 M cacodylate buffer, the samples were post fixed in 1:1 2% OsO4 and 0.2 M cacodylate buffer for 1 hour. After 3 water washes, samples were dehydrated in a graded ethanol series and embedded in an epoxy resin (Sigma-Aldrich). Ultrathin sections (60-70 nm) were obtained with an Ultrotome V (LKB) ultramicrotome, counterstained with uranyl acetate and lead citrate and viewed with a Tecnai G^2 (FEI) transmission electron microscope operating at 100 kV. Images were captured with a Veleta (Olympus Soft Imaging System) digital camera. Quantification of mitochondria perimeter and area was performed by using ImageJ software.

ELISA. GABA levels were determined from fly brains using the GABA ELISA Enzyme immunoassay (IBL, ID59301). Briefly, total brain lysates, isolated mitochondria and vesicles (Depner et al., 2014; Yoon et al., 2017) were used for GABA derivatization. The samples were incubated with a polyclonal antibody against GABA-derivative, together with assay reagent containing GABA-derivative (tracer). The concentration of antibody-bound tracer is inverse proportional to the GABA concentration in the sample. Peroxidase conjugate was added detect the tracer and tetramethylbenzidine (TMB) served as a peroxidase substrate. The absorbance was measured in a microplate photometer at 450nm.

REFERENCES

Aditi, K., Shakarad, M.N., and Agrawal, N. (2016). Altered lipid metabolism in Drosophila model of Huntington's disease. Sci Rep *6*, 31411.

Akarsu, S., Torun, D., Bolu, A., Erdem, M., Kozan, S., Ak, M., Akar, H., and Uzun, O. (2014). Mitochondrial complex I and III gene mRNA levels in schizophrenia, and their relationship with clinical features. J Mol Psychiatry *2*, 6.

Alexa, A., Rahnenfuhrer, J., and Lengauer, T. (2006). Improved scoring of functional groups from gene expression data by decorrelating GO graph structure. Bioinformatics *22*, 1600-1607.

Amberger, J.S., Bocchini, C.A., Schiettecatte, F., Scott, A.F., and Hamosh, A. (2015). OMIM.org: Online Mendelian Inheritance in Man (OMIM(R)), an online catalog of human genes and genetic disorders. Nucleic Acids Res *43*, D789-798.

Amoedo, N.D., Punzi, G., Obre, E., Lacombe, D., De Grassi, A., Pierri, C.L., and Rossignol, R. (2016). AGC1/2, the mitochondrial aspartate-glutamate carriers. Biochim Biophys Acta *1863*, 2394-2412.

Anholt, R.R., and Mackay, T.F. (2012). Genetics of aggression. Annu Rev Genet *46*, 145-164.

Anitei, M., Stange, C., Parshina, I., Baust, T., Schenck, A., Raposo, G., Kirchhausen, T., and Hoflack, B. (2010). Protein complexes containing CYFIP/Sra/PIR121 coordinate Arf1 and Rac1 signalling during clathrin-AP-1-coated carrier biogenesis at the TGN. Nat Cell Biol *12*, 330-340.

Anitha, A., Nakamura, K., Thanseem, I., Yamada, K., Iwayama, Y., Toyota, T., Matsuzaki, H., Miyachi, T., Yamada, S., Tsujii, M.*, et al.* (2012). Brain region-specific altered expression and association of mitochondria-related genes in autism. Molecular autism *3*, 12.

Aoki, Y., and Cortese, S. (2016). Mitochondrial Aspartate/Glutamate Carrier SLC25A12 and Autism Spectrum Disorder: a Meta-Analysis. Mol Neurobiol *53*, 1579-1588.

Aronson, A.R., and Lang, F.M. (2010). An overview of MetaMap: historical perspective and recent advances. J Am Med Inform Assoc *17*, 229-236.

Ashburner, M., Ball, C.A., Blake, J.A., Botstein, D., Butler, H., Cherry, J.M., Davis, A.P., Dolinski, K., Dwight, S.S., Eppig, J.T.*, et al.* (2000). Gene ontology: tool for the unification of biology. The Gene Ontology Consortium. Nat Genet *25*, 25-29.

Attrill, H., Falls, K., Goodman, J.L., Millburn, G.H., Antonazzo, G., Rey, A.J., Marygold, S.J., and FlyBase, C. (2016). FlyBase: establishing a Gene Group resource for Drosophila melanogaster. Nucleic Acids Res *44*, D786-792.

Bachmann, S.O., Sledziowska, M., Cross, E., Kalbassi, S., Waldron, S., Chen, F., Ranson, A., and Baudouin, S.J. (2019). Behavioral training rescues motor deficits in Cyfip1 haploinsufficiency mouse model of autism spectrum disorders. Translational psychiatry *9*, 29.

Badal, K.K., Akhmedov, K., Lamoureux, P., Liu, X.A., Reich, A., Fallahi-Sichani, M., Swarnkar, S., Miller, K.E., and Puthanveettil, S.V. (2019). Synapse Formation Activates a Transcriptional Program for Persistent Enhancement in the Bi-directional Transport of Mitochondria. Cell Rep *26*, 507-517 e503.

Balijepalli, S., Boyd, M.R., and Ravindranath, V. (1999). Inhibition of mitochondrial complex I by haloperidol: the role of thiol oxidation. Neuropharmacology *38*, 567-577.

Bastock, M. (1956). A gene mutation which changes a behaviour pattern. Evolution *10*, 421–439.

Bastock, M.M., A. (1955). The courtship of Drosophila melanogaster

. Behaviour *8*, 85–111.

Ben-Ari, Y. (2017). NKCC1 Chloride Importer Antagonists Attenuate Many Neurological and Psychiatric Disorders. Trends Neurosci *40*, 536-554.

Ben-Ari, Y., Khalilov, I., Kahle, K.T., and Cherubini, E. (2012). The GABA excitatory/inhibitory shift in brain maturation and neurological disorders. Neuroscientist *18*, 467-486.

Benke, D., and Mohler, H. (2017). Impact on GABA systems in monogenetic developmental CNS disorders: Clues to symptomatic treatment. Neuropharmacology.

Bergman, O., and Ben-Shachar, D. (2016). Mitochondrial Oxidative Phosphorylation System (OXPHOS) Deficits in Schizophrenia: Possible Interactions with Cellular Processes. Canadian journal of psychiatry Revue canadienne de psychiatrie *61*, 457-469.

Besson, M., and Martin, J.R. (2005). Centrophobism/thigmotaxis, a new role for the mushroom bodies in Drosophila. J Neurobiol *62*, 386-396.

Boccuto, L., Chen, C.F., Pittman, A.R., Skinner, C.D., McCartney, H.J., Jones, K., Bochner, B.R., Stevenson, R.E., and Schwartz, C.E. (2013). Decreased tryptophan metabolism in patients with autism spectrum disorders. Molecular autism *4*, 16.

Bonnighausen, J., Gebhard, D., Kroger, C., Hadeler, B., Tumforde, T., Lieberei, R., Bergemann, J., Schafer, W., and Bormann, J. (2015). Disruption of the GABA shunt affects mitochondrial respiration and virulence in the cereal pathogen Fusarium graminearum. Mol Microbiol *98*, 1115-1132.

Bozdagi, O., Sakurai, T., Dorr, N., Pilorge, M., Takahashi, N., and Buxbaum, J.D. (2012). Haploinsufficiency of Cyfip1 produces fragile X-like phenotypes in mice. PloS one *7*, e42422.

Braat, S., and Kooy, R.F. (2015). The GABAA Receptor as a Therapeutic Target for Neurodevelopmental Disorders. Neuron *86*, 1119-1130.

Brambilla, P., Perez, J., Barale, F., Schettini, G., and Soares, J.C. (2003). GABAergic dysfunction in mood disorders. Molecular psychiatry *8*, 721-737, 715.

Brand, A.H., and Perrimon, N. (1993). Targeted gene expression as a means of altering cell fates and generating dominant phenotypes. Development *118*, 401-415.

Cafferkey, M., Ahn, J.W., Flinter, F., and Ogilvie, C. (2014). Phenotypic features in patients with 15q11.2(BP1-BP2) deletion: further delineation of an emerging syndrome. Am J Med Genet A *164A*, 1916-1922.

Carillo, P. (2018). GABA Shunt in Durum Wheat. Front Plant Sci *9*, 100.

Castora, F.J. (2019). Mitochondrial function and abnormalities implicated in the pathogenesis of ASD. Prog Neuropsychopharmacol Biol Psychiatry *92*, 83-108.

Castro, J.P., Wardelmann, K., Grune, T., and Kleinridders, A. (2018). Mitochondrial Chaperones in the Brain: Safeguarding Brain Health and Metabolism? Front Endocrinol (Lausanne) *9*, 196.

Cellot, G., and Cherubini, E. (2014). GABAergic signaling as therapeutic target for autism spectrum disorders. Frontiers in pediatrics *2*, 70.

Chateauvieux, S., Morceau, F., Dicato, M., and Diederich, M. (2010). Molecular and therapeutic potential and toxicity of valproic acid. Journal of biomedicine & biotechnology *2010*.

Chen, N., Koopmans, F., Gordon, A., Paliukhovich, I., Klaassen, R.V., van der Schors, R.C., Peles, E., Verhage, M., Smit, A.B., and Li, K.W. (2015). Interaction proteomics of canonical Caspr2 (CNTNAP2) reveals the presence of two Caspr2 isoforms with overlapping interactomes. Biochim Biophys Acta *1854*, 827-833.

Chen, Y., Cunningham, F., Rios, D., McLaren, W.M., Smith, J., Pritchard, B., Spudich, G.M., Brent, S., Kulesha, E., Marin-Garcia, P., *et al.* (2010a). Ensembl variation resources. BMC Genomics *11*, 293.

Chen, Z., Borek, D., Padrick, S.B., Gomez, T.S., Metlagel, Z., Ismail, A.M., Umetani, J., Billadeau, D.D., Otwinowski, Z., and Rosen, M.K. (2010b). Structure and control of the actin regulatory WAVE complex. Nature *468*, 533-538.

Coghlan, S., Horder, J., Inkster, B., Mendez, M.A., Murphy, D.G., and Nutt, D.J. (2012). GABA system dysfunction in autism and related disorders: from synapse to symptoms. Neurosci Biobehav Rev *36*, 2044-2055.

Cox, D.M., and Butler, M.G. (2015). The 15q11.2 BP1-BP2 microdeletion syndrome: a review. International journal of molecular sciences *16*, 4068-4082.

Dankert, H., Wang, L., Hoopfer, E.D., Anderson, D.J., and Perona, P. (2009). Automated monitoring and analysis of social behavior in Drosophila. Nat Methods *6*, 297-303.

Das, D.K., Tapias, V., D'Aiuto, L., Chowdari, K.V., Francis, L., Zhi, Y., Ghosh, B.A., Surti, U., Tischfield, J., Sheldon, M., *et al.* (2015). Genetic and morphological features of human iPSC-derived neurons with chromosome 15q11.2 (BP1-BP2) deletions. Molecular neuropsychiatry *1*, 116-123.

Davenport, E.C., Szulc, B.R., Drew, J., Taylor, J., Morgan, T., Higgs, N.F., Lopez-Domenech, G., and Kittler, J.T. (2019). Autism and Schizophrenia-Associated CYFIP1 Regulates the Balance of Synaptic Excitation and Inhibition. Cell Rep *26*, 2037-2051 e2036.

Davis, M.I., Gross, S., Shen, M., Straley, K.S., Pragani, R., Lea, W.A., Popovici-Muller, J., DeLaBarre, B., Artin, E., Thorne, N., *et al.* (2014). Biochemical, cellular, and biophysical characterization of a potent inhibitor of mutant isocitrate dehydrogenase IDH1. J Biol Chem *289*, 13717-13725.

De Rubeis, S., He, X., Goldberg, A.P., Poultney, C.S., Samocha, K., Cicek, A.E., Kou, Y., Liu, L., Fromer, M., Walker, S., *et al.* (2014). Synaptic, transcriptional and chromatin genes disrupted in autism. Nature *515*, 209-215.

De Rubeis, S., Pasciuto, E., Li, K.W., Fernández, E., Di Marino, D., Buzzi, A., Ostroff, L.E., Klann, E., Zwartkruis, F.J., Komiyama, N.H., *et al.* (2013). CYFIP1 coordinates mRNA translation and cytoskeleton remodeling to ensure proper dendritic spine formation. Neuron *79*, 1169-1182.

De Wolf, V., Brison, N., Devriendt, K., and Peeters, H. (2013). Genetic counseling for susceptibility loci and neurodevelopmental disorders: the del15q11.2 as an example. Am J Med Genet A *161A*, 2846-2854.

Depner, H., Lutzkendorf, J., Babkir, H.A., Sigrist, S.J., and Holt, M.G. (2014). Differential centrifugation-based biochemical fractionation of the Drosophila adult CNS. Nat Protoc *9*, 2796-2808.

Di Marino, D., Chillemi, G., De Rubeis, S., Tramontano, A., Achsel, T., and Bagni, C. (2015). MD and Docking Studies Reveal That the Functional Switch of CYFIP1 is Mediated by a Butterfly-like Motion. J Chem Theory Comput *11*, 3401-3410.

Domínguez-Iturza, N., Lo, A.C., Shah, D., Armendáriz, M., Vannelli, A., Mercaldo, V., Trusel, M., Li, K.W., Gastaldo, D., Santos, A.R., *et al.* (2019). The autism- and schizophrenia-associated protein CYFIP1 regulates bilateral brain connectivity and behaviour. Nature Communications *10*, 3454.

Edden, R.A., Crocetti, D., Zhu, H., Gilbert, D.L., and Mostofsky, S.H. (2012). Reduced GABA concentration in attention-deficit/hyperactivity disorder. Arch Gen Psychiatry *69*, 750-753.

Eden, S., Rohatgi, R., Podtelejnikov, A.V., Mann, M., and Kirschner, M.W. (2002). Mechanism of regulation of WAVE1-induced actin nucleation by Rac1 and Nck. Nature *418*, 790-793.

Ejima, A., and Griffith, L.C. (2007). Measurement of Courtship Behavior in Drosophila melanogaster. CSH Protoc *2007*, pdb prot4847.

Foss-Feig, J.H., Adkinson, B.D., Ji, J.L., Yang, G., Srihari, V.H., McPartland, J.C., Krystal, J.H., Murray, J.D., and Anticevic, A. (2017). Searching for Cross-Diagnostic Convergence: Neural Mechanisms Governing Excitation and Inhibition Balance in Schizophrenia and Autism Spectrum Disorders. Biol Psychiatry *81*, 848-861.

Friedman, S.D., Shaw, D.W., Artru, A.A., Richards, T.L., Gardner, J., Dawson, G., Posse, S., and Dager, S.R. (2003). Regional brain chemical alterations in young children with autism spectrum disorder. Neurology *60*, 100-107.

Fryea, E.R.N.K.R. (2011). Autistic disorder with complex IV overactivity: A new mitochondrial syndrome. Journal of Pediatric Neurology *09*, 427-434.

Gallart-Ayala, H., Konz, I., Mehl, F., Teav, T., Oikonomidi, A., Peyratout, G., van der Velpen, V., Popp, J., and Ivanisevic, J. (2018). A global HILIC-MS approach to measure polar human cerebrospinal fluid metabolome: Exploring gender-associated variation in a cohort of elderly cognitively healthy subjects. Analytica Chimica Acta.

Galy, A., Schenck, A., Sahin, H.B., Qurashi, A., Sahel, J.A., Diebold, C., and Giangrande, A. (2011). CYFIP dependent actin remodeling controls specific aspects of Drosophila eye morphogenesis. Dev Biol *359*, 37-46.

Gandal, M.J., Haney, J.R., Parikshak, N.N., Leppa, V., Ramaswami, G., Hartl, C., Schork, A.J., Appadurai, V., Buil, A., Werge, T.M.*, et al.* (2018). Shared molecular neuropathology across major psychiatric disorders parallels polygenic overlap. Science *359*, 693-697.

Garcia, M.J., and Teets, N.M. (2019). Cold stress results in sustained locomotor and behavioral deficits in Drosophila melanogaster. J Exp Zool A Ecol Integr Physiol *331*, 192-200.

Garcia-Cazorla, A., Artuch, R., and Bayes, A. (2018). Synaptic metabolism and brain circuitries in inborn errors of metabolism. J Inherit Metab Dis *41*, 909-910.

Genheden, M., Kenney, J.W., Johnston, H.E., Manousopoulou, A., Garbis, S.D., and Proud, C.G. (2015). BDNF stimulation of protein synthesis in cortical neurons requires the MAP kinase-interacting kinase MNK1. The Journal of neuroscience : the official journal of the Society for Neuroscience *35*, 972-984.

Ghanizadeh, A., Berk, M., Farrashbandi, H., Alavi Shoushtari, A., and Villagonzalo, K.A. (2013). Targeting the mitochondrial electron transport chain in autism, a systematic review and synthesis of a novel therapeutic approach. Mitochondrion *13*, 515-519.

Goldenthal, M.J., Damle, S., Sheth, S., Shah, N., Melvin, J., Jethva, R., Hardison, H., Marks, H., and Legido, A. (2015). Mitochondrial enzyme dysfunction in autism spectrum disorders; a novel biomarker revealed from buccal swab analysis. Biomarkers in medicine *9*, 957-965.

Griffiths, K.K., and Levy, R.J. (2017). Evidence of Mitochondrial Dysfunction in Autism: Biochemical Links, Genetic-Based Associations, and Non-Energy-Related Mechanisms. Oxidative medicine and cellular longevity *2017*, 4314025.

Han, S., Tai, C., Jones, C.J., Scheuer, T., and Catterall, W.A. (2014). Enhancement of inhibitory neurotransmission by GABAA receptors having alpha2,3-subunits ameliorates behavioral deficits in a mouse model of autism. Neuron *81*, 1282-1289.

Han, S., Tai, C., Westenbroek, R.E., Yu, F.H., Cheah, C.S., Potter, G.B., Rubenstein, J.L., Scheuer, T., de la Iglesia, H.O., and Catterall, W.A. (2012).

Autistic-like behaviour in Scn1a+/- mice and rescue by enhanced GABA-mediated neurotransmission. Nature *489*, 385-390.
Hollis, F., Kanellopoulos, A.K., and Bagni, C. (2017). Mitochondrial dysfunction in Autism Spectrum Disorder: clinical features and perspectives. Current opinion in neurobiology *45*, 178-187.
Homberg, U., and Muller, M. (2016). Ultrastructure of GABA- and Tachykinin-Immunoreactive Neurons in the Lower Division of the Central Body of the Desert Locust. Front Behav Neurosci *10*, 230.
Hsiao, K., Harony-Nicolas, H., Buxbaum, J.D., Bozdagi-Gunal, O., and Benson, D.L. (2016). Cyfip1 Regulates Presynaptic Activity during Development. The Journal of neuroscience : the official journal of the Society for Neuroscience *36*, 1564-1576.
Hsu, C.T., and Bhandawat, V. (2016). Organization of descending neurons in Drosophila melanogaster. Sci Rep *6*, 20259.
Hu, Y., Flockhart, I., Vinayagam, A., Bergwitz, C., Berger, B., Perrimon, N., and Mohr, S.E. (2011). An integrative approach to ortholog prediction for disease-focused and other functional studies. BMC Bioinformatics *12*, 357.
Kanellopoulos, A.K., Semelidou, O., Kotini, A.G., Anezaki, M., and Skoulakis, E.M. (2012). Learning and memory deficits consequent to reduction of the fragile X mental retardation protein result from metabotropic glutamate receptor-mediated inhibition of cAMP signaling in Drosophila. The Journal of neuroscience : the official journal of the Society for Neuroscience *32*, 13111-13124.
Kann, O., and Kovacs, R. (2007). Mitochondria and neuronal activity. American journal of physiology Cell physiology *292*, C641-657.
Khacho, M., and Slack, R.S. (2018). Mitochondrial dynamics in the regulation of neurogenesis: From development to the adult brain. Dev Dyn *247*, 47-53.
Koganezawa, M., Kimura, K., and Yamamoto, D. (2016). The Neural Circuitry that Functions as a Switch for Courtship versus Aggression in Drosophila Males. Curr Biol *26*, 1395-1403.
Kolodziejczyk, A., Sun, X., Meinertzhagen, I.A., and Nassel, D.R. (2008). Glutamate, GABA and acetylcholine signaling components in the lamina of the Drosophila visual system. PloS one *3*, e2110.
Konradi, C., and Ongur, D. (2017). Role of mitochondria and energy metabolism in schizophrenia and psychotic disorders. Schizophrenia research.
Kosmidis, S., Botella, J.A., Mandilaras, K., Schneuwly, S., Skoulakis, E.M., Rouault, T.A., and Missirlis, F. (2011). Ferritin overexpression in Drosophila glia leads to iron deposition in the optic lobes and late-onset behavioral defects. Neurobiol Dis *43*, 213-219.
Krumschnabel, G., Fontana-Ayoub, M., Sumbalova, Z., Heidler, J., Gauper, K., Fasching, M., and Gnaiger, E. (2015). Simultaneous high-resolution measurement of mitochondrial respiration and hydrogen peroxide production. Methods Mol Biol *1264*, 245-261.
Kuo, H.Y., and Liu, F.C. (2019). Synaptic Wiring of Corticostriatal Circuits in Basal Ganglia: Insights into the Pathogenesis of Neuropsychiatric Disorders. eNeuro *6*.
Leblond, C.S., Heinrich, J., Delorme, R., Proepper, C., Betancur, C., Huguet, G., Konyukh, M., Chaste, P., Ey, E., Rastam, M.*, et al.* (2012). Genetic and functional analyses of SHANK2 mutations suggest a multiple hit model of autism spectrum disorders. PLoS Genet *8*, e1002521.
Lee, D., Su, H., and O'Dowd, D.K. (2003). GABA receptors containing Rdl subunits mediate fast inhibitory synaptic transmission in Drosophila neurons. The Journal of neuroscience : the official journal of the Society for Neuroscience *23*, 4625-4634.

Legido, A., Jethva, R., and Goldenthal, M.J. (2013). Mitochondrial dysfunction in autism. Semin Pediatr Neurol *20*, 163-175.

Lepagnol-Bestel, A.M., Maussion, G., Boda, B., Cardona, A., Iwayama, Y., Delezoide, A.L., Moalic, J.M., Muller, D., Dean, B., Yoshikawa, T.*, et al.* (2008). SLC25A12 expression is associated with neurite outgrowth and is upregulated in the prefrontal cortex of autistic subjects. Molecular psychiatry *13*, 385-397.

Li, Z., Okamoto, K., Hayashi, Y., and Sheng, M. (2004). The importance of dendritic mitochondria in the morphogenesis and plasticity of spines and synapses. Cell *119*, 873-887.

Liu, X., and Davis, R.L. (2009). The GABAergic anterior paired lateral neuron suppresses and is suppressed by olfactory learning. Nat Neurosci *12*, 53-59.

Maguire, S.E., Rhoades, S., Chen, W.F., Sengupta, A., Yue, Z., Lim, J.C., Mitchell, C.H., Weljie, A.M., and Sehgal, A. (2015). Independent Effects of gamma-Aminobutyric Acid Transaminase (GABAT) on Metabolic and Sleep Homeostasis. J Biol Chem *290*, 20407-20416.

Marland, J.R., Hasel, P., Bonnycastle, K., and Cousin, M.A. (2016). Mitochondrial Calcium Uptake Modulates Synaptic Vesicle Endocytosis in Central Nerve Terminals. J Biol Chem *291*, 2080-2086.

Masuda-Nakagawa, L.M., Ito, K., Awasaki, T., and O'Kane, C.J. (2014). A single GABAergic neuron mediates feedback of odor-evoked signals in the mushroom body of larval Drosophila. Frontiers in neural circuits *8*, 35.

McGuire, S.E., Le, P.T., Osborn, A.J., Matsumoto, K., and Davis, R.L. (2003). Spatiotemporal rescue of memory dysfunction in Drosophila. Science *302*, 1765-1768.

McGuire, S.E., Mao, Z., and Davis, R.L. (2004). Spatiotemporal gene expression targeting with the TARGET and gene-switch systems in Drosophila. Science's STKE : signal transduction knowledge environment *2004*, pl6.

Mergenthaler, P., Lindauer, U., Dienel, G.A., and Meisel, A. (2013). Sugar for the brain: the role of glucose in physiological and pathological brain function. Trends Neurosci *36*, 587-597.

Michaeli, S., Fait, A., Lagor, K., Nunes-Nesi, A., Grillich, N., Yellin, A., Bar, D., Khan, M., Fernie, A.R., Turano, F.J.*, et al.* (2011). A mitochondrial GABA permease connects the GABA shunt and the TCA cycle, and is essential for normal carbon metabolism. Plant J *67*, 485-498.

Midani, F.S., Wynn, M.L., and Schnell, S. (2017). The importance of accurately correcting for the natural abundance of stable isotopes. Analytical biochemistry *520*, 27-43.

Mitchell, J.A., Aronson, A.R., Mork, J.G., Folk, L.C., Humphrey, S.M., and Ward, J.M. (2003). Gene indexing: characterization and analysis of NLM's GeneRIFs. AMIA Annu Symp Proc, 460-464.

Morais, V.A., Verstreken, P., Roethig, A., Smet, J., Snellinx, A., Vanbrabant, M., Haddad, D., Frezza, C., Mandemakers, W., Vogt-Weisenhorn, D.*, et al.* (2009). Parkinson's disease mutations in PINK1 result in decreased Complex I activity and deficient synaptic function. EMBO Mol Med *1*, 99-111.

Mukherjee, A., Carvalho, F., Eliez, S., and Caroni, P. (2019). Long-Lasting Rescue of Network and Cognitive Dysfunction in a Genetic Schizophrenia Model. Cell *178*, 1387-1402 e1314.

Napoli, I., Mercaldo, V., Boyl, P.P., Eleuteri, B., Zalfa, F., De Rubeis, S., Di Marino, D., Mohr, E., Massimi, M., Falconi, M.*, et al.* (2008). The fragile X syndrome protein represses activity-dependent translation through CYFIP1, a new 4E-BP. Cell *134*, 1042-1054.

Napolioni, V., Persico, A.M., Porcelli, V., and Palmieri, L. (2011). The mitochondrial aspartate/glutamate carrier AGC1 and calcium homeostasis: physiological links and abnormalities in autism. Mol Neurobiol *44*, 83-92.

Nebel, R.A., Zhao, D., Pedrosa, E., Kirschen, J., Lachman, H.M., Zheng, D., and Abrahams, B.S. (2016). Reduced CYFIP1 in Human Neural Progenitors Results in Dysregulation of Schizophrenia and Epilepsy Gene Networks. PloS one *11*, e0148039.

Nevado, J., Mergener, R., Palomares-Bralo, M., Souza, K.R., Vallespin, E., Mena, R., Martinez-Glez, V., Mori, M.A., Santos, F., Garcia-Minaur, S.*, et al.* (2014). New microdeletion and microduplication syndromes: A comprehensive review. Genet Mol Biol *37*, 210-219.

Oguro-Ando, A., Rosensweig, C., Herman, E., Nishimura, Y., Werling, D., Bill, B.R., Berg, J.M., Gao, F., Coppola, G., Abrahams, B.S.*, et al.* (2015). Increased CYFIP1 dosage alters cellular and dendritic morphology and dysregulates mTOR. Molecular psychiatry *20*, 1069-1078.

Orefice, L.L., Zimmerman, A.L., Chirila, A.M., Sleboda, S.J., Head, J.P., and Ginty, D.D. (2016). Peripheral Mechanosensory Neuron Dysfunction Underlies Tactile and Behavioral Deficits in Mouse Models of ASDs. Cell *166*, 299-313.

Palmieri, F. (2013). The mitochondrial transporter family SLC25: identification, properties and physiopathology. Mol Aspects Med *34*, 465-484.

Panja, D., Kenney, J.W., D'Andrea, L., Zalfa, F., Vedeler, A., Wibrand, K., Fukunaga, R., Bagni, C., Proud, C.G., and Bramham, C.R. (2014). Two-stage translational control of dentate gyrus LTP consolidation is mediated by sustained BDNF-TrkB signaling to MNK. Cell Rep *9*, 1430-1445.

Pardo, B., Contreras, L., and Satrustegui, J. (2013). De novo Synthesis of Glial Glutamate and Glutamine in Young Mice Requires Aspartate Provided by the Neuronal Mitochondrial Aspartate-Glutamate Carrier Aralar/AGC1. Front Endocrinol (Lausanne) *4*, 149.

Pathania, M., Davenport, E.C., Muir, J., Sheehan, D.F., Lopez-Domenech, G., and Kittler, J.T. (2014). The autism and schizophrenia associated gene CYFIP1 is critical for the maintenance of dendritic complexity and the stabilization of mature spines. Translational psychiatry *4*, e374.

Patowary, A., Nesbitt, R., Archer, M., Bernier, R., and Brkanac, Z. (2017). Next Generation Sequencing Mitochondrial DNA Analysis in Autism Spectrum Disorder. Autism research : official journal of the International Society for Autism Research.

Pech, U., Dipt, S., Barth, J., Singh, P., Jauch, M., Thum, A.S., Fiala, A., and Riemensperger, T. (2013). Mushroom body miscellanea: transgenic Drosophila strains expressing anatomical and physiological sensor proteins in Kenyon cells. Frontiers in neural circuits *7*, 147.

Pech, U., Revelo, N.H., Seitz, K.J., Rizzoli, S.O., and Fiala, A. (2015). Optical dissection of experience-dependent pre- and postsynaptic plasticity in the Drosophila brain. Cell Rep *10*, 2083-2095.

Perry, S.W., Norman, J.P., Barbieri, J., Brown, E.B., and Gelbard, H.A. (2011). Mitochondrial membrane potential probes and the proton gradient: a practical usage guide. Biotechniques *50*, 98-115.

Picard, M. (2015). Mitochondrial synapses: intracellular communication and signal integration. Trends Neurosci *38*, 468-474.

Raefsky, S.M., and Mattson, M.P. (2017). Adaptive responses of neuronal mitochondria to bioenergetic challenges: Roles in neuroplasticity and disease resistance. Free Radic Biol Med *102*, 203-216.

Reichardt, J., and Bornholdt, S. (2006). Statistical mechanics of community detection. Phys Rev E Stat Nonlin Soft Matter Phys *74*, 016110.

Reynolds, M.F., Sisk, E.C., and Rasgon, N.L. (2007). Valproate and neuroendocrine changes in relation to women treated for epilepsy and bipolar disorder: a review. Current medicinal chemistry *14*, 2799-2812.

Robinson, J.E., and Gradinaru, V. (2018). Dopaminergic dysfunction in neurodevelopmental disorders: recent advances and synergistic technologies to aid basic research. Current opinion in neurobiology *48*, 17-29.

Roci, I., Gallart-Ayala, H., Schmidt, A., Watrous, J., Jain, M., Wheelock, C.E., and Nilsson, R. (2016). Metabolite Profiling and Stable Isotope Tracing in Sorted Subpopulations of Mammalian Cells. Analytical chemistry *88*, 2707-2713.

Rosenfeld, M., Brenner-Lavie, H., Ari, S.G., Kavushansky, A., and Ben-Shachar, D. (2011). Perturbation in mitochondrial network dynamics and in complex I dependent cellular respiration in schizophrenia. Biol Psychiatry *69*, 980-988.

Rossignol, D.A., and Frye, R.E. (2012). Mitochondrial dysfunction in autism spectrum disorders: a systematic review and meta-analysis. Molecular psychiatry *17*, 290-314.

Sakurai, T., Ramoz, N., Barreto, M., Gazdoiu, M., Takahashi, N., Gertner, M., Dorr, N., Gama Sosa, M.A., De Gasperi, R., Perez, G.*, et al.* (2010). Slc25a12 disruption alters myelination and neurofilaments: a model for a hypomyelination syndrome and childhood neurodevelopmental disorders. Biol Psychiatry *67*, 887-894.

Salwinski, L., Miller, C.S., Smith, A.J., Pettit, F.K., Bowie, J.U., and Eisenberg, D. (2004). The Database of Interacting Proteins: 2004 update. Nucleic Acids Res *32*, D449-451.

Schenck, A., Bardoni, B., Langmann, C., Harden, N., Mandel, J.L., and Giangrande, A. (2003). CYFIP/Sra-1 controls neuronal connectivity in Drosophila and links the Rac1 GTPase pathway to the fragile X protein. Neuron *38*, 887-898.

Schriml, L.M., Arze, C., Nadendla, S., Chang, Y.W., Mazaitis, M., Felix, V., Feng, G., and Kibbe, W.A. (2012). Disease Ontology: a backbone for disease semantic integration. Nucleic Acids Res *40*, D940-946.

Schwarz, T.L. (2013). Mitochondrial trafficking in neurons. Cold Spring Harb Perspect Biol *5*.

Schwede, M., Nagpal, S., Gandal, M.J., Parikshak, N.N., Mirnics, K., Geschwind, D.H., and Morrow, E.M. (2018). Strong correlation of downregulated genes related to synaptic transmission and mitochondria in post-mortem autism cerebral cortex. J Neurodev Disord *10*, 18.

Selimbeyoglu, A., Kim, C.K., Inoue, M., Lee, S.Y., Hong, A.S.O., Kauvar, I., Ramakrishnan, C., Fenno, L.E., Davidson, T.J., Wright, M.*, et al.* (2017). Modulation of prefrontal cortex excitation/inhibition balance rescues social behavior in CNTNAP2-deficient mice. Sci Transl Med *9*.

Siegel, R.W., and Hall, J.C. (1979). Conditioned responses in courtship behavior of normal and mutant Drosophila. Proc Natl Acad Sci U S A *76*, 3430-3434.

Silva, A.I., Haddon, J.E., Ahmed Syed, Y., Trent, S., Lin, T.-C.E., Patel, Y., Carter, J., Haan, N., Honey, R.C., Humby, T.*, et al.* (2019). Cyfip1 haploinsufficient rats show white matter changes, myelin thinning, abnormal oligodendrocytes and behavioural inflexibility. Nature Communications *10*, 3455.

Simon, A.F., Chou, M.T., Salazar, E.D., Nicholson, T., Saini, N., Metchev, S., and Krantz, D.E. (2012). A simple assay to study social behavior in Drosophila: measurement of social space within a group. Genes Brain Behav *11*, 243-252.

Sohal, V.S., and Rubenstein, J.L.R. (2019). Excitation-inhibition balance as a framework for investigating mechanisms in neuropsychiatric disorders. Molecular psychiatry.

Sokolowski, M.B. (2001). Drosophila: genetics meets behaviour. Nat Rev Genet *2*, 879-890.

Sokolowski, M.B. (2010). Social interactions in "simple" model systems. Neuron *65*, 780-794.

Son, G., and Han, J. (2018). Roles of mitochondria in neuronal development. BMB Rep *51*, 549-556.

Spinazzi, M., Casarin, A., Pertegato, V., Salviati, L., and Angelini, C. (2012). Assessment of mitochondrial respiratory chain enzymatic activities on tissues and cultured cells. Nat Protoc *7*, 1235-1246.

Stathopoulos, S., Gaujoux, R., and O'Ryan, C. (2018). Genome-wide DNA methylation patterns in Autism Spectrum Disorder and mitochondrial function. bioRxiv.

Stefansson, H., Meyer-Lindenberg, A., Steinberg, S., Magnusdottir, B., Morgen, K., Arnarsdottir, S., Bjornsdottir, G., Walters, G.B., Jonsdottir, G.A., Doyle, O.M.*, et al.* (2014). CNVs conferring risk of autism or schizophrenia affect cognition in controls. Nature *505*, 361-366.

Stradal, T.E., and Scita, G. (2006). Protein complexes regulating Arp2/3-mediated actin assembly. Curr Opin Cell Biol *18*, 4-10.

Sun, J., Xu, A.Q., Giraud, J., Poppinga, H., Riemensperger, T., Fiala, A., and Birman, S. (2018). Neural Control of Startle-Induced Locomotion by the Mushroom Bodies and Associated Neurons in Drosophila. Front Syst Neurosci *12*, 6.

Tam, G.W., van de Lagemaat, L.N., Redon, R., Strathdee, K.E., Croning, M.D., Malloy, M.P., Muir, W.J., Pickard, B.S., Deary, I.J., Blackwood, D.H.*, et al.* (2010). Confirmed rare copy number variants implicate novel genes in schizophrenia. Biochem Soc Trans *38*, 445-451.

Tauber, J.M., Vanlandingham, P.A., and Zhang, B. (2011). Elevated levels of the vesicular monoamine transporter and a novel repetitive behavior in the Drosophila model of fragile X syndrome. PloS one *6*, e27100.

Taurines, R., Thome, J., Duvigneau, J.C., Forbes-Robertson, S., Yang, L., Klampfl, K., Romanos, J., Muller, S., Gerlach, M., and Mehler-Wex, C. (2010). Expression analyses of the mitochondrial complex I 75-kDa subunit in early onset schizophrenia and autism spectrum disorder: increased levels as a potential biomarker for early onset schizophrenia. Eur Child Adolesc Psychiatry *19*, 441-448.

Tochitani, S., and Kondo, S. (2013). Immunoreactivity for GABA, GAD65, GAD67 and Bestrophin-1 in the meninges and the choroid plexus: implications for non-neuronal sources for GABA in the developing mouse brain. PloS one *8*, e56901.

Toker, L., and Agam, G. (2015). Mitochondrial dysfunction in psychiatric morbidity: current evidence and therapeutic prospects. Neuropsychiatr Dis Treat *11*, 2441-2447.

Traag, V.A., and Bruggeman, J. (2009). Community detection in networks with positive and negative links. Phys Rev E Stat Nonlin Soft Matter Phys *80*, 036115.

Ugur, B., Bao, H., Stawarski, M., Duraine, L.R., Zuo, Z., Lin, Y.Q., Neely, G.G., Macleod, G.T., Chapman, E.R., and Bellen, H.J. (2017). The Krebs Cycle Enzyme

Isocitrate Dehydrogenase 3A Couples Mitochondrial Metabolism to Synaptic Transmission. Cell Rep *21*, 3794-3806.

Urraca, N., Cleary, J., Brewer, V., Pivnick, E.K., McVicar, K., Thibert, R.L., Schanen, N.C., Esmer, C., Lamport, D., and Reiter, L.T. (2013). The interstitial duplication 15q11.2-q13 syndrome includes autism, mild facial anomalies and a characteristic EEG signature. Autism research : official journal of the International Society for Autism Research *6*, 268-279.

Valenti, D., de Bari, L., De Filippis, B., Henrion-Caude, A., and Vacca, R.A. (2014). Mitochondrial dysfunction as a central actor in intellectual disability-related diseases: an overview of Down syndrome, autism, Fragile X and Rett syndrome. Neurosci Biobehav Rev *46 Pt 2*, 202-217.

Vanlerberghe, C., Petit, F., Malan, V., Vincent-Delorme, C., Bouquillon, S., Boute, O., Holder-Espinasse, M., Delobel, B., Duban, B., Vallee, L.*, et al.* (2015). 15q11.2 microdeletion (BP1-BP2) and developmental delay, behaviour issues, epilepsy and congenital heart disease: a series of 52 patients. Eur J Med Genet *58*, 140-147.

Vilella, A.J., Severin, J., Ureta-Vidal, A., Heng, L., Durbin, R., and Birney, E. (2009). EnsemblCompara GeneTrees: Complete, duplication-aware phylogenetic trees in vertebrates. Genome Res *19*, 327-335.

Vos, M., Lauwers, E., and Verstreken, P. (2010). Synaptic mitochondria in synaptic transmission and organization of vesicle pools in health and disease. Front Synaptic Neurosci *2*, 139.

Wang, J., Tao, Y., Song, F., Sun, Y., Ott, J., and Saffen, D. (2015). Common Regulatory Variants of CYFIP1 Contribute to Susceptibility for Autism Spectrum Disorder (ASD) and Classical Autism. Ann Hum Genet.

Wang, P., Zhao, D., Lachman, H.M., and Zheng, D. (2018). Enriched expression of genes associated with autism spectrum disorders in human inhibitory neurons. Translational psychiatry *8*, 13.

Williams, G.S., Boyman, L., Chikando, A.C., Khairallah, R.J., and Lederer, W.J. (2013). Mitochondrial calcium uptake. Proc Natl Acad Sci U S A *110*, 10479-10486.

Williams, S.G., Nakev, A., Guo, H., Frain, S., Tenin, G., Liakhovitskaia, A., Saha, P., Priest, J.R., Hentges, K.E., and Keavney, B.D. (2019). Large-scale examination of neuropsychiatric, cognitive and cardiovascular phenotypic associations with 15q11.2 BP1-BP2 deletion in ~500,000 UK Biobank individuals. bioRxiv, 722504.

Woo, Y.J., Kanellopoulos, A.K., Hemati, P., Kirschen, J., Nebel, R.A., Wang, T., Bagni, C., and Abrahams, B.S. (2019). Domain-specific cognitive impairments in humans and flies with reduced CYFIP1 dosage. Biological Psychiatry.

Woo, Y.J., Wang, T., Guadalupe, T., Nebel, R.A., Vino, A., Del Bene, V.A., Molholm, S., Ross, L.A., Zwiers, M.P., Fisher, S.E.*, et al.* (2016). A Common CYFIP1 Variant at the 15q11.2 Disease Locus Is Associated with Structural Variation at the Language-Related Left Supramarginal Gyrus. PloS one *11*, e0158036.

Wu, C.L., Shih, M.F., Lai, J.S., Yang, H.T., Turner, G.C., Chen, L., and Chiang, A.S. (2011). Heterotypic gap junctions between two neurons in the drosophila brain are critical for memory. Curr Biol *21*, 848-854.

Yang, M., Bozdagi, O., Scattoni, M.L., Wohr, M., Roullet, F.I., Katz, A.M., Abrams, D.N., Kalikhman, D., Simon, H., Woldeyohannes, L.*, et al.* (2012). Reduced excitatory neurotransmission and mild autism-relevant phenotypes in adolescent Shank3 null mutant mice. The Journal of neuroscience : the official journal of the Society for Neuroscience *32*, 6525-6541.

Yao, C.H., Wang, R., Wang, Y., Kung, C.P., Weber, J.D., and Patti, G.J. (2019). Mitochondrial fusion supports increased oxidative phosphorylation during cell proliferation. Elife *8*.

Yizhar, O., Fenno, L.E., Prigge, M., Schneider, F., Davidson, T.J., O'Shea, D.J., Sohal, V.S., Goshen, I., Finkelstein, J., Paz, J.T.*, et al.* (2011). Neocortical excitation/inhibition balance in information processing and social dysfunction. Nature *477*, 171-178.

Yoon, K.J., Nguyen, H.N., Ursini, G., Zhang, F., Kim, N.S., Wen, Z., Makri, G., Nauen, D., Shin, J.H., Park, Y.*, et al.* (2014). Modeling a genetic risk for schizophrenia in iPSCs and mice reveals neural stem cell deficits associated with adherens junctions and polarity. Cell stem cell *15*, 79-91.

Yoon, W.H., Sandoval, H., Nagarkar-Jaiswal, S., Jaiswal, M., Yamamoto, S., Haelterman, N.A., Putluri, N., Putluri, V., Sreekumar, A., Tos, T.*, et al.* (2017). Loss of Nardilysin, a Mitochondrial Co-chaperone for alpha-Ketoglutarate Dehydrogenase, Promotes mTORC1 Activation and Neurodegeneration. Neuron *93*, 115-131.

Yuan, Q., Song, Y., Yang, C.H., Jan, L.Y., and Jan, Y.N. (2014). Female contact modulates male aggression via a sexually dimorphic GABAergic circuit in Drosophila. Nat Neurosci *17*, 81-88.

Yuen, R., Merico, D., Bookman, M., J, L.H., Thiruvahindrapuram, B., Patel, R.V., Whitney, J., Deflaux, N., Bingham, J., Wang, Z.*, et al.* (2017). Whole genome sequencing resource identifies 18 new candidate genes for autism spectrum disorder. Nat Neurosci *20*, 602-611.

Zars, T., Fischer, M., Schulz, R., and Heisenberg, M. (2000). Localization of a short-term memory in Drosophila. Science *288*, 672-675.

Zhang, H., Tan, J., Reynolds, E., Kuebler, D., Faulhaber, S., and Tanouye, M. (2002). The Drosophila slamdance gene: a mutation in an aminopeptidase can cause seizure, paralysis and neuronal failure. Genetics *162*, 1283-1299.

Zhao, Q., Li, T., Zhao, X., Huang, K., Wang, T., Li, Z., Ji, J., Zeng, Z., Zhang, Z., Li, K.*, et al.* (2013). Rare CNVs and tag SNPs at 15q11.2 are associated with schizophrenia in the Han Chinese population. Schizophr Bull *39*, 712-719.

Zoghbi, H.Y., and Bear, M.F. (2012). Synaptic dysfunction in neurodevelopmental disorders associated with autism and intellectual disabilities. Cold Spring Harb Perspect Biol *4*.

Zorova, L.D., Popkov, V.A., Plotnikov, E.Y., Silachev, D.N., Pevzner, I.B., Jankauskas, S.S., Babenko, V.A., Zorov, S.D., Balakireva, A.V., Juhaszova, M.*, et al.* (2018). Mitochondrial membrane potential. Anal Biochem *552*, 50-59.

Zwarts, L., Magwire, M.M., Carbone, M.A., Versteven, M., Herteleer, L., Anholt, R.R., Callaerts, P., and Mackay, T.F. (2011). Complex genetic architecture of Drosophila aggressive behavior. Proc Natl Acad Sci U S A *108*, 17070-17075.

FIGURE LEGENDS

Figure 1. Deficits in social behavior in flies harboring the *Cyfip* haploinsufficiency. (A) Control (*w1118*), *Cyfip*$^{85.1}$/+, TM3/+ and *Cyfip*$^{85.1}$/TM3 flies were analyzed for total number of social interactions in a competition for food assay. n > 20 groups of 8 flies each or (B) in a courtship assay. n > 20 flies. (C) Grooming behavior. The percentage of time spent grooming was monitored over a period of 3 minutes in control and *Cyfip*$^{85.1}$/+ flies. n = 10-12 individual flies for each genotype. (D) Social space behavior. Left, representative images of an open field assay. Red circles indicate flies staying close together. Middle, quantification of the distance of a fly to its closest neighbor in control and *Cyfip*$^{85.1}$/+ flies. n = 8 groups of 30 flies for each genotype. Right, *Cyfip*$^{85.1}$/+ flies keep longer distance from the wall of an open arena. n = 8 replicates of 30 flies for each genotype. For all paradigms data are shown with box and whisker plots where the line inside the box indicates the median, ****$p < 0.0001$, ***$p < 0.001$, **$p < 0.01$, Mann–Whitney test.

Figure 2. *Cyfip* haploinsufficiency proteome revealed maladaptive mitochondrial function and energy production. (A) Clustering of the Fly CYFIP PPI network. The Modularity-based Potts and simulated annealing algorithms available in R. were used. GO "mitochondrion" related genes are shown in peach, "cytoskeleton" related genes in navy-blue, and "synaptic vesicle" related genes in orange. Enriched clustered, using the Hypergeometric test corrected for using a permutation study, for "mitochondrion", "cytoskeleton" and "synaptic vesicle" related GO terms are also highlighted. Community 3, $p = 2.4 \times 10^{-6}$, permutated p = 0% and Community 18, p = 0.0194816, permutated p = 0.92375%. (B) Gene ontology cellular component analysis and (C) Gene ontology biological functions analysis of *Cyfip*$^{85.1}$/+ flies compared to controls. Enrichment values were calculated using the Topology-based Elimination Fisher method. (D) Disease enrichment values for the deregulated genes of *Cyfip*$^{85.1}$/+ flies compared to controls using combined OMIM/geneRIF/Ensembl variation annotation data. Enrichment values were calculated using the Topology-based Elimination Fisher method; N = number of disease genes found in the dataset; p-values making use of the full HDO ontology tree (6331 terms).

Figure 3. Increased brain mitochondrial activity, membrane potential and size in *Cyfip* haploinsufficient flies. (A) A representative graph of high-resolution respirometry experiment in control and *Cyfip*$^{85.1}$/+ fly brains. The blue line represents the oxygen concentration and the red line the oxygen consumption flux. (B) Quantification of the oxygen consumption normalized per unit (1 unit corresponding to 1 brain) of control and *Cyfip*$^{85.1}$/+. n ≥ 6 independent experiments per genotype (each with 10 fly brains), mean ± s.e.m. **p < 0.01, multiple *t* test, corrected for multiple comparisons using the Sidak-Bonferroni method. (C) Same as in (B) of *Cyfip*$^{85.1}$/+ fly bodies (no heads). Normalization by protein concentration mg. n ≥ 7 independent experiments per genotype, mean ± s.e.m. ns, not significant, multiple *t*-test, corrected for multiple comparisons using the Sidak-Bonferroni method. (D) Measurement of the mitochondrial membrane potential. Left, representative Z projections of confocal images of fly brains stained with TMRE. The antenna lobes (AL) area was quantified. The antenna lobes (AL) area was quantified (highlighted with a red circle). Right, quantification of the TMRE staining from control and *Cyfip*$^{85.1}$/+. Shown is the fold change in TMRE fluorescence intensity from the AL area. n = 15-16 brains per genotype, mean ± s.e.m., **p < 0.01, Mann–Whitney test. (E) Mitochondrial DNA copy number measured in control and *Cyfip*$^{85.1}$/+ fly brains relative to nuclear DNA. n = 4 (groups of 10 fly brains), mean ± s.e.m, ns, not significant, Mann-Whitney test. (F) Left, representative EM images of mitochondria from control and *Cyfip*$^{85.1}$/+ fly brains. Right panel, quantification of the mitochondria perimeter and area. n = 160-165 mitochondria per genotype, mean ± s.e.m. ****p < 0.0001, Mann–Whitney test.

Figure 4. Altered TCA cycle and metabolism in *Cyfip* haploinsufficient flies. (A) Simplified representation of TCA cycle and metabolites measured in fly brains. (B) Quantification of metabolites from the TCA cycle in *Cyfip*$^{85.1}$/+ brains normalized to control. n = 5 (groups of 10 fly brains), mean ± s.e.m. ***p < 0.001, **p < 0.01, *p < 0.05, Kruskal-Wallis test, Dunn's multiple comparison test. (C) Enzymatic activity of IDH-NAD dependent from *Cyfip*$^{85.1}$/+ brains normalized to control. n = 3-4 (group of 10 fly brains), mean ± s.e.m. **p < 0.01, Mann-Whitney test. (D) same as in (C) for αKG enzymatic activity. n = 3-4 (groups of 10 fly brains), mean ± s.e.m. *p < 0.05, Mann-Whitney test. (E) Relative levels of NAD total and (F) NADH of fly brains from control and *Cyfip*$^{85.1}$/+. n = 4 (groups of 10 fly brains), mean ± s.e.m. *p < 0.05, Mann-Whitney test. (G) Contribution of [U-$^{13}C_6$]glucose to TCA-cycle metabolites in

Drosophila brain tissue following 6 hours feeding with [^{13}C]glucose. The x-axis denotes the ^{13}C-isotopologue profile (i.e. the mass isotopologue distribution - MID) of labeled metabolites following the incorporation of [^{13}C] glucose skeleton. The catabolism of ^{13}C labeled glucose leads to M+3 pyruvate. The decarboxylation of pyruvate makes M+2 acetyl-CoA in the mitochondria, which is then incorporated into M+2 citrate. All TCA cycle intermediates, downstream of citrate, will have a mass of M+2. Values shown are mean ± sem. n = 5 (10 brains were pooled per each sample). ***p < 0.001, **p < 0.01, *p < 0.05, Sidak's multiple comparisons test.

Figure 5. TCA cycle and mitochondrial complex I inhibition restores social deficits in *Cyfip* mutant flies.

(A) Social behavior of *Cyfip*$^{85.1}$*/+* upon genetic reduction of *idh3a,* n > 10 groups of 8 flies for each genotype were analyzed, ***p < 0.001, **p < 0.01, Kruskal-Wallis test, Dunn's multiple comparison test. (B) Social behavior upon treatment with 5 μM of ML309 for 1 (1d) or 3 days (3d) of *Cyfip*$^{85.1}$*/+* flies and (C) upon pan-neuronal IDH overexpression (29^{o}C) in adults. n > 10 groups of 8 flies for each genotype, **p < 0.01, ****p < 0.0001, ***p < 0.001, Kruskal-Wallis test, Dunn's multiple comparison test. (D) Quantification of the oxygen consumption normalized per unit upon treatment with 5 μM of ML309 for 3 days (3d) of control and *Cyfip*$^{85.1}$*/+*. n ≥ 4 independent experiments per genotype (each with 10 fly brains), mean ± s.e.m. *p < 0.05, multiple *t* test, corrected for multiple comparisons using the Sidak-Bonferroni method. (E) Competition for food upon feeding with 10 μM rotenone for 1 (1d), 2 (2d) and 4 days (4d) in *Cyfip*$^{85.1}$*/+* flies and (F) upon genetic reduction of *pink1* or *ndufs3,* n > 10 groups of 8 flies for each genotype were analyzed, ****p < 0.0001, Kruskal-Wallis test, Dunn's multiple comparison test.

Figure 6. Social deficits in *Cyfip*$^{85.1}$*/+* flies are due to defects in GABA signalling.

(A) Abrogation of *Cyfip* in cholinergic, (B) GABAergic neurons and (C) in subsets of interneurons in the anterior paired lateral neurons (APLGal4), antenna lobe interneurons (LN1Gal4, LN2Gal4), and the dorsal paired medial neurons (DPMGal4). Flies were analyzed for total number of social interactions in a food competition assay. n = 14 groups of 8 flies per genotype, ****p < 0.0001, ***p < 0.001, **p < 0.01, Kruskal-Wallis test, Dunn's multiple comparison test. **(**D) Left, representative Z projections of confocal images of control and *Cyfip*$^{85.1}$*/+* and *Cyfip*$^{85.1}$*/+* fed flies for 5 days (5d) with

50 µM GABA and stained with α-GABA. Right, data quantification (n = 15 brains). Scale bars, 100 µm. ****p < 0.0001, Kruskal-Wallis test, Dunn's multiple comparison test. (E) Expression of syp-pHTomato in GABAergic neurons to measure synaptic release. (F) Dynamics and maximal change of monitored syp-pHTomato fluorescence in GABAergic neurons of control and *Cyfip*$^{85.1}$*/+* flies. n = 10 flies. All traces indicate mean ± s.e.m. The scale bars represent 20 µm; *p < 0.05; two-sample t test. (G) GABA levels determined by HILIC-MS/MS in control and *Cyfip*$^{85.1}$*/+* brains. n = 5 (groups of 10 brains) per genotype, mean ± s.e.m, ns, not significant, Mann-Whitney test. (H) Analysis of GABA levels from control and *Cyfip*$^{85.1}$*/+,* into enriched fractions of mitochondria and vesicles by ELISA. n > 3, mean ± s.e.m. **p < 0.01, Kruskal-Wallis test, Dunn's multiple comparison test. (I) Competition for food of *Cyfip*$^{85.1}$*/+* flies upon treatment (2-5 days) with 50 µM GABA, n > 10 groups of 8 flies, ****p < 0.0001, ***p < 0.001, **p < 0.01, Kruskal-Wallis test, Dunn's multiple comparison test.

Figure 7. Aralar is a novel mitochondrial GABA transporter. (A) Genetic screening for changes in competition for food behavior. Flies mutant for mitochondrial carriers were crossed with *Cyfip*$^{85.1}$*/+* mutant flies, tested and compared to control and *Cyfip*$^{85.1}$*/+* flies. Threshold line indicates the control levels of behavior. # shows the genotype that is significantly different from *Cyfip*$^{85.1}$*/+* and not different from the control. mean ± s.e.m, n > 10 groups of 8 flies, Kruskal-Wallis test, Dunn's multiple comparison test. (B) Competition for food, (C) grooming behavior and (D) social space behavior in control, *Cyfip*$^{85.1}$/+ and *Aralar*^{MI07552}*/Cyfip*$^{85.1}$ flies. n > 8 independent experiments with groups of 8 and 30 flies in (B) and (D), respectively. All comparisons refer to the control. ***p < 0.001, **p < 0.01, *p < 0.05, Kruskal-Wallis test, Dunn's multiple comparison test. (E) Analysis of GABA levels by ELISA in cytosolic and mitochondrial fractions from control, *Cyfip*$^{85.1}$*/+, Aralar*^{MI07552}*/+* and *Aralar*^{MI07552}*/Cyfip*$^{85.1}$ flies. n > 3, mean ± s.e.m. **p < 0.01, *p < 0.05, Kruskal-Wallis test, Dunn's multiple comparison test. (F) Upon treatment with 500 µM oligomycin, mitochondrial membrane potential was analyzed by staining using TMRE, n = 8-9 brains. (G) Competition for food of control flies upon treatment (1 day) with 500 µM of oligomycin, n = 10 groups of 8 flies each. (H) GABA levels measured by ELISA in fractionated mitochondria. n = 5, mean ± s.e.m., ***p < 0.001, *p < 0.05, Kruskal-Wallis test.

Figure 8. Model. Aralar drives GABA uptake into polarized mitochondria. When *Cyfip* level is reduced, the TCA cycle produces increased levels of succinate and NADH leading to higher mitochondrial activity that next leads to hyperpolarization of mitochondria. As a consequence, the increased polarization activates the GABA carrier Aralar driving GABA into mitochondria. The excessive unidirectional GABA transport into the mitochondria reduces its homeostatic levels required for proper synapse functioning and behavior.

Figure 1

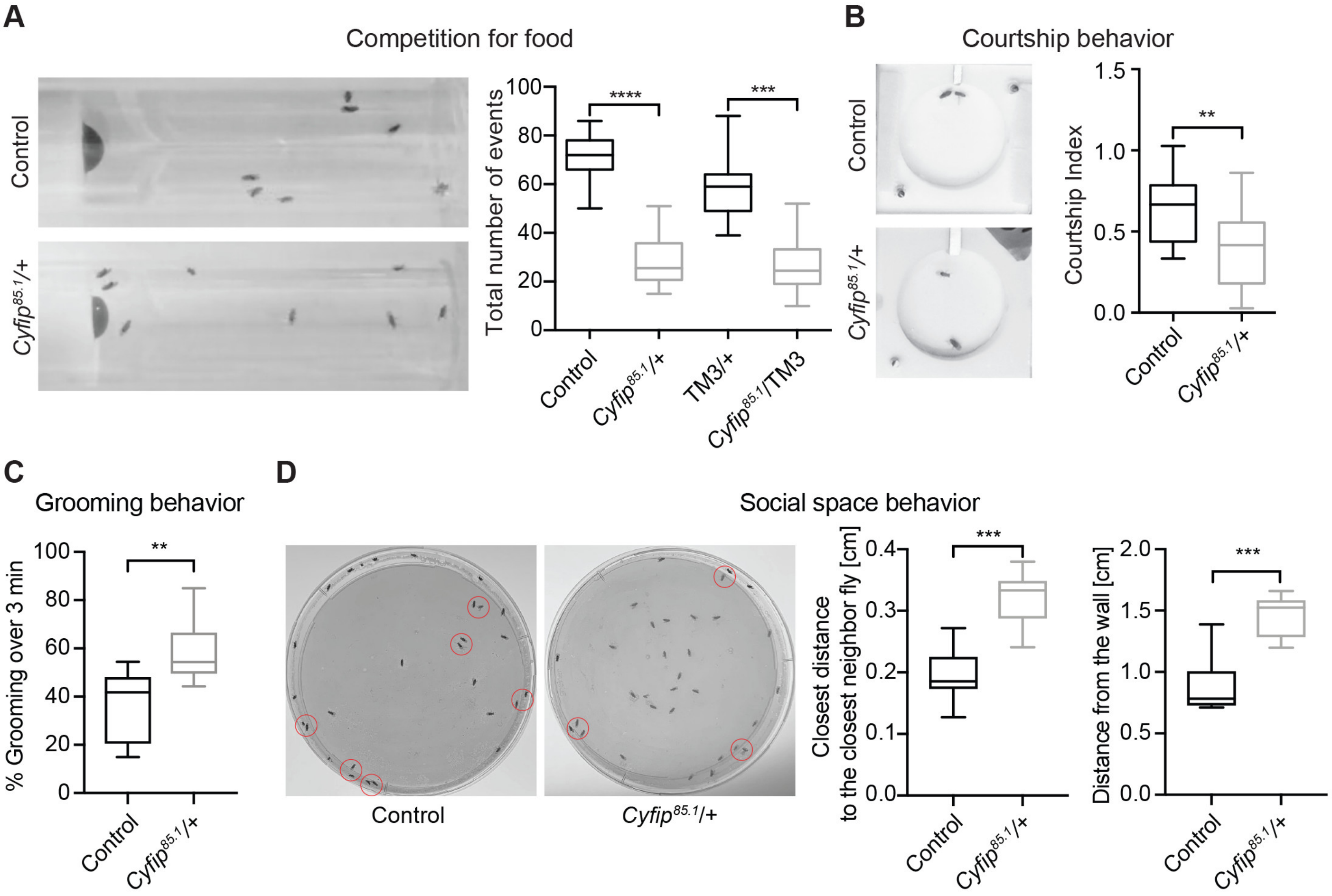
A
Competition for food
Control
Cyfip85.1/+
Total number of events
100
80
60
40
20
0
****
***
Control
Cyfip85.1/+
TM3/+
Cyfip85.1/TM3
B
Courtship behavior
Control
Cyfip85.1/+
Courtship Index
1.5
1.0
0.5
0.0
**
Control
Cyfip85.1/+
C
Grooming behavior
% Grooming over 3 min
100
80
60
40
20
0
**
Control
Cyfip85.1/+
D
Social space behavior
Control
Cyfip85.1/+
Closest distance to the closest neighbor fly [cm]
0.4
0.3
0.2
0.1
0.0
***
Control
Cyfip85.1/+
Distance from the wall [cm]
2.0
1.5
1.0
0.5
0.0
***
Control
Cyfip85.1/+

Figure 2

A

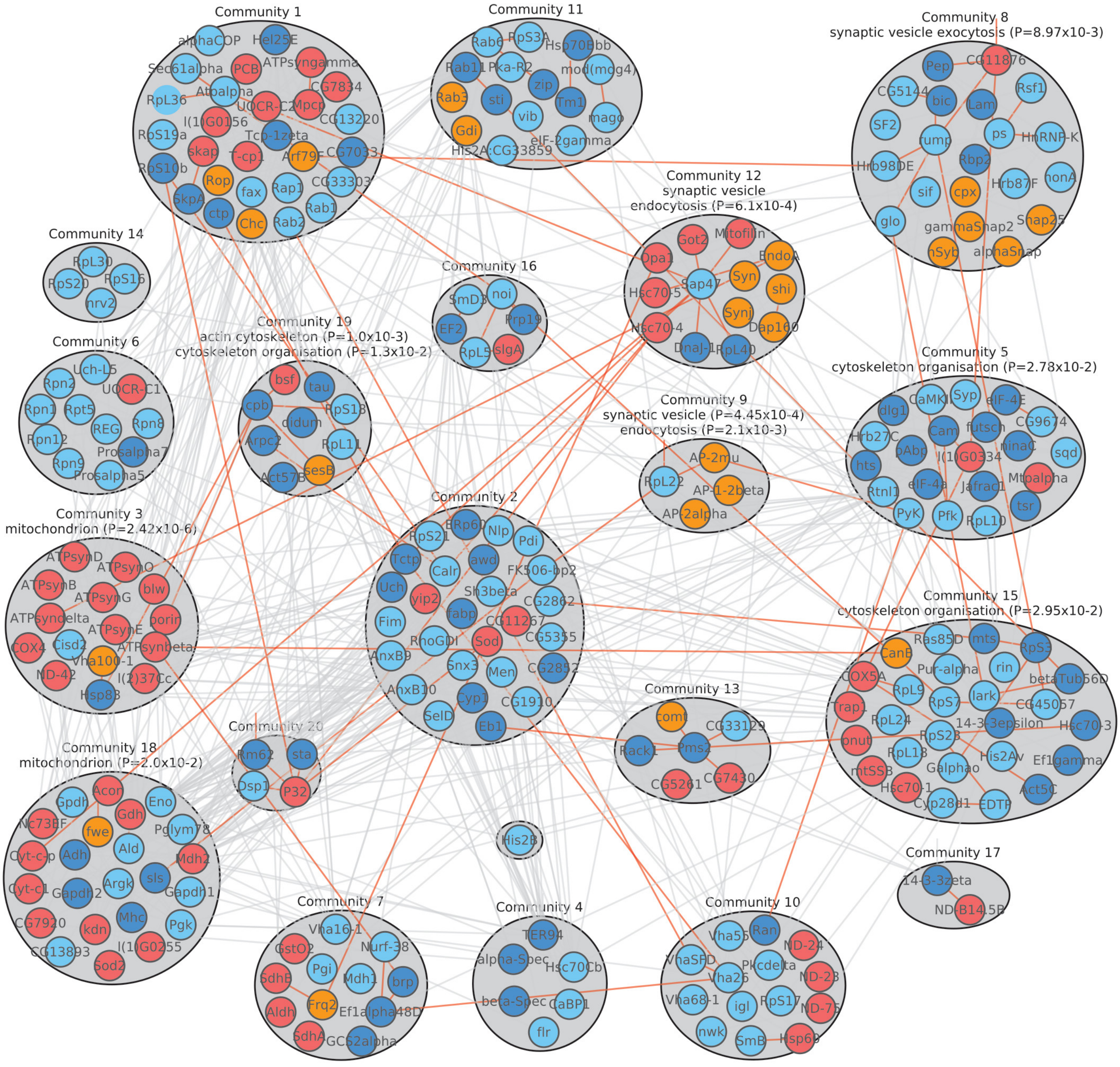

B

Clipped GO Cellular Component tree

GO.ID	GO CC Term	Elim Fisher	hits	Bonferroni for elim Fisher
GO:0005737	Cytoplasm	7.7e-28	185	***
GO:0005840	Ribosome	2.9e-10	24	***
GO:0005759	Mitochondrial matrix	2.7e-09	25	***
GO:0005739	Mitochondrion	1.5e-06	82	***
GO:0030529	Ribonucleoprotein complex	4.6e-06	31	***
GO:0000275	Mitochondrial proton-transporting ATP synt.	5.4e-06	5	***
GO:0005747	Mitochondrial respiratory chain complex I	3.8e-05	9	***
GO:0005743	Mitochondrial inner membrane	0.00012	37	**

C

GO Biological functions analysis

GO.ID	GO Biological Function Description	Annotated	Significant	elim Fisher
GO:0000022	mitotic spindle elongation	82	19	5.50E-13
GO:0006457	protein folding	104	20	5.50E-12
GO:0006099	tricarboxylic acid cycle	39	13	1.70E-11
GO:0006096	glycolytic process	27	10	1.20E-09
GO:0015986	ATP synthesis coupled proton transport	21	9	1.80E-09
GO:0007269	neurotransmitter secretion	122	23	6.10E-09
GO:0048790	maintenance of presynaptic active zone s.	6	5	9.00E-08
GO:0051298	centrosome duplication	85	15	2.70E-07
GO:0008103	oocyte microtubule cytoskeleton polariza...	23	7	1.90E-06
GO:0048172	regulation of short-term neuronal synapt...	5	4	2.70E-06
GO:0006537	glutamate biosynthetic process	6	4	8.10E-06
GO:0000281	mitotic cytokinesis	65	10	1.00E-05
GO:0007317	regulation of pole plasm oskar mRNA loca..	29	7	1.00E-05
GO:0015991	ATP hydrolysis coupled proton transport	40	8	1.10E-05
GO:0009408	response to heat	87	11	2.50E-05
GO:0008340	determination of adult lifespan	160	15	3.50E-05
GO:0006414	translational elongation	24	6	3.70E-05
GO:0006120	mitochondrial electron transport, NADH t...	35	7	3.90E-05
GO:0045454	cell redox homeostasis	49	8	5.10E-05

D

Human Disease Ontology analysis

Disease	N	OMIM/ geneRIF/ Ensembl Variable	Disease Ontology ID
Schizophrenia	66	3.2x10-12	5419
Frontotemporal dementia	20	4.6x10-12	9255
Alzheimer's disease	50	6.3x10-9	10652
Epilepsy syndrome	27	1.0x10-4	1826
Parkinson's disease	23	1.8x10-4	14330
Huntington's disease	9	4.0x10-3	12858
Infantile epileptic encephalopathy	4	9.2x10-3	2481
Hypertension	24	3.9x10-2	10763
Autistic disorder	13	5.9x10-2	12849
Autism spectrum disorder	13	6.5x10-2	60041
Bipolar disorder	22	8.1x10-2	3312

Figure 3

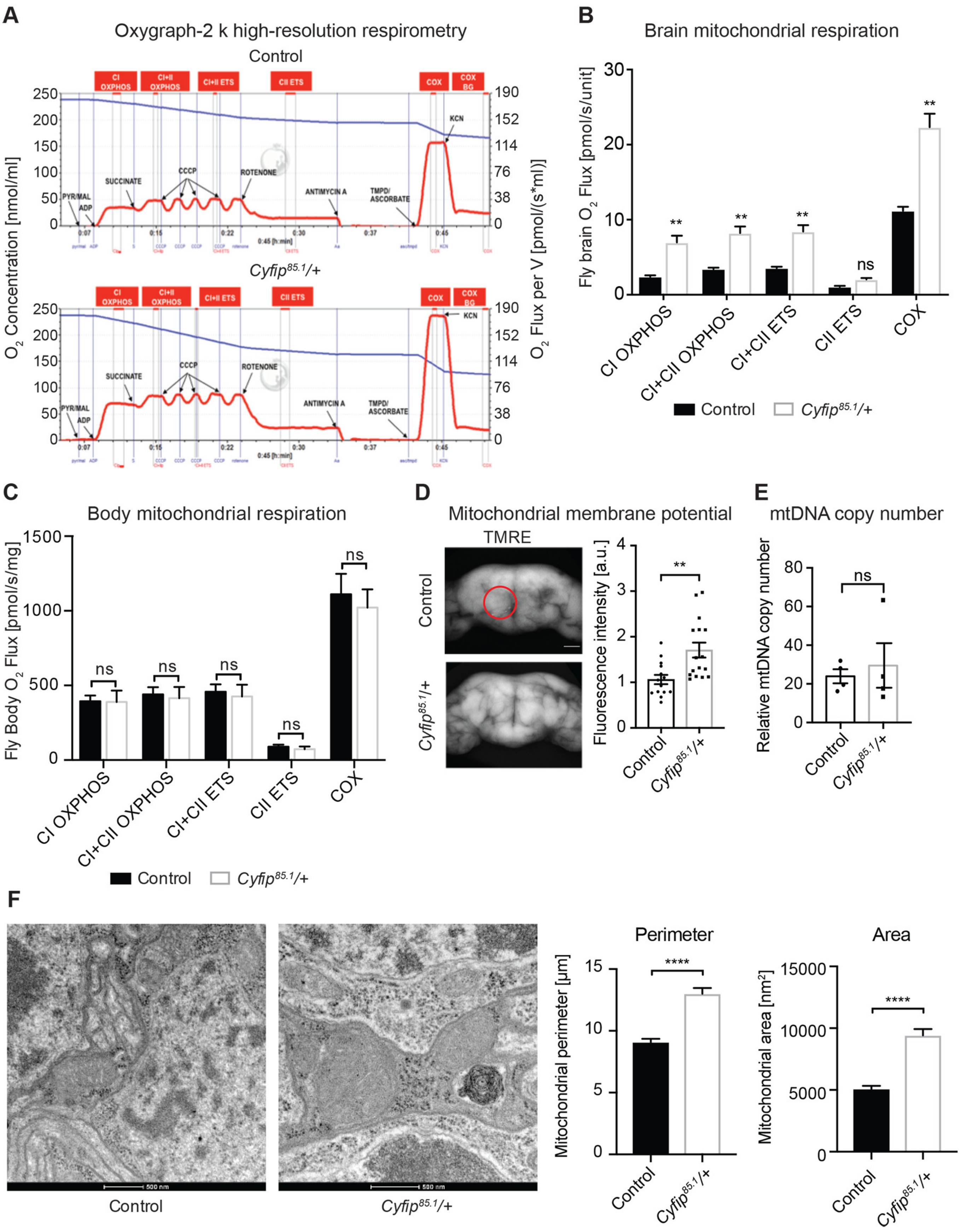
A
Oxygraph-2 k high-resolution respirometry
Control
CI OXPHOS
CI+II OXPHOS
CI+II ETS
CII ETS
COX
COX BG
PYR/MAL
ADP
SUCCINATE
CCCP
ROTENONE
ANTIMYCIN A
TMPD/ ASCORBATE
KCN
0:07
0:15
0:22
0:30
0:37
0:45
0:45 [h:min]
Cyfip85.1/+
O2 Concentration [nmol/ml]
O2 Flux per V [pmol/(s*ml)]
250
200
150
100
50
0
190
152
114
76
38
0
B
Brain mitochondrial respiration
Fly brain O2 Flux [pmol/s/unit]
30
20
10
0
**
**
**
ns
**
CI OXPHOS
CI+CII OXPHOS
CI+CII ETS
CII ETS
COX
Control
Cyfip85.1/+
C
Body mitochondrial respiration
Fly Body O2 Flux [pmol/s/mg]
1500
1000
500
0
ns
ns
ns
ns
ns
CI OXPHOS
CI+CII OXPHOS
CI+CII ETS
CII ETS
COX
Control
Cyfip85.1/+
D
Mitochondrial membrane potential
TMRE
Control
Cyfip85.1/+
Fluorescence intensity [a.u.]
4
3
2
1
0
**
Control
Cyfip85.1/+
E
mtDNA copy number
Relative mtDNA copy number
80
60
40
20
0
ns
Control
Cyfip85.1/+
F
500 nm
500 nm
Control
Cyfip85.1/+
Perimeter
Mitochondrial perimeter [µm]
15
10
5
0
****
Control
Cyfip85.1/+
Area
Mitochondrial area [nm2]
15000
10000
5000
0
****
Control
Cyfip85.1/+

Figure 4

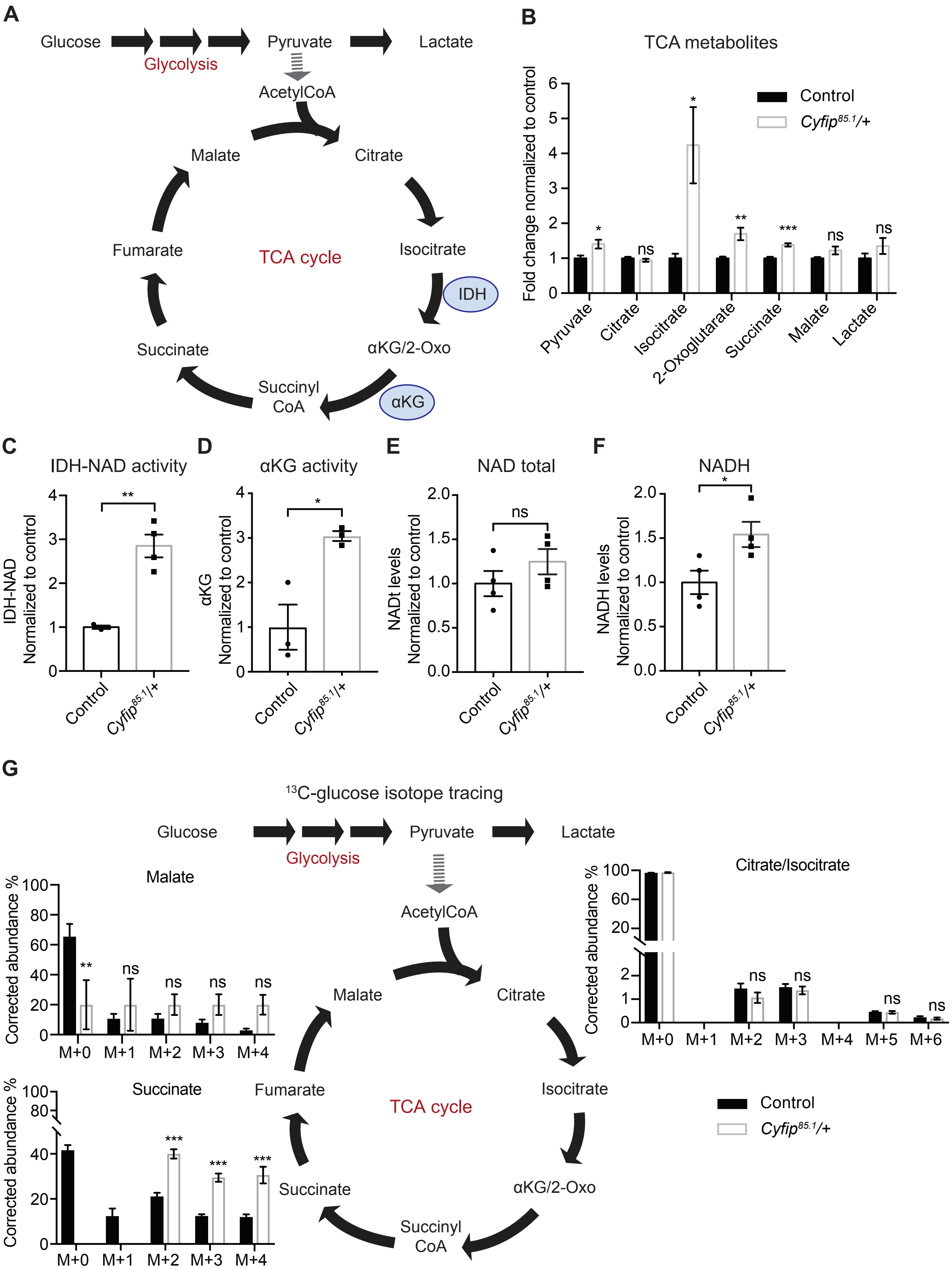
A
Glucose
Glycolysis
Pyruvate
Lactate
AcetylCoA
Malate
Citrate
Isocitrate
IDH
αKG/2-Oxo
Succinyl CoA
αKG
Succinate
Fumarate
TCA cycle
B
TCA metabolites
Fold change normalized to control
0
1
2
3
4
5
6
Control
Cyfip85.1/+
*
ns
*
**
***
ns
ns
Pyruvate
Citrate
Isocitrate
2-Oxoglutarate
Succinate
Malate
Lactate
C
IDH-NAD activity
IDH-NAD Normalized to control
**
Control
Cyfip85.1/+
D
αKG activity
αKG Normalized to control
*
E
NAD total
NADt levels Normalized to control
ns
0.0
0.5
1.0
1.5
2.0
F
NADH
NADH levels Normalized to control
*
G
13C-glucose isotope tracing
Glucose
Glycolysis
Pyruvate
Lactate
AcetylCoA
Malate
Citrate
Isocitrate
αKG/2-Oxo
Succinyl CoA
Succinate
Fumarate
TCA cycle
Malate
Corrected abundance %
0
20
40
60
80
100
**
ns
ns
ns
ns
M+0
M+1
M+2
M+3
M+4
Succinate
***
***
***
Citrate/Isocitrate
ns
ns
ns
ns
M+5
M+6
Control
Cyfip85.1/+

Figure 5

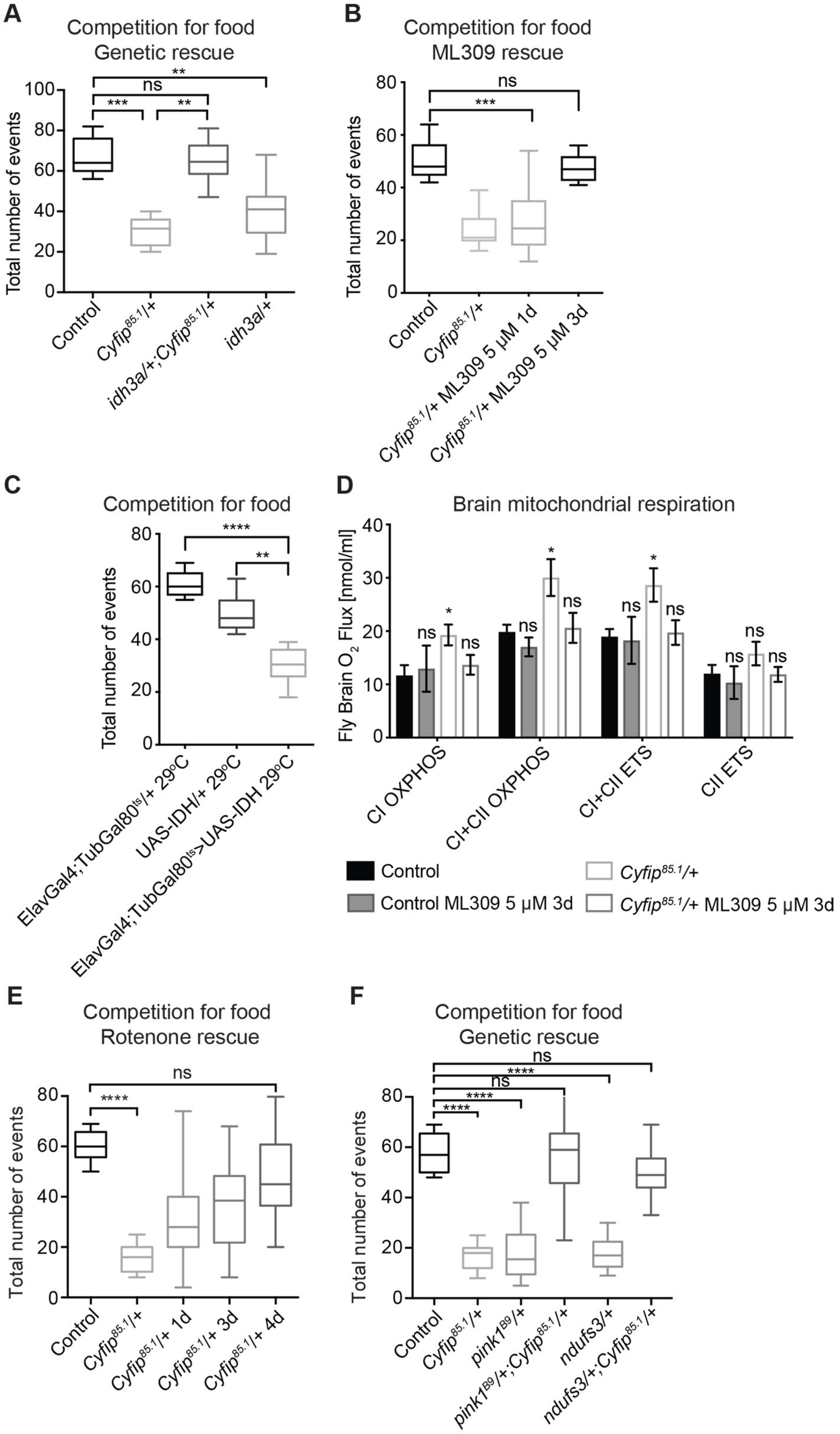
A
Competition for food
Genetic rescue
Total number of events
0
20
40
60
80
100
***
ns
**
**
Control
Cyfip85.1/+
idh3a/+;Cyfip85.1/+
idh3a/+
B
Competition for food
ML309 rescue
Total number of events
0
20
40
60
80
ns
***
Control
Cyfip85.1/+
Cyfip85.1/+ ML309 5 μM 1d
Cyfip85.1/+ ML309 5 μM 3d
C
Competition for food
Total number of events
0
20
40
60
80
****
**
ElavGal4;TubGal80ts/+ 29oC
UAS-IDH/+ 29oC
ElavGal4;TubGal80ts>UAS-IDH 29oC
D
Brain mitochondrial respiration
Fly Brain O2 Flux [nmol/ml]
0
10
20
30
40
ns
*
ns
ns
*
ns
ns
*
ns
ns
ns
ns
CI OXPHOS
CI+CII OXPHOS
CI+CII ETS
CII ETS
Control
Control ML309 5 μM 3d
Cyfip85.1/+
Cyfip85.1/+ ML309 5 μM 3d
E
Competition for food
Rotenone rescue
Total number of events
0
20
40
60
80
ns
****
Control
Cyfip85.1/+
Cyfip85.1/+ 1d
Cyfip85.1/+ 3d
Cyfip85.1/+ 4d
F
Competition for food
Genetic rescue
Total number of events
0
20
40
60
80
ns
****
ns
****
****
Control
Cyfip85.1/+
pink1B9/+
pink1B9/+;Cyfip85.1/+
ndufs3/+
ndufs3/+;Cyfip85.1/+

Figure 6

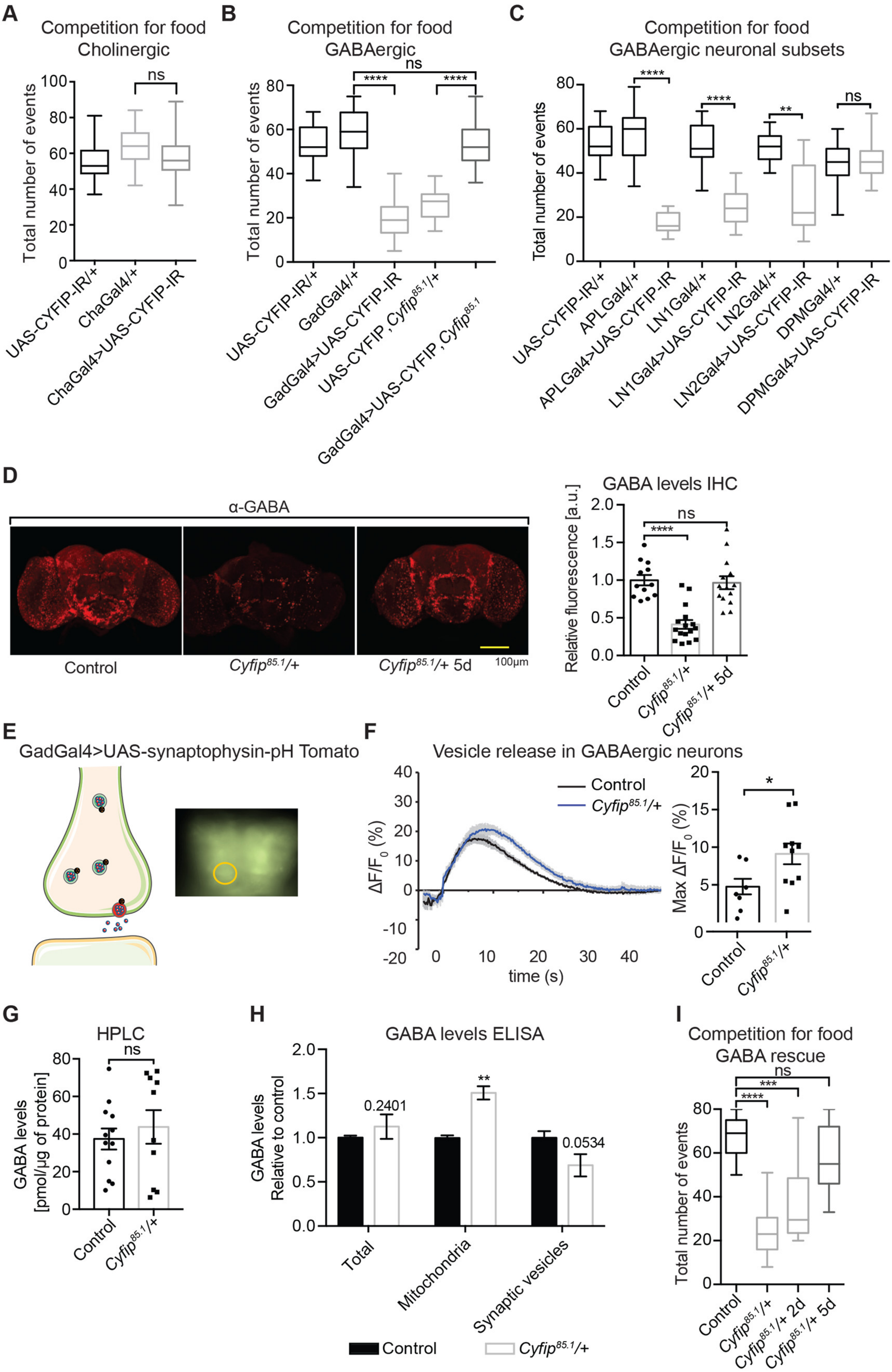
A
Competition for food
Cholinergic
Total number of events
100
80
60
40
20
0
ns
UAS-CYFIP-IR/+
ChaGal4/+
ChaGal4>UAS-CYFIP-IR
B
Competition for food
GABAergic
ns
****
****
80
60
40
20
0
Total number of events
UAS-CYFIP-IR/+
GadGal4/+
GadGal4>UAS-CYFIP-IR
UAS-CYFIP, Cyfip85.1/+
GadGal4>UAS-CYFIP, Cyfip85.1
C
Competition for food
GABAergic neuronal subsets
****
****
**
ns
80
60
40
20
0
Total number of events
UAS-CYFIP-IR/+
APLGal4/+
APLGal4>UAS-CYFIP-IR
LN1Gal4/+
LN1Gal4>UAS-CYFIP-IR
LN2Gal4/+
LN2Gal4>UAS-CYFIP-IR
DPMGal4/+
DPMGal4>UAS-CYFIP-IR
D
α-GABA
Control
Cyfip85.1/+
Cyfip85.1/+ 5d
100μm
GABA levels IHC
ns
****
2.0
1.5
1.0
0.5
0.0
Relative fluorescence [a.u.]
Control
Cyfip85.1/+
Cyfip85.1/+ 5d
E
GadGal4>UAS-synaptophysin-pH Tomato
F
Vesicle release in GABAergic neurons
40
30
20
10
0
-10
-20
ΔF/F0 (%)
Control
Cyfip85.1/+
0
10
20
30
40
time (s)
20
15
10
5
0
Max ΔF/F0 (%)
*
Control
Cyfip85.1/+
G
HPLC
ns
80
60
40
20
0
GABA levels
[pmol/μg of protein]
Control
Cyfip85.1/+
H
GABA levels ELISA
2.0
1.5
1.0
0.5
0.0
GABA levels
Relative to control
0.2401
**
0.0534
Total
Mitochondria
Synaptic vesicles
Control
Cyfip85.1/+
I
Competition for food
GABA rescue
ns
***
****
80
60
40
20
0
Total number of events
Control
Cyfip85.1/+
Cyfip85.1/+ 2d
Cyfip85.1/+ 5d

Figure 7

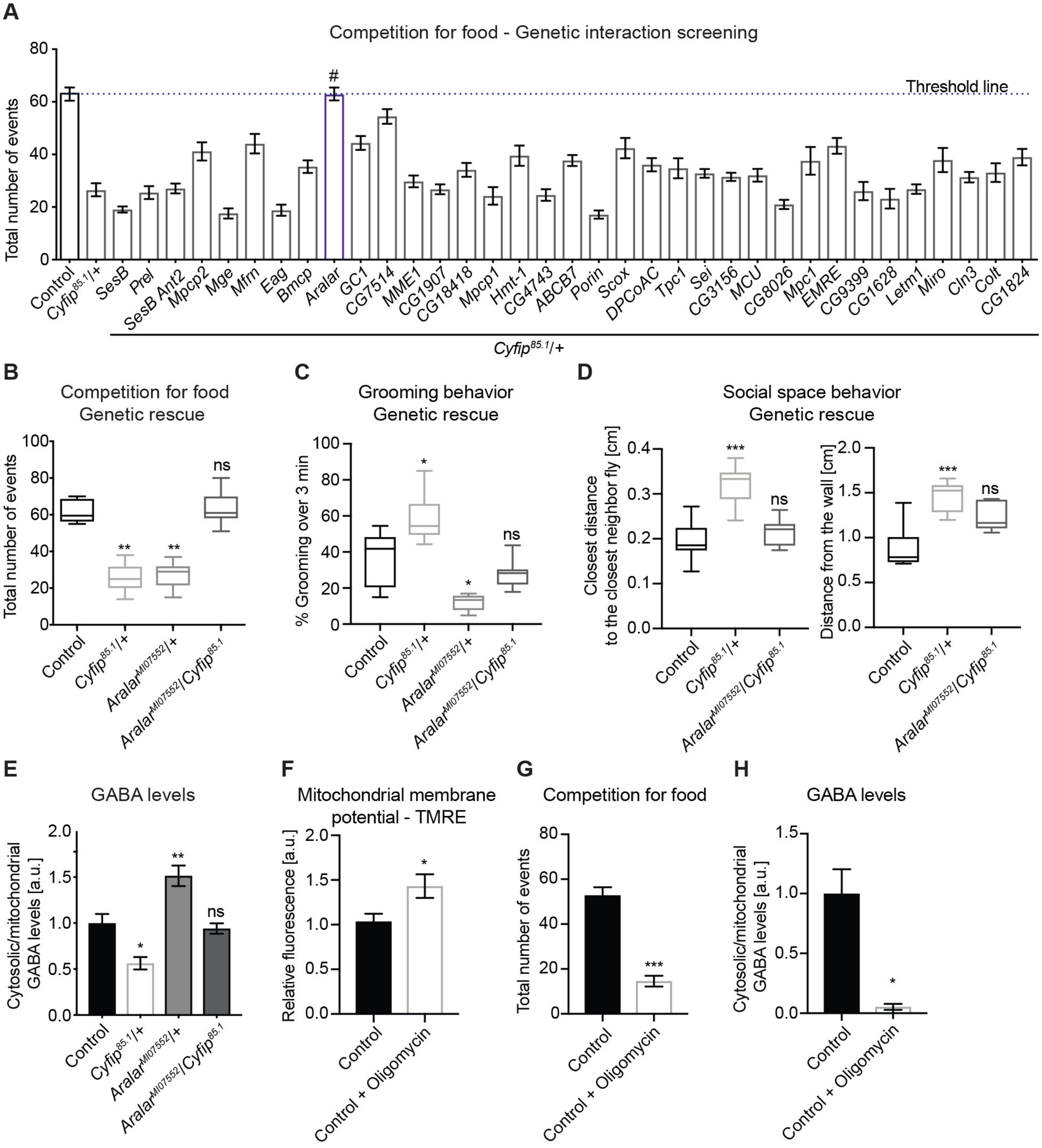
A
Competition for food - Genetic interaction screening
Total number of events
0
20
40
60
80
#
Threshold line
Control
Cyfip85.1/+
SesB
Prel
SesB Ant2
Mpcp2
Mge
Mfrn
Eag
Bmcp
Aralar
GC1
CG7514
MME1
CG1907
CG18418
Mpcp1
Hmt-1
CG4743
ABCB7
Porin
Scox
DPCoAC
Tpc1
Sei
CG3156
MCU
CG8026
Mpc1
EMRE
CG9399
CG1628
Letm1
Miro
Cln3
Colt
CG1824
Cyfip85.1/+
B
Competition for food
Genetic rescue
Total number of events
0
20
40
60
80
100
**
**
ns
Control
Cyfip85.1/+
AralarMI07552/+
AralarMI07552/Cyfip85.1
C
Grooming behavior
Genetic rescue
% Grooming over 3 min
0
20
40
60
80
100
*
*
ns
Control
Cyfip85.1/+
AralarMI07552/+
AralarMI07552/Cyfip85.1
D
Social space behavior
Genetic rescue
Closest distance
to the closest neighbor fly [cm]
0.0
0.1
0.2
0.3
0.4
***
ns
Control
Cyfip85.1/+
AralarMI07552/Cyfip85.1
Distance from the wall [cm]
0.0
0.5
1.0
1.5
2.0
***
ns
Control
Cyfip85.1/+
AralarMI07552/Cyfip85.1
E
GABA levels
Cytosolic/mitochondrial
GABA levels [a.u.]
0.0
0.5
1.0
1.5
2.0
*
**
ns
Control
Cyfip85.1/+
AralarMI07552/+
AralarMI07552/Cyfip85.1
F
Mitochondrial membrane
potential - TMRE
Relative fluorescence [a.u.]
0.0
0.5
1.0
1.5
2.0
*
Control
Control + Oligomycin
G
Competition for food
Total number of events
0
20
40
60
80
***
Control
Control + Oligomycin
H
GABA levels
Cytosolic/mitochondrial
GABA levels [a.u.]
0.0
0.5
1.0
1.5
*
Control
Control + Oligomycin

Figure 8

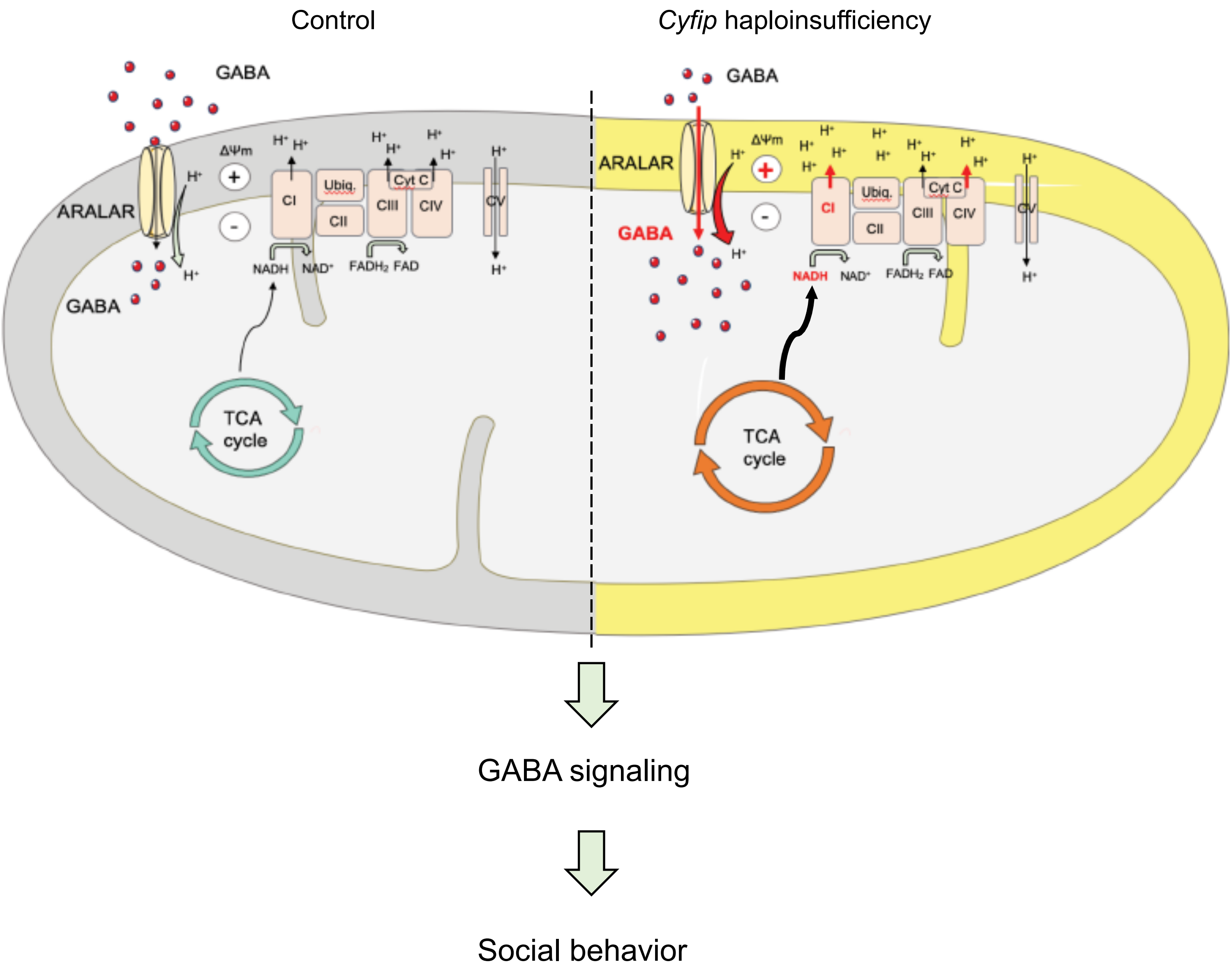
Control
Cyfip haploinsufficiency
GABA
ARALAR
ΔΨm
+
-
H⁺
CI
Ubiq.
CII
Cyt C
CIII
CIV
CV
NADH
NAD⁺
FADH₂
FAD
GABA
TCA cycle
GABA
ARALAR
ΔΨm
+
-
H⁺
GABA
CI
Ubiq.
CII
Cyt C
CIII
CIV
CV
NADH
NAD⁺
FADH₂
FAD
TCA cycle
GABA signaling
Social behavior

Kanellopoulos et al. Supplemental Information

Figure and Table Legends

Figure S1. *Cyfip* haploinsufficiency flies have deficits in social behavior and hyperactivity. (A) Female *Cyfip*$^{85.1}$/+ flies show a decreased competition for food. Control (*w1118*) and *Cyfip*$^{85.1}$/+ female flies were analyzed for total number of social interactions in a competition for food assay. n > 12 groups of 8 flies. Data are shown with box and whisker plots where the line inside the box indicates the median, ***$p < 0.001$, Mann–Whitney test. (B, C) Male *Cyfip*$^{85.1}$/+ flies are hyperactive. (B) Locomotion activity of control and *Cyfip*$^{85.1}$/+ flies was monitored over 24 hours and (C) during the morning period ZT0-ZT6. n > 40 flies for each genotype were tested. mean ± s.e.m., **$p < 0.01$, ns, not significant, Mann–Whitney test. (D, E) No negative geotaxis phenotype in *Cyfip*$^{85.1}$/+ flies. Negative geotaxis response was measured in 5 days old *Cyfip*$^{85.1}$/+ and control male (D) and female (E) flies. n > 30 flies for each genotype, mean ± s.e.m. ns, not significant, Mann–Whitney test. (F) *Cyfip* mRNA levels are decreased in adult brains upon pan-neuronal *Cyfip* knockdown (29°C) in comparison to parental control strains. The levels of *Cyfip* were normalized to *rpl13* mRNA. n = 3 for each genotype, mean ± s.e.m. *$p < 0.05$, Kruskal-Wallis test, Dunn's multiple comparison test. (G) Acute knock down of *Cyfip* in adult male flies is sufficient to produce the phenotype in the competition for food assay. Adult-specific abrogation of *Cyfip* (UAS-CYFIP-IR) (29°C) pan-neuronally compared with uninduced (18°C), transgene-alone and driver-alone control flies were analyzed for total number of social interactions. Conditional overexpression of CYFIP in the mutant background (genetic rescue, UAS-CYFIP, *Cyfip*$^{85.1}$/+) in comparison with the uninduced transgene (18°C) reverses social defects of *Cyfip*$^{85.1}$/+ flies. n = 14 independent experiments with 8 flies per genotype, ****$p < 0.0001$, **$p < 0.01$, Kruskal-Wallis test, Dunn's multiple comparison test.

Figure S2. The proteome of the *Cyfip*$^{85.1}$/+ mutant flies revealed maladaptive mitochondrial function and altered TCA cycle. (A) Electron transport chain and (B) TCA cycle modified from WikiPathways (wikipathways.org) for *Drosophila melanogaster*. Proteomic analysis of *Cyfip*$^{85.1}$/+ flies uncovered several dysregulated mitochondrial proteins (highlighted) in comparison to control flies.

Figure S3. Increased mitochondrial Complex I subunit in *Cyfip*$^{85.1}$/+ fly brains. (A) Mitochondrial membrane potential is increased in *Cyfip*$^{85.1}$/+ brains. Left, representative Z projection of confocal images of fly brains from control and *Cyfip*$^{85.1}$/+ stained with Rhodamine 123. Right, quantification of fold change in Rhodamine 123 fluorescence intensity from the antenna lobes (AL) area. n = 11-12 brains per genotype, mean ± s.e.m., $^{*}p = 0.0167$, Kruskal-Wallis test, Dunn's multiple comparison test. (B, C) Upregulation of Complex I subunit NDUFS3 in *Cyfip*$^{85.1}$/+ flies (B) Left panel, representative Western blotting of protein extracts from fly brains using antibodies to detect the mitochondrial proteins HSP60, ATPB, NDUFS3 and TOM20. Right panel, quantification upon normalization to Syntaxin, n = 4 per genotype, mean ± s.e.m $^{*}p < 0.05$. Kruskal-Wallis test, Dunn's multiple comparison test. (C) VDAC/Porin level does not change in the *Cyfip*$^{85.1}$/+ flies. Left panel, representative Western blotting of protein extracts from fly brains using an antibody to detect the mitochondrial marker VDAC/Porin. Right panel, quantification upon normalization to Tubulin, n = 4 per genotype, mean ± s.e.m, ns, not significant, Mann–Whitney test. (D) Citrate synthase (CS) activity does not change in the *Cyfip*$^{85.1}$/+ flies. Measurement of mitochondrial CS activity in control and *Cyfip*$^{85.1}$/+ fly brains. n = 5 per genotype, mean ± s.e.m., ns, not significant, Mann–Whitney test. (E, F) Feeding behavior is not altered in the *Cyfip*$^{85.1}$/+ flies. (E) Food consumption during the day time. Groups of 5-7-day-old flies were analyzed every 2 hours (ZT0, ZT2, ZT4, ZT6). (F) Quantification of food consumption over 24 hours (see Methods). At the given time points, flies were collected, homogenized, and the absorbance of the supernatant measured at 625 nm (to read the blue dye in the food). mean ± s.e.m., ns, not significant, Mann–Whitney test.

Figure S4. *Cyfip*$^{85.1}$/+ fly brains have high levels of amino acids related to the TCA cycle. (A) Liquid chromatography-mass spectrometry revealed that specific amino acids related to the TCA cycle are higher in *Cyfip*$^{85.1}$/+ brains compared to control flies. Amino acids in *Cyfip*$^{85.1}$/+ brains normalized to control and µg of protein (n = 5, groups of 10 fly brains), mean ± s.e.m. $^{*}p < 0.05$, $^{**}p < 0.01$, Kruskal-Wallis test, Dunn's multiple comparison test. (B) Specific chemical reactions of the TCA cycle are affected in the *Cyfip*$^{85.1}$/+ brains. Contribution of [U-$^{13}C_6$] glucose to the TCA-cycle metabolites such as glutamate, glutamine and aspartate in *Drosophila* brain tissue following 6 hours feeding with [^{13}C] glucose. The x-axis denotes the ^{13}C-isotopologue profile (i.e. the mass isotopologue distribution - MID) of labeled metabolites following the incorporation of [^{13}C] glucose skeleton. The catabolism of ^{13}C labeled glucose leads to M+3 pyruvate. The decarboxylation of pyruvate makes M+2 acetyl-CoA in the mitochondria, which is then incorporated into M+2 citrate. All the TCA cycle intermediates, downstream of citrate, have a mass of M+2. Values shown are mean ± sem (n = 5, 10 brains were pooled per each sample). * $p < 0.05$; ** $p < 0.01$, ***$p < 0.001$, 2way ANOVA, Sidak's multiple comparisons test.

Figure S5. Rotenone treatment restores social deficits but does not restore hyperactivity of *Cyfip*$^{85.1}$/+ flies. (A) Rotenone treatment does not affect control flies. Competition for food upon treatment with different concentrations of rotenone in control flies. (B) The positive effect of rotenone treatment is reversible in *Cyfip*$^{85.1}$/+ flies. *Cyfip* mutant flies were treated for 4 days (4d) with 10 μM rotenone and then tested for 5 days of the post-treatment period in competition for food assay. The comparison was with the control in each case. n > 10 groups of 8 flies for each condition were tested. mean ± s.e.m., ****$p < 0.0001$, **$p < 0.01$, Kruskal-Wallis test, Dunn's multiple comparison test. (C) Rotenone does not rescue hyperactivity in *Cyfip*$^{85.1}$/+ flies. Locomotion upon treatment with 10 μM rotenone for 4 days (4d) was analyzed in *Cyfip*$^{85.1}$/+ flies. Locomotion was monitored over 24 hours. n > 40 flies for each condition were tested. mean ± s.e.m., ** $p < 0.01$, Kruskal-Wallis test, Dunn's multiple comparison test.

Figure S6. GABA-dependent excitability and number of GABAergic neurons are not affected in the *Cyfip*$^{85.1}$/+ flies. (A) Decreased *Cyfip* mRNA levels upon *Cyfip* knockdown in GABAergic neurons (FACS sorted cells) (white bar) in comparison to control flies (black bar). The levels of *Cyfip* were normalized to *rpl13* mRNA. n = 3 for each genotype, mean ± s.e.m. **$p < 0.01$, Mann–Whitney test. (B) Scheme of the GABAergic neuronal subsets where CYFIP was knock-down. APL (GABAergic and Octopaminergic) and DPM (GABAergic and Serotonergic). The LN (GABAergic) neurons regulate the Projections neurons (PN). (C) No changes in presynaptic excitability. Representative false color-coded image showing pre-synaptic Ca^{2+} influx in GABAergic (n > 8) and APL (n > 6) neurons upon depolarization (50 mM KCl). The traces indicate the dynamics of Ca^{2+} influx, quantified as $\Delta F/F_0$ (%) in synaptophysin-

G-CaMP fluorescence over time (t0 indicates KCl delivery). The bar diagram indicates Max $\Delta F/F_0$ (%). mean ± s.e.m, $p > 0.05$, Mann-Whitney test. (D-F) No changes in the number of GABAergic neurons. (D) Left, representative Z projections of confocal images of control and *Cyfip*$^{85.1}$/+ fly brains stained with nc82 (neuropil) and GAD1 antibody. Right, quantification of GAD1 relative fluorescence ($n > 11$). White box indicates the area of quantification. Scale bar, 100 µm. Mann-Whitney test. (E) Left, representative Western blotting of GAD1 levels from control and *Cyfip*$^{85.1}$/+ adult head lysates. Left, quantification of relative levels to neuronal marker syntaxin. $n = 4$, mean ± s.e.m, Mann-Whitney test. (F) Real-time PCR detecting *Gad1* mRNA level normalized to *rpl13* mRNA. $n = 3$ for each genotype, mean ± s.e.m, Mann-Whitney test.

Figure S7. GABA supplement restores social deficits in Cyfip haploinsufficient flies. (A) No changes in glutamate levels as determined by HILIC-MS/MS in control and *Cyfip*$^{85.1}$/+ brains. $n = 5$ (group of 10 brains) per genotype, mean ± s.e.m, Mann-Whitney test. (B) Subcellular fractionation and enrichment in mitochondria and synaptosomes. Shown is a Western blot of the respective fractions. Bruchpilot (BRP) was used as synaptic marker and ATP5B was used as mitochondrial marker. (C-E) Increasing GABA availability rescues competition for food behavior. (C) Competition for food of *Cyfip*$^{85.1}$/+ flies upon treatment (2-5 days) with 100 µM DABA, and (D) 1 mM VPA. (E) Conditional abrogation (29°C) of CYFIP pan-neuronally in adults upon GABA treatment for 5 days in comparison with the uninduced (18°C) and induced (29°C) controls. Flies tested for social interactions. $n > 14$ independent experiments (group of 8 flies) for each genotype, mean ± s.e.m., ***$p < 0.001$, Kruskal Wallis test, Dunn's multiple comparison test. (F) Decreased GABA production phenocopies *Cyfip* mutation. Competition for food upon GAD1 abrogation pan-neuronally in adults. $n > 10$ independent experiments (each with 8 flies) for each genotype, mean ± s.e.m., ***$p < 0.001$, Kruskal-Wallis test, Dunn's multiple comparison test. (G) Excess of GABA affects behavior in control flies. Competition for food was monitored upon treatment with 50µM GABA for 5 days (5d), in control flies. $n > 10$ independent experiments (each with 8 flies) for each genotype, mean ± s.e.m., *$p < 0.05$, Mann-Whitney test. (H) GABA$_A$R agonist rescues CYFIP mutant behavior. Competition for food of *Cyfip*$^{85.1}$/+ flies upon treatment (1d) with 50 µM Diazepam. (I) Competition for food was rescued upon treatment with VPA, GABA, DABA, in flies with reduced CYFIP in

GABAergic neurons. For all the experiments n > 10 (group of 8 flies), **p < 0.01, ***p < 0.001, ****p < 0.0001, Kruskal-Wallis test, Dunn's multiple comparison test. (J) Temporal effect of GABA treatment in competition for food. *Cyfip*$^{85.1}$/+ flies were treated for 5 days with GABA (GABA 5d) and then tested for 5 days of the post-treatment period. The comparison was with the control in each case. n > 10 groups of 8 flies for each condition were tested. mean ± s.e.m., ****p < 0.0001, **p < 0.01, Kruskal-Wallis test, Dunn's multiple comparison test.

Figure S8: Characterization of Aralar synthesis in *Cyfip* haploinsufficiency. (A) Aralar haploinsufficiency does not rescue hyperactivity deficits of Cyfip mutant flies. Locomotor activity was monitored over 24 hours. n > 40 flies for each genotype were tested. mean ± s.e.m., **p < 0.01, ***p < 0.001, Kruskal-Wallis test, Dunn's multiple comparison test. (B) Aralar inhibition by pyridoxal 5'-phosphate (PLP) restores social deficits in *Cyfip* haploinsufficient flies. Competition for food of control and *Cyfip*$^{85.1}$/+ flies upon treatment (2 days) with 50 µM PLP. n > 10 (groups of 8 flies each), **p < 0.01, *p < 0.05, Mann–Whitney test. (C, D) Aralar expression does not change in the *Cyfip*$^{85.1}$/+ flies. (C) *Aralar* mRNA level was measured in control and *Cyfip*$^{85.1}$/+ fly brains by RT-qPCR and quantified upon normalization to the ribosomal protein *l13* mRNA. n = 4 (groups of 10 fly brains each), mean ± s.e.m, Mann-Whitney test (D) Translational efficiency of *Aralar* mRNA is comparable in control and *Cyfip*$^{85.1}$/+ flies. Distribution of *Aralar* mRNA on polysomes and mRNPs. Bars indicate the percentage *Aralar* mRNA on polysomes over the total (polysomes + mRNPs). n = 3 groups of 100 fly heads for each genotype, mean ± s.e.m. Mann–Whitney test.

Table S1. List of the identified proteins in control and *Cyfip*$^{85.1}$/+ fly brains.

Table S2. GO biological functions and cellular components in control and *Cyfip*$^{85.1}$/+ fly brains.

Table S3. GO analysis of mitochondrial GABA carrier candidates.

Table S1. List of the identified proteins in control and *Cyfip*$_{85.1}$/+ mutant flies

Fly brain		
SWISS-PROT accession number	**Gene name**	**Ratio Cyfip$_{85.1}$/Control**
Q59E30	fax	112.80
Q02645	hts	100.08
X2JC31	Chc	96.41
X2JCJ4	sif	61.44
M9PDK5	VhaSFD	59.61
X2JE15	shi	56.32
Q9VB69	Men-b	51.84
E1JIJ5	Vha55	50.43
Q23983	alphaSnap	46.58
G3M3A2	RpS3	46.57
O18333	Rab2	46.09
Q9V3N7	CRMP	40.35
A4V134	CaMKII	39.14
A4V4U5	slgA	38.98
Q94523	SdhA	38.97
A0A0B4LJ12	awd	37.16
Q7KN62	TER94	37.10
Q9VFF0	UQCR-C1	34.77
Q9VL70	yip2	34.69
Q9VVL7	CG7430	34.26
M9PBL3	Hsp83	33.27
P52029	Pgi	30.89
P36975	Snap25	30.85
Q7K5K3	CG11876	30.84
Q9VU35	CG11267	28.22
Q00963	beta-Spec	27.70
M9PE40	Uch	27.55
Q24560	betaTub56D	26.34
Q0E8E8	Mpcp	25.95
A0A0B4LFM0	Cbp53E	25.44
X2JDP6	CG4747	23.41
Q4AB57	His2A:CG33859	22.36
P05661	Mhc	21.78
M9PH10	comt	21.74
P13060	EF2	21.18
M9PD18	Vha68-1	20.39
Q9VL16	CG5676	20.38
M9NGG5	futsch	20.31
Q9W2X6	ATPsyndelta	20.23
Q9VWX8	Frq2	19.97
O77062	Eaat1	19.46
M9PET0	Gpdh	19.05
P41094	RpS18	18.90
A0A0B4K6V0	brp	18.42
Q24208	eIF-2gamma	18.41
A0A0B4KHH8	Syp	18.34
Q9V3W7	SF2	17.82
E1JJ37	cpx	17.62
Q9VLB7	Gdi	17.50
B7YZQ7	Nurf-38	17.46
Q9VAJ9	CG1907	16.99

P13395	alpha-Spec	16.67
Q9VAM6	Cisd2	16.53
Q8IML5	Vha100-1	16.29
Q9VGM2	fabp	16.29
Q9VIU8	CG10132	15.82
C6TP87	Ef1alpha48D	15.76
Q9VBI2	Dak1	15.72
B7Z0L1	Fas1	14.82
P13607	Atpalpha	14.66
Q7JS69	nrv3	13.71
X2JB48	sesB	13.70
A8JNU6	Nc73EF	13.45
Q9VJZ4	ND-B22	13.45
M9PDC7	Dap160	13.43
O18335	Rab11	13.31
Q7K2X5	CG14762	13.09
Q9VGF7	GC1	12.37
Q24253	AP-1-2beta	12.34
P22465	AnxB10	12.24
Q8IQW5	CG14207-RB	12.13
Q0KHZ6	CG7834	12.01
Q24439	ATPsynO	11.89
Q9VSY4	CG3967	11.43
A0A0B4LGZ5	RpL11	11.43
A4V383	ND-42	11.29
M9PEL1	Rop	11.20
X2JDU0	RpL9	11.16
X2JGP4	Pdi	11.12
Q9VNX4	P5CDh1	10.86
Q9W401	kdn	10.80
C6KI54	COII	10.68
A0A023GQA5	l(2)37Cc	10.59
Q9VIQ8	COX4	10.58
P50887	RpL22	10.34
Q9V597	RpL31	10.25
A4V110	CaMKI	10.25
O18332	Rab1	10.23
X2JC35	RpL36	10.22
Q9VW68	CG7433	10.19
Q6NP72	CG13220	10.00
F3YDH0	Hsc70-3	9.84
Q9VKW5	CG5355	9.80
M9PDW0	nSyb	9.77
Q7KM15	bic	9.64
Q9VEB1	Mdh2	9.57
A0A0B4KH34	AnxB9	9.55
A0A0B4LGD3	kcc	9.38
O01666	ATPsyngamma	9.14
M9PGX2	prtp	9.13
P06605	alphaTub84D	9.12
E1JHQ1	Gs1	9.11
A0A0B4LFD2	Hsc70-5	9.07
M9PCG1	CG5261	8.91
B5RIU6	EndoA	8.89
O02649	Hsp60	8.81
A0A0B4JCW4	skap	8.71
Q7JPS2	igl	8.51
P17704	RpS17	8.31

Q9VXQ5	Tcp-1zeta	8.30
Q8IMI7	RpS7	8.25
X2J6D4	Cyt-c-p	8.09
X2JH42	ATPsynbeta	8.00
Q9VD58	CG6439	7.95
Q9VXB0	CG9132	7.88
A0A0B4LGS4	Vha26	7.78
Q9VVA6	nudC	7.76
X2JCX8	RpS14b	7.70
A0A0B4KGN2	Mitofilin	7.69
C7LA75	Hsc70-4	7.69
X2JC80	sta	7.63
Q99323	zip	7.56
Q7KMP8	Rpn9	7.46
A4V4A5	Ran	7.44
M9PH99	Gad1	7.42
Q9W141	CG4692	7.37
A4V3Q6	Ef1alpha100E	7.33
Q9VKM8	CG33129	7.33
Q9VKM3	ATPsynG	7.30
P21914	SdhB	7.26
A0A0B4KGE6	Rpn8	7.23
O18373	SelD	7.20
P00334	Adh	7.18
X2JCP8	Act5C	7.14
Q95083	Prosalpha5	7.12
P25228	Rab3	7.10
A0A0B4KFZ9	His4r	7.08
Q9VFT4	rin	6.95
P45594	tsr	6.91
Q3YMU0	ERp60	6.86
A4V449	ND-75	6.86
M9PD75	porin	6.79
Q9VGQ1	CG5214	6.77
A0A0B4LH71	Sap47	6.76
Q8STG9	Sec61alpha	6.70
M9NEQ9	RpS10b	6.70
M9NFH8	CG9674	6.54
P54385	Gdh	6.49
P35381	blw	6.46
X2JE06	RpL24	6.43
Q8I0J1	CG1910	6.40
Q9VG58	Hsp70Bbb	6.37
Q9VQM2	ND-B14.5B	6.36
Q9V3P3	REG	6.35
P55828	RpS20	6.34
A0A0B4LHL7	ATPsynD	6.22
Q9VKZ7	CG4972-RA	6.19
Q9VWH4	l(1)G0156	6.17
Q9VV75	UQCR-C2	6.15
Q9VRL0	Cyt-c1	6.13
Q960M4	Prx5	6.09
P92177	14-3-3epsilon	6.01
Q9VSY2	CG3689	6.01
Q7KN85	ATPCL	5.98
Q9VTU2	ND-SGDH	5.95
Q04047	nonA	5.92
Q94516	ATPsynB	5.87

M9MRQ9	Scsalpha	5.80
A0A0B4KHG5	chp	5.58
Q9VQ61	Got2	5.57
P02283	His2B	5.56
Q95T12	fwe	5.49
Q9VF27	ND-23	5.44
A0A0B4KFT0	COX5A	5.42
Q7KV27	CG1640	5.36
Q53ZT0	DnaJ-1	5.32
A0A0B4LF57	Cam	5.31
Q95T61	BcDNA:GH02439	5.26
Q9VLC5	Aldh	5.23
P16914	elav	5.19
M9PG22	Arf79F	5.17
Q9V3V6	Rpt5	5.14
Q9V4N3	Cyt-b5	5.09
X2JEN8	CG13865	5.03
E1JJ68	Rm62	5.01
Q9W392	CG7033	4.89
M9PEL3	qm	4.88
Q9VIE8	Acon	4.86
Q9V438	CaBP1	4.86
A1ZBJ2	CG7461	4.85
Q9V3E7	Ref1	4.84
Q9W227	CG2852	4.84
P48588	RpS25	4.83
P08646	Ras85D	4.70
M9PCC1	Rack1	4.69
P16378	Galphao	4.68
Q7KUX7	Rbp2	4.66
P25007	Cyp1	4.62
Q27415	Nlp	4.61
Q9I7R0	CG18815	4.56
A0A0B4LGQ1	Sod2	4.55
Q9VD29	Sar1	4.53
M9NG39	Pep	4.53
M9PJN8	Gapdh2	4.53
Q86B87	mod(mdg4)	4.50
R9Q794	RpL5	4.49
A0A0B4KFY5	ps	4.47
A0A0B4LG52	RpS16	4.46
Q7JYK1	RpL40	4.45
Q7KMM4	GCS2alpha	4.43
Q9VC31	RabX4	4.38
C8VV14	Ald	4.37
P48375	FK506-bp2	4.36
O97066	twr	4.31
P53501	Act57B	4.29
P21187	pAbp	4.29
Q9W4H6	l(1)G0334	4.27
Q9TVP3	jdp	4.26
E1JGN7	HnRNP-K	4.20
Q9V3P6	Rpn2	4.16
P52034	Pfk	4.14
P55830	RpS3A	4.11
M9MRQ6	Sh3beta	4.09
A0A0B4KEH0	14-3-3zeta	3.94
M9NFW6	CanB	3.92

O76927	RpS21	3.75
P22700	Ca-P60A	3.73
A0A0B4K661	Tm1	3.72
Q7JZK1	ND-B14	3.65
Q1RL12	nrv2	3.64
Q24491	Rsf1	3.63
M9NE89	Lam	3.63
E1JHA4	Hrb27C	3.61
Q8SYD9	EndoB	3.60
M9PIM0	RpL10	3.59
Q8IRQ5	l(1)G0255	3.59
Q86BQ4	CG2862	3.57
E1JHR5	Eno	3.54
A0A0B4K6U6	sqd	3.52
A8JNP2	Argk	3.51
A0A0B4KGI5	Ace	3.47
E1JHT6	Rtnl1	3.45
P07909	Hrb98DE	3.43
E2QD65	RpS19a	3.38
A0A0B4JD11	Ef1gamma	3.33
Q7JXC4	P32	3.27
Q9VU68	flr	3.22
Q24537	Dsp1	3.17
E2QCP0	His3.3A	3.04
Q9VAN7	Pglym78	2.99
Q95RR6	Pur-alpha	2.77
O62619	PyK	2.74
Q2PDW1	CG3662	2.70
A1Z700	didum	2.67
Q9VAC1	CG7920	2.66
Q4ABD8	His1:CG33807	2.63
Q7KLW9	Prp19	2.57
Q9VYJ5	CG12717-RA	2.49
O77134	ATPsynE	2.49
Q7JYV2	Syngr	2.49
E6EK18	PMCA	2.46
Q9VW59	RhoGDI	2.45
A8JNP1	Argk	2.44
Q9V436	Rpn12	2.42
Q9VMB9	COX5B	2.37
Q8IPE8	Mtpalpha	2.36
Q9VKX2	Mdh1	2.32
M9NFZ9	CG45057	2.25
Q9VNB9	RpL35A	2.25
Q76NQ0	CG33303	2.19
Q962I2	Rala	2.19
Q6NN06	bol	2.17
X2JDI1	mts	2.13
Q94901	lark	2.11
Q05856	SmB	2.09
M9PCE0	Pgk	2.09
Q9VDY8	vib	2.08
Q9V5C6	Prosalpha7	2.07
Q27268	Hel25E	2.00
Q9VGH5	glo	2.00
P49028	mago	1.99
E1JGZ9	CG30382	1.98
Q9VSL4	GstO2	1.98

Q9VJ19	RpL30	1.97
Q5U0V7	Synj	1.96
P29613	Tpi	1.95
Q9VW54	Rpn1	1.79
Q9VG51	Snx3	1.74
M9NDP1	ctp	1.66
Q9VYN1	Pkcdelta	1.64
P07486	Gapdh1	1.55
Q9I7K5	eca	1.53
M9MRT6	Rap1	1.47
P48598	eIF-4E	1.46
P54622	mtSSB	1.42
M9PDS8	sls	1.42
X2JF59	Jafrac1	1.32
P48810	Hrb87F	1.31
Q9W0C3	CG13928	1.30
M9PCU0	ninaC	1.30
H8F4T6	CG16935-RA	1.26
O77430	SkpA	1.26
Q9VZ77	CG17150	1.22
P82713	Cyp309a2	1.22
A8JV30	CG34327-RA	1.14
Q9W0K2	Trh	1.14
O44437	SmD3	1.11
Q9XZ61	Uch-L5	1.08
X2JAI2	Arpc2	1.03
Q9VUC1	Hsc70Cb	0.96
O46106	noi	0.95
A0A0B4LFB8	Opa1	0.94
Q9VT32	CG6767	0.93
A4V391	T-cp1	0.89
Q9VEI2	CG14329	0.87
P31007	dlg1	0.85
D2NUK9	hoip	0.78
P29843	Hsc70-1	0.75
Q9VST4	CG5144	0.72
Q9VHC7	rump	0.70
A0A0B4LHV0	tau	0.69
P91659	D3-100EF	0.67
M9PHM6	RpL18	0.67
Q9W0B8	alphaCOP	0.67
E1JGX2	Gprk1	0.64
Q9VIG0	CG9257	0.59
Q8IQZ8	Fim	0.58
P40797	pnut	0.58
P61851	Sod	0.55
Q9VMR0	CG7382	0.52
A1ZA03	Pms2	0.51
Q9VTY8	sti	0.50
A1Z6L9	Trap1	0.48
Q9VE01	Cyp12a5	0.46
Q9VQR9	CG17593-RA	0.45
A0A0B4KH25	His2Av	0.39
O62530	AP-2mu	0.37
M9PEB9	CG17258	0.36
Q9VH25	gammaSnap2	0.32
Q8SYC4	CG13893	0.28
O96881	TfIIEbeta	0.28

A0A0B4LGP3	emp	0.23
Q9VU60	CG14111	0.21
A0A0B4KGK0	Pcmt	0.20
A0A0B4LFD9	RpS23	0.13

Table S2. GO biological functions and cellular components analysis of control and *Cyfip 85.1*/+ mutant flies.

Fly brain						
GO.ID	**GO Biological Function**	**Annotated**	**Significant**	**classic Fisher**	**Elim Fisher**	**Hits**
GO:0000022	mitotic spindle elongation	82	19	5.5e-13	5.50E-13	19
GO:0006457	protein folding	104	20	5.5e-12	5.50E-12	20
GO:0006099	tricarboxylic acid cycle	39	13	1.7e-11	1.70E-11	13
GO:0006096	glycolytic process	27	10	1.2e-09	1.20E-09	10
GO:0015986	ATP synthesis coupled proton transport	21	9	1.8e-09	1.80E-09	9
GO:0007269	neurotransmitter secretion	122	23	2.1e-13	6.10E-09	23
GO:0048790	maintenance of presynaptic active zone s...	6	5	9.0e-08	9.00E-08	5
GO:0051298	centrosome duplication	85	15	9.0e-09	2.70E-07	15
GO:0008103	oocyte microtubule cytoskeleton polariza...	23	7	1.9e-06	1.90E-06	7
GO:0048172	regulation of short-term neuronal synapt...	5	4	2.7e-06	2.70E-06	4
GO:0006537	glutamate biosynthetic process	6	4	8.1e-06	8.10E-06	4
GO:0000281	mitotic cytokinesis	65	10	1.0e-05	1.00E-05	10
GO:0007317	regulation of pole plasm oskar mRNA loca...	29	7	1.0e-05	1.00E-05	7
GO:0015991	ATP hydrolysis coupled proton transport	40	8	1.1e-05	1.10E-05	8
GO:0009408	response to heat	87	11	2.5e-05	2.50E-05	11
GO:0008340	determination of adult lifespan	160	15	3.5e-05	3.50E-05	15
GO:0006414	translational elongation	24	6	3.7e-05	3.70E-05	6
GO:0006120	mitochondrial electron transport, NADH t...	35	7	3.9e-05	3.90E-05	7
GO:0045454	cell redox homeostasis	49	8	5.1e-05	5.10E-05	8
GO:0016082	synaptic vesicle priming	16	5	5.2e-05	5.20E-05	5
GO:0051130	positive regulation of cellular componen...	189	18	4.6e-06	5.50E-05	18
GO:0006108	malate metabolic process	9	4	6.3e-05	6.30E-05	4
GO:0007274	neuromuscular synaptic transmission	70	9	0.00012	0.00012	9
GO:0008104	protein localization	522	41	1.2e-09	0.00016	41
GO:0006119	oxidative phosphorylation	84	18	9.5e-12	0.00018	18
GO:0007009	plasma membrane organization	47	7	0.00027	0.00027	7
GO:0006886	intracellular protein transport	261	23	8.6e-07	0.00030	23
GO:0008360	regulation of cell shape	114	11	0.00030	0.00030	11
GO:0007520	myoblast fusion	48	7	0.00031	0.00031	7
GO:0009612	response to mechanical stimulus	48	7	0.00031	0.00031	7
GO:0000398	mRNA splicing, via spliceosome	270	25	1.1e-07	0.00033	25
GO:0051881	regulation of mitochondrial membrane pot...	6	3	0.00039	0.00039	3
GO:0000381	regulation of alternative mRNA splicing,...	65	8	0.00039	0.00039	8
GO:0007067	mitotic nuclear division	265	18	0.00039	0.00039	18
GO:0022900	electron transport chain	88	18	2.2e-11	0.00044	18
GO:0016183	synaptic vesicle coating	14	4	0.00045	0.00045	4
GO:0033227	dsRNA transport	25	5	0.00052	0.00052	5
GO:0045451	pole plasm oskar mRNA localization	68	13	3.3e-08	0.00057	13
GO:0048488	synaptic vesicle endocytosis	53	10	1.5e-06	0.00059	10
GO:0051533	positive regulation of NFAT protein impo...	15	4	0.00060	0.00060	4
GO:0007298	border follicle cell migration	125	11	0.00066	0.00066	11
GO:0030721	spectrosome organization	7	3	0.00066	0.00066	3
GO:0031629	synaptic vesicle fusion to presynaptic m...	7	3	0.00066	0.00066	3
GO:0055114	oxidation-reduction process	556	53	1.2e-15	0.00071	53
GO:1901215	negative regulation of neuron death	27	5	0.00075	0.00075	5
GO:0000028	ribosomal small subunit assembly	2	2	0.00075	0.00075	2
GO:0000447	endonucleolytic cleavage in ITS1 to sepa...	2	2	0.00075	0.00075	2
GO:0000461	endonucleolytic cleavage to generate mat...	2	2	0.00075	0.00075	2
GO:0006086	acetyl-CoA biosynthetic process from pyr...	2	2	0.00075	0.00075	2
GO:0042062	long-term strengthening of neuromuscular...	2	2	0.00075	0.00075	2

GO:0043525	positive regulation of neuron apoptotic ...	2	2	0.00075	0.00075	2
GO:0046598	positive regulation of viral entry into ...	2	2	0.00075	0.00075	2
GO:2000427	positive regulation of apoptotic cell cl...	2	2	0.00075	0.00075	2
GO:0007406	negative regulation of neuroblast prolif...	28	5	0.00089	0.00089	5
GO:0006090	pyruvate metabolic process	37	15	1.6e-14	0.00095	15
GO:0030865	cortical cytoskeleton organization	50	9	7.5e-06	0.00101	9

GO.ID	GO Cellular Component	Annotated	Significant	classic Fisher	Elim Fisher	Hits
GO:0005811	lipid particle	207	86	1.00E-30	1.00E-30	86
GO:0005875	microtubule associated complex	369	82	1.00E-30	1.00E-30	82
GO:0022627	cytosolic small ribosomal subunit	40	14	3.8e-12	3.80E-12	14
GO:0005737	cytoplasm	3313	250	1.00E-30	2.50E-11	250
GO:0005759	mitochondrial matrix	161	25	9.9e-12	3.40E-09	25
GO:0045169	fusome	36	11	4.3e-09	4.30E-09	11
GO:0008021	synaptic vesicle	71	14	1.7e-08	1.70E-08	14
GO:0030018	Z disc	33	10	2.4e-08	2.40E-08	10
GO:0043195	terminal bouton	42	11	2.6e-08	2.60E-08	11
GO:0022625	cytosolic large ribosomal subunit	54	12	4.5e-08	4.50E-08	12
GO:0031430	M band	9	6	5.2e-08	5.20E-08	6
GO:0071011	precatalytic spliceosome	147	18	3.6e-07	3.60E-07	18
GO:0071013	catalytic step 2 spliceosome	125	16	8.8e-07	8.80E-07	16
GO:0005739	mitochondrion	656	82	3.4e-30	9.90E-07	82
GO:0000275	mitochondrial proton-transporting ATP sy...	9	5	2.6e-06	2.60E-06	5
GO:0005829	cytosol	823	71	1.1e-16	2.70E-06	71
GO:0043025	neuronal cell body	66	11	3.4e-06	3.40E-06	11
GO:0005747	mitochondrial respiratory chain complex ...	49	9	1.2e-05	1.20E-05	9
GO:0005703	polytene chromosome puff	38	8	1.3e-05	1.30E-05	8
GO:0031594	neuromuscular junction	54	9	2.7e-05	2.70E-05	9
GO:0005743	mitochondrial inner membrane	193	37	5.1e-20	5.30E-05	37
GO:0048786	presynaptic active zone	16	5	7.6e-05	7.60E-05	5
GO:0070938	contractile ring	16	5	7.6e-05	7.60E-05	5
GO:0030122	AP-2 adaptor complex	4	3	0.00010	0.00010	3
GO:0098800	inner mitochondrial membrane protein com...	129	28	7.0e-17	0.00024	28
GO:0005853	eukaryotic translation elongation factor...	5	3	0.00025	0.00025	3
GO:0045254	pyruvate dehydrogenase complex	5	3	0.00025	0.00025	3
GO:0000221	vacuolar proton-transporting V-type ATPa...	13	4	0.00045	0.00045	4
GO:0045170	spectrosome	6	3	0.00049	0.00049	3
GO:0005874	microtubule	64	8	0.00059	0.00059	8
GO:0000276	mitochondrial proton-transporting ATP sy...	14	4	0.00061	0.00061	4
GO:0033181	plasma membrane proton-transporting V-ty...	14	4	0.00061	0.00061	4
GO:0098803	respiratory chain complex	87	17	5.7e-10	0.00064	17
GO:0005813	centrosome	98	10	0.00066	0.00066	10
GO:0005746	mitochondrial respiratory chain	88	17	6.8e-10	0.00078	17
GO:0045495	pole plasm	39	6	0.00095	0.00095	6
GO:0045172	germline ring canal	27	5	0.00107	0.00107	5
GO:0048471	perinuclear region of cytoplasm	55	7	0.00116	0.00116	7
GO:0005886	plasma membrane	933	56	2.7e-07	0.00127	56
GO:0005832	chaperonin-containing T-complex	8	3	0.00131	0.00131	3
GO:0005890	sodium:potassium-exchanging ATPase compl...	8	3	0.00131	0.00131	3
GO:0015629	actin cytoskeleton	107	16	9.9e-08	0.00143	16
GO:0030140	trans-Golgi network transport vesicle	9	3	0.00192	0.00192	3
GO:0008091	spectrin	3	2	0.00260	0.00260	2
GO:0031475	myosin V complex	3	2	0.00260	0.00260	2
GO:0035062	omega speckle	3	2	0.00260	0.00260	2
GO:0008541	proteasome regulatory particle, lid subc...	10	3	0.00269	0.00269	3

GO:0016460	myosin II complex	10	3	0.00269	0.00269	3
GO:0072686	mitotic spindle	35	5	0.00354	0.00354	5
GO:0044444	cytoplasmic part	2582	212	1.00E-30	0.00369	212
GO:0030424	axon	112	18	4.8e-09	0.00399	18
GO:0008540	proteasome regulatory particle, base sub...	12	3	0.00472	0.00472	3
GO:0019773	proteasome core complex, alpha-subunit c...	12	3	0.00472	0.00472	3

Table S3. GO analysis for potential mitochondrial GABA carriers

GO:0005741 mitochondrial outer membrane

Flybase ID	Gene	Candidate	Direct annotation
FBgn0031881	MME1	yes	acyl carnitine transport|mitochondrial transport|magnesium ion transmembrane transporter activity|magnesium ion transmembrane transport|magnesium ion export from mitochondrion|carnitine transport|carnitine:acyl carnitine antiporter activity|mitochondrial inner membrane|cellular magnesium ion homeostasis
FBgn0035568	CG18418	yes	alpha-ketoglutarate transport|oxoglutarate:malate antiporter activity|mitochondrial transport|mitochondrial inner membrane|malate transport
FBgn0035567	CG7514	yes	alpha-ketoglutarate transport|oxoglutarate:malate antiporter activity|mitochondrial transport|mitochondrial inner membrane|malate transport
FBgn0039674	CG1907	yes	alpha-ketoglutarate transport|oxoglutarate:malate antiporter activity|mitochondrial transport|mitochondrion|mitochondrial inner membrane|malate transport
FBgn0038376	Hmt-1	yes	ATP binding|ATPase activity, coupled to transmembrane movement of substances|heme transporter activity|integral component of membrane|response to cadmium ion|vacuolar membrane|mitochondrial inner membrane|heme transport
FBgn0030403	CG1824	yes	ATP binding|ATPase activity, coupled to transmembrane movement of substances|transmembrane transport|integral component of membrane|mitochondrial inner membrane|transporter activity
FBgn0023536	CG3156	yes	ATP binding|ATPase activity, coupled to transmembrane movement of substances|transmembrane transport|mitochondrial transport|heme biosynthetic process|integral component of membrane|transporter activity|mitochondrial inner membrane
FBgn0263026	CG43321	yes	biological_process|integral component of mitochondrial inner membrane|calcium import into the mitochondrion|uniplex complex|mitochondrial calcium ion homeostasis|cellular_component|molecular_function|mitochondrial calcium ion transmembrane transport
FBgn0039140	Miro	yes	cellular homeostasis|microtubule cytoskeleton organization|Rho protein signal transduction|mitochondrion organization|integral component of mitochondrial outer membrane|magnesium ion binding|GTP binding|protein binding|synaptic vesicle transport|mitochondrial outer membrane permeabilization|GTPase activity|mitochondrion transport along microtubule|calcium ion binding|mitochondrion|establishment of mitochondrion localization, microtubule-mediated|axonal transport of mitochondrion|regulation of mitochondrion organization|mitochondrion localization
FBgn0035244	ABCB7	yes	cellular iron ion homeostasis|ATP binding|ATPase activity, coupled to transmembrane movement of substances|transmembrane transport|heme transporter activity|integral component of membrane|mitochondrial inner membrane|heme transport|iron-sulfur cluster assembly
FBgn0260453	CG17140	yes	channel activity|transmembrane transport|mitochondrial outer membrane
FBgn0262467	Scox	yes	copper ion transport|cellular copper ion homeostasis|positive regulation of ATP biosynthetic process|mitochondrion|copper chaperone activity|cytochrome complex assembly|respiratory chain complex IV assembly|mitochondrial inner membrane
FBgn0033391	CG8026	yes	folic acid transport|folic acid transmembrane transporter activity|transmembrane transport|mitochondrial transport|FAD transmembrane transporter activity|mitochondrial inner membrane
FBgn0062440	EMRE	yes	integral component of mitochondrial inner membrane|calcium import into the mitochondrion|uniplex complex|positive regulation of innate immune response|defense response to Gram-negative bacterium|mitochondrial calcium ion homeostasis|mitochondrial calcium ion transmembrane transport

<table>
<tr><td>FBgn0037715</td><td>CG9399</td><td>yes</td><td>integral component of mitochondrial inner membrane|integral component of membrane|mitochondrial pyruvate transmembrane transport|pyruvate transmembrane transporter activity</td></tr>
<tr><td>FBgn0037714</td><td>CG9396</td><td>yes</td><td>integral component of mitochondrial inner membrane|integral component of membrane|mitochondrial pyruvate transmembrane transport|pyruvate transmembrane transporter activity</td></tr>
<tr><td>FBgn0052832</td><td>CG32832</td><td>yes</td><td>integral component of mitochondrial inner membrane|mitochondrial pyruvate transmembrane transport|pyruvate transmembrane transporter activity</td></tr>
<tr><td>FBgn0038662</td><td>Mpc1</td><td>yes</td><td>integral component of mitochondrial inner membrane|mitochondrion|mitochondrial pyruvate transmembrane transport|pyruvate metabolic process|pyruvate transmembrane transporter activity</td></tr>
<tr><td>FBgn0042185</td><td>MCU</td><td>yes</td><td>integral component of mitochondrial inner membrane|uniplex complex|calcium import into the mitochondrion|anesthesia-resistant memory|calcium channel activity|mitochondrion|medium-term memory|mitochondrial calcium ion homeostasis|uniporter activity|mitochondrial calcium ion transmembrane transport</td></tr>
<tr><td>FBgn0019830</td><td>colt</td><td>yes</td><td>liquid clearance, open tracheal system|acyl carnitine transport|mitochondrial transport|epithelial cell morphogenesis|integral component of membrane|carnitine transport|carnitine:acyl carnitine antiporter activity|mitochondrial inner membrane</td></tr>
<tr><td>FBgn0036756</td><td>Cln3</td><td>yes</td><td>lysosome organization|regulation of Notch signaling pathway|determination of adult lifespan|late endosome|regulation of JNK cascade|lysosome|response to oxidative stress|microvillus membrane|regulation of intracellular pH|mitochondrial membrane|arginine transport|vesicle|apical plasma membrane</td></tr>
<tr><td>FBgn0037970</td><td>GC2</td><td>yes</td><td>malate-aspartate shuttle|L-aspartate transmembrane transporter activity|L-glutamate transmembrane transport|mitochondrial inner membrane|high-affinity glutamate transmembrane transporter activity|aspartate transmembrane transport|L-glutamate transmembrane transporter activity</td></tr>
<tr><td>FBgn0260743</td><td>GC1</td><td>yes</td><td>malate-aspartate shuttle|L-aspartate transmembrane transporter activity|L-glutamate transmembrane transport|mitochondrial inner membrane|high-affinity glutamate transmembrane transporter activity|aspartate transmembrane transport|L-glutamate transmembrane transporter activity</td></tr>
<tr><td>FBgn0033413</td><td>prel</td><td>yes</td><td>mitochondrial intermembrane space|mitochondrion morphogenesis|mitochondrial crista|mitochondrion|phospholipid transport|phosphatidic acid transporter activity|dendrite morphogenesis</td></tr>
<tr><td>FBgn0030218</td><td>CG1628</td><td>yes</td><td>mitochondrial L-ornithine transmembrane transport|L-ornithine transmembrane transporter activity|amino acid transmembrane transporter activity|mitochondrial inner membrane|amino acid transmembrane transport</td></tr>
<tr><td>FBgn0284252</td><td>Letm1</td><td>yes</td><td>mitochondrial membrane|potassium ion transmembrane transport|mitochondrion morphogenesis|potassium:proton antiporter activity|calcium ion binding|ribosome binding|mitochondrion|proton transmembrane transport|cellular response to hypoxia|calcium:sodium antiporter activity|mitochondrial calcium ion transmembrane transport|neurotransmitter secretion</td></tr>
<tr><td>FBgn0067783</td><td>DPCoAC</td><td>yes</td><td>mitochondrial transmembrane transport|defense response to Gram-negative bacterium|positive regulation of innate immune response|antiporter activity|integral component of mitochondrial membrane|integral component of membrane</td></tr>
<tr><td>FBgn0039561</td><td>mfrn</td><td>yes</td><td>multicellular organismal iron ion homeostasis|iron ion transmembrane transporter activity|mitochondrion|spermatid differentiation|iron import into the mitochondrion|mitochondrial inner membrane</td></tr>
<tr><td>FBgn0003360</td><td>sesB</td><td>yes</td><td>muscle cell cellular homeostasis|transmembrane transport|locomotion|ATP:ADP antiporter activity|determination of adult lifespan|positive regulation of ATP biosynthetic process|regulation of cytosolic calcium ion concentration|chemical synaptic transmission|mitochondrial inner membrane|neuron cellular homeostasis|synaptic growth at neuromuscular junction|mitochondrial transport|synaptic vesicle transport|oogenesis|negative regulation of autophagy|mitochondrial calcium ion homeostasis|mitochondrion|cellular response to oxidative stress|action potential|ATP transport|ADP transport|regulation of mitochondrial depolarization</td></tr>
<tr><td>FBgn0034497</td><td>Mpcp1</td><td>yes</td><td>phosphate ion transmembrane transporter activity|inorganic phosphate transmembrane transporter activity|integral component of mitochondrial inner membrane|phosphate ion transport|mitochondrial envelope|phosphate ion transmembrane transport</td></tr>
<tr><td>FBgn0026409</td><td>Mpcp2</td><td>yes</td><td>phosphate ion transmembrane transporter activity|inorganic phosphate transmembrane transporter activity|integral component of mitochondrial inner membrane|phosphate ion transport|mitochondrion|wing disc dorsal/ventral pattern formation|mitochondrial envelope|phosphate ion transmembrane transport</td></tr>
</table>

FBgn0003353	sei	yes	potassium ion transport|sensory perception of sound|voltage-gated potassium channel activity|integral component of plasma membrane|transmembrane transport|regulation of membrane potential|potassium ion transmembrane transport|voltage-gated potassium channel complex|voltage-gated cation channel activity
FBgn0035473	mge	yes	P-P-bond-hydrolysis-driven protein transmembrane transporter activity|mitochondrion|mitochondrial outer membrane translocase complex
FBgn0036199	Bmcp	yes	sulfate transport|transmembrane transport|transmembrane transporter activity|antiporter activity|oxaloacetate transmembrane transporter activity|succinate transmembrane transporter activity|malate transmembrane transporter activity|mitochondrial inner membrane|sensory perception of sound|thiosulfate transport|oxaloacetate transport|regulation of metabolic process|succinate transmembrane transport|malate transmembrane transport|phosphate ion transmembrane transport|thiosulfate transmembrane transporter activity|sulfate transmembrane transporter activity
FBgn0037852	Tpc1	yes	thiamine transmembrane transporter activity|integral component of mitochondrial inner membrane|antiporter activity|mitochondrial thiamine pyrophosphate transmembrane transport|thiamine pyrophosphate transmembrane transport
JniProtKB:Q9W0Y	Tpc2	yes	thiamine transmembrane transporter activity|integral component of mitochondrial inner membrane|thiamine pyrophosphate transmembrane transport
FBgn0025111	Ant2	yes	transmembrane transport|ATP:ADP antiporter activity|ATP transport|ADP transport|mitochondrial inner membrane
FBgn0260454	CG17139	yes	transmembrane transport|mitochondrial outer membrane
FBgn0000535	eag	yes	transmembrane transport|potassium ion transmembrane transport|voltage-gated potassium channel complex|perineurial glial growth|regulation of heart contraction|voltage-gated cation channel activity|learning|plasma membrane|learning or memory|potassium ion transport|phosphorelay sensor kinase activity|voltage-gated potassium channel activity|integral component of plasma membrane|regulation of membrane potential|phosphorelay signal transduction system|courtship behavior|sensory perception of smell|behavioral response to ether|protein complex oligomerization
FBgn0039357	CG4743	yes	transmembrane transport|S-adenosyl-L-methionine transmembrane transporter activity|S-adenosyl-L-methionine transport|mitochondrial inner membrane
FBgn0069354	Porin2	yes	voltage-gated anion channel activity|ion transport|porin activity|mitochondrial transport|anion transmembrane transport|mitochondrion|cation channel activity|mitochondrial outer membrane
FBgn0004363	porin	yes	voltage-gated anion channel activity|ion transport|sperm individualization|mitochondrial transport|anion transmembrane transport|mitochondrion|sperm mitochondrion organization|mitochondrial outer membrane|phototransduction|mitochondrion organization|Nebenkern
FBgn0028646	aralar1	yes	wound healing|identical protein binding|malate-aspartate shuttle|mitochondrial transport|transmembrane transporter activity|calcium ion binding|mitochondrion|L-aspartate transmembrane transporter activity|L-glutamate transmembrane transport|mitochondrial inner membrane|aspartate transmembrane transport|L-glutamate transmembrane transporter activity
Excluded from the screening			
FBgn0266599	Hsc70-4	protein	ATPase activity|chaperone-mediated protein folding|nervous system development|axon guidance|late endosomal microautophagy|response to unfolded protein|axonal fasciculation|mRNA splicing, via spliceosome|ATP binding|vesicle-mediated transport|protein binding involved in protein folding|cellular response to heat|embryonic development via the syncytial blastoderm|catalytic step 2 spliceosome|perichromatin fibrils|precatalytic spliceosome|ovarian follicle cell development|chaperone binding|cytosol|cellular response to unfolded protein|heterochromatin organization involved in chromatin silencing|misfolded protein binding|membrane organization|heat shock protein binding|chaperone cofactor-dependent protein refolding|unfolded protein
FBgn0265265	CG32727	protein	biological_process|protein import into mitochondrial matrix|PAM complex, Tim23 associated import motor|protein transporter activity|cellular_component|ATPase activator activity|molecular_function
FBgn0027360	Tim10	protein	defense response to Gram-negative bacterium|mitochondrial intermembrane space protein transporter complex|protein import into mitochondrial inner membrane|protein transporter activity|negative regulation of innate immune response|TIM22 mitochondrial import inner membrane insertion complex|mitochondrial inner membrane

FBgn0036928	Tom20	protein	protein targeting to mitochondrion|integral component of mitochondrial outer membrane|mitochondrion targeting sequence binding|mitochondrial outer membrane translocase complex assembly|protein transmembrane transporter activity|protein import into mitochondrial matrix|P-P-bond-hydrolysis-driven protein transmembrane transporter activity|mitochondrion|tRNA import into mitochondrion|mitochondrial outer membrane translocase complex
FBgn0037828	tomboy20	protein	protein targeting to mitochondrion|mitochondrion targeting sequence binding|integral component of mitochondrial outer membrane|mitochondrial outer membrane translocase complex assembly|protein transmembrane transporter activity|protein import into mitochondrial matrix|P-P-bond-hydrolysis-driven protein transmembrane transporter activity|tRNA import into mitochondrion|mitochondrial outer membrane translocase complex
FBgn0051229	CG31229	protein	protein targeting to mitochondrion|mitochondrion targeting sequence binding|TIM23 mitochondrial import inner membrane translocase complex|protein transmembrane transporter activity|P-P-bond-hydrolysis-driven protein transmembrane transporter activity|protein import into mitochondrial inner membrane|TIM22 mitochondrial import inner membrane insertion complex
FBgn0032397	Tom70	protein	protein targeting to mitochondrion|P-P-bond-hydrolysis-driven protein transmembrane transporter activity|mitochondrial outer membrane translocase complex
FBgn0033357	Tom7	protein	protein targeting to mitochondrion|P-P-bond-hydrolysis-driven protein transmembrane transporter activity|mitochondrial outer membrane translocase complex
FBgn0033074	tomboy40	protein	protein targeting to mitochondrion|protein import into mitochondrial matrix|protein transmembrane transporter activity|P-P-bond-hydrolysis-driven protein transmembrane transporter activity|mitochondrial intermembrane space protein transporter complex|mitochondrion|mitochondrial outer membrane translocase complex
FBgn0016041	Tom40	protein	protein targeting to mitochondrion|protein transmembrane transporter activity|protein import into mitochondrial matrix|P-P-bond-hydrolysis-driven protein transmembrane transporter activity|mitochondrion|cellular response to hypoxia|mitochondrial outer membrane translocase complex
FBgn0263977	Tim17b	protein	protein targeting to mitochondrion|TIM23 mitochondrial import inner membrane translocase complex|integral component of mitochondrial inner membrane|protein import into mitochondrial matrix|protein transmembrane transporter activity|mitochondrion
FBgn0038018	Tim17a1	protein	protein targeting to mitochondrion|TIM23 mitochondrial import inner membrane translocase complex|integral component of mitochondrial inner membrane|protein import into mitochondrial matrix|protein transmembrane transporter activity|P-P-bond-hydrolysis-driven protein transmembrane transporter activity
FBgn0037307	Tim17a2	protein	protein targeting to mitochondrion|TIM23 mitochondrial import inner membrane translocase complex|integral component of mitochondrial inner membrane|protein import into mitochondrial matrix|protein transmembrane transporter activity|P-P-bond-hydrolysis-driven protein transmembrane transporter activity
FBgn0031164	CG1724	protein	protein targeting to mitochondrion|TIM23 mitochondrial import inner membrane translocase complex|integral component of mitochondrial inner membrane|protein transmembrane transporter activity|protein import into mitochondrial matrix|P-P-bond-hydrolysis-driven protein transmembrane transporter activity
FBgn0037310	Tim17b1	protein	protein targeting to mitochondrion|TIM23 mitochondrial import inner membrane translocase complex|integral component of mitochondrial inner membrane|protein transmembrane transporter activity|protein import into mitochondrial matrix|P-P-bond-hydrolysis-driven protein transmembrane transporter activity
FBgn0020371	Tim17b2	protein	protein targeting to mitochondrion|TIM23 mitochondrial import inner membrane translocase complex|integral component of mitochondrial inner membrane|protein transmembrane transporter activity|protein import into mitochondrial matrix|P-P-bond-hydrolysis-driven protein transmembrane transporter activity
FBgn0027359	Tim8	protein	protein targeting to mitochondrion|TIM23 mitochondrial import inner membrane translocase complex|mitochondrial intermembrane space|P-P-bond-hydrolysis-driven protein transmembrane transporter activity|chaperone-mediated protein transport|mitochondrion
FBgn0030480	Tim9a	protein	protein targeting to mitochondrion|TIM23 mitochondrial import inner membrane translocase complex|P-P-bond-hydrolysis-driven protein transmembrane transporter activity
FBgn0027358	Tim9b	protein	protein targeting to mitochondrion|TIM23 mitochondrial import inner membrane translocase complex|P-P-bond-hydrolysis-driven protein transmembrane transporter activity|mitochondrial intermembrane space protein transporter complex|cellular response to hypoxia
FBgn0036204	Tim13	protein	protein targeting to mitochondrion|TIM23 mitochondrial import inner membrane translocase complex|P-P-bond-hydrolysis-driven protein transmembrane transporter activity|mitochondrial intermembrane space protein transporter complex|protein import into mitochondrial inner membrane|protein transporter activity
FBgn0038683	CG11779	protein	protein targeting to mitochondrion|TIM23 mitochondrial import inner membrane translocase complex|protein import into mitochondrial matrix|P-P-bond-hydrolysis-driven protein transmembrane transporter activity|chaperone binding|cellular response to hypoxia|mitochondrial inner membrane

FBgn0038355	CG4520	protein	protein transmembrane transporter activity|protein import into mitochondrial matrix|mitochondrial outer membrane translocase complex
FBgn0267976	Tim23	protein	TIM23 mitochondrial import inner membrane translocase complex|integral component of mitochondrial inner membrane|protein import into mitochondrial matrix|protein transmembrane transporter activity
FBgn0036173	CG7394	protein	TIM23 mitochondrial import inner membrane translocase complex|protein import into mitochondrial matrix|PAM complex, Tim23 associated import motor|protein transporter activity|ATPase activator activity
FBgn0014391	sun	H+	ATPase activity|mitochondrial proton-transporting ATP synthase complex, catalytic core F(1)|G protein-coupled receptor binding|response to oxidative stress|extracellular space|protein binding|determination of adult lifespan|proton transmembrane transport|ATP synthesis coupled proton transport|mitochondrial inner membrane|positive regulation of G protein-coupled receptor signaling pathway|proton-transporting ATP synthase activity, rotational mechanism
FBgn0051477	TPsynepsilor	H+	ATPase activity|mitochondrial proton-transporting ATP synthase complex, catalytic core F(1)|proton transmembrane transport|ATP synthesis coupled proton transport|mitochondrial inner membrane|proton-transporting ATP synthase activity, rotational mechanism
FBgn0031108	CG15459	H+	biological_process|molecular_function|mitochondrial proton-transporting ATP synthase complex
FBgn0040651	CG15458	H+	biological_process|molecular_function|mitochondrial proton-transporting ATP synthase complex
FBgn0083167	Neb-cGP	H+	extracellular space|hormone activity|regulation of growth|mitochondrial proton-transporting ATP synthase complex
FBgn0035805	CG7506	H+	mitochondrial proton-transporting ATP synthase complex assembly|integral component of mitochondrial membrane
FBgn0036568	ATPsynbetaL	H+	mitochondrial proton-transporting ATP synthase complex, catalytic core F(1)|ATP binding|determination of adult lifespan|proton transmembrane transport|spermatid differentiation|proton-transporting ATPase activity, rotational mechanism|regulation of proton transport|ATP synthesis coupled proton transport|proton-transporting ATP synthase activity, rotational mechanism
FBgn0010217	ATPsynbeta	H+	mitochondrial proton-transporting ATP synthase complex, catalytic core F(1)|ATP binding|mitochondrion|proton transmembrane transport|proton-transporting ATPase activity, rotational mechanism|ATP synthesis coupled proton transport|proton-transporting ATP synthase activity, rotational mechanism
FBgn0028342	ATPsyndelta	H+	mitochondrial proton-transporting ATP synthase complex, catalytic core F(1)|mitochondrion|proton transmembrane transport|ATP synthesis coupled proton transport|proton-transporting ATP synthase activity, rotational mechanism
FBgn0020235	TPsyngamm	H+	mitochondrial proton-transporting ATP synthase complex, catalytic core F(1)|mitochondrion|proton transmembrane transport|proton-transporting ATPase activity, rotational mechanism|ATP biosynthetic process|ATP synthesis coupled proton transport|proton-transporting ATP synthase activity, rotational mechanism
FBgn0039830	ATPsynC	H+	mitochondrial proton-transporting ATP synthase complex, coupling factor F(o)|ATP hydrolysis coupled proton transport|proton-transporting ATP synthase complex, coupling factor F(o)|proton transmembrane transport|ATP synthesis coupled proton transport|proton-transporting ATP synthase activity, rotational mechanism
FBgn0031941	ATPsynGL	H+	mitochondrial proton-transporting ATP synthase complex, coupling factor F(o)|ATP metabolic process|ATP synthesis coupled proton transport|proton-transporting ATP synthase activity, rotational mechanism
FBgn0036345	mel\CG1730	H+	mitochondrial proton-transporting ATP synthase complex, coupling factor F(o)|ATP synthesis coupled proton transport|proton-transporting ATP synthase activity, rotational mechanism
FBgn0035032	ATPsynF	H+	mitochondrial proton-transporting ATP synthase complex, coupling factor F(o)|ATPase activity|mitochondrion|proton transmembrane transport

FBgn0035585	ATPsynCF6L	H+	mitochondrial proton-transporting ATP synthase complex, coupling factor F(o)|ATPase activity|proton transmembrane transporter activity|ATP metabolic process|ATP synthesis coupled proton transport
FBgn0019644	ATPsynB	H+	mitochondrial proton-transporting ATP synthase complex, coupling factor F(o)|mitochondrion|proton transmembrane transport|ATP synthesis coupled proton transport|proton-transporting ATP synthase activity, rotational mechanism
FBgn0013672	mt:ATPase6	H+	mitochondrial proton-transporting ATP synthase complex, coupling factor F(o)|neuron cellular homeostasis|muscle cell cellular homeostasis|locomotion|determination of adult lifespan|mitochondrion|proton transmembrane transport|proton-exporting ATPase activity, phosphorylative mechanism|mitochondrial ATP synthesis coupled proton transport|ATP synthesis coupled proton transport|proton-transporting ATP synthase activity, rotational mechanism
FBgn0010612	ATPsynG	H+	mitochondrial proton-transporting ATP synthase complex, coupling factor F(o)|proton transmembrane transport|ATP synthesis coupled proton transport|proton-transporting ATP synthase activity, rotational mechanism
FBgn0038224	ATPsynE	H+	mitochondrial proton-transporting ATP synthase complex, coupling factor F(o)|proton transmembrane transport|ATP synthesis coupled proton transport|proton-transporting ATP synthase activity, rotational mechanism
FBgn0034081	CG10731	H+	mitochondrial proton-transporting ATP synthase complex, coupling factor F(o)|proton transmembrane transport|molecular_function
FBgn0013673	mt:ATPase8	H+	mitochondrial proton-transporting ATP synthase complex, coupling factor F(o)|proton transmembrane transporter activity|ATP synthesis coupled proton transport
FBgn0016120	ATPsynD	H+	mitochondrial proton-transporting ATP synthase complex, coupling factor F(o)|response to oxidative stress|mitochondrial proton-transporting ATP synthase, stator stalk|regulation of mitochondrial membrane potential|negative regulation of ERK1 and ERK2 cascade|determination of adult lifespan|mitochondrion|ATP metabolic process|proton transmembrane transport|negative regulation of TOR signaling|ATP synthesis coupled proton transport|proton-transporting ATP synthase activity, rotational mechanism
FBgn0016119	ATPsynCF6	H+	mitochondrial proton-transporting ATP synthase, central stalk|mitochondrial proton-transporting ATP synthase complex, coupling factor F(o)|ATPase activity|proton transmembrane transporter activity|mitochondrion|proton transmembrane transport|ATP synthesis coupled proton transport
FBgn0016691	ATPsynO	H+	mitochondrial proton-transporting ATP synthase, central stalk|mitochondrion|proton transmembrane transport|mitochondrial ATP synthesis coupled proton transport|proton-transporting ATP synthase activity, rotational mechanism
FBgn0034133	CG7813-RA	H+	mitochondrial proton-transporting ATP synthase, stator stalk|ATP synthesis coupled proton transport|proton-transporting ATP synthase activity, rotational mechanism
FBgn0031757	Ucp4C	H+	response to cold|oxidative phosphorylation uncoupler activity|proton transmembrane transport|mitochondrial inner membrane
FBgn0031758	Ucp4B	H+	response to cold|proton transmembrane transport|oxidative phosphorylation uncoupler activity|mitochondrial inner membrane
FBgn0030872	Ucp4A	H+	response to oxidative stress|response to cold|oxidative phosphorylation uncoupler activity|proton transmembrane transport|mitochondrial inner membrane
FBgn0036222	SdhAL	electron	anaerobic respiration|plasma membrane succinate dehydrogenase complex|succinate dehydrogenase (ubiquinone) activity|mitochondrial respiratory chain complex II, succinate dehydrogenase complex (ubiquinone)|flavin adenine dinucleotide binding|electron transfer activity|respiratory electron transport chain|mitochondrial electron transport, succinate to ubiquinone|tricarboxylic acid cycle|succinate dehydrogenase activity
FBgn0011211	blw	electron	ATPase activity|lipid storage|electron transport chain|ADP binding|regulation of choline O-acetyltransferase activity|ATP biosynthetic process|proton-transporting ATP synthase activity, rotational mechanism|mitochondrial proton-transporting ATP synthase complex, catalytic core F(1)|ATP binding|response to oxidative stress|mitochondrion|ATP metabolic process|ATP synthesis coupled proton transport
FBgn0032833	COX4	electron	cell proliferation|cytochrome-c oxidase activity|negative regulation of neuroblast proliferation|Golgi organization|mitochondrion|mitochondrial electron transport, cytochrome c to oxygen|mitochondrial respiratory chain complex IV|mitotic cell cycle

FBgn0013675	mt:CoII	electron	cytochrome-c oxidase activity|copper ion binding|integral component of membrane|ATP synthesis coupled electron transport|mitochondrial respiratory chain complex IV
FBgn0034877	levy	electron	cytochrome-c oxidase activity|determination of adult lifespan|regulation of catalytic activity|mitochondrial electron transport, cytochrome c to oxygen|aerobic respiration|mitochondrial respiratory chain complex IV|enzyme regulator activity
FBgn0036830	VIa	electron	cytochrome-c oxidase activity|mitochondrial electron transport, cytochrome c to oxygen|aerobic respiration|mitochondrial respiratory chain complex IV|enzyme regulator activity
iProtKB:A0A0B4LF	CG44296	electron	cytochrome-c oxidase activity|mitochondrial electron transport, cytochrome c to oxygen|mitochondrial respiratory chain complex IV
FBgn0033020	COX4L	electron	cytochrome-c oxidase activity|mitochondrial electron transport, cytochrome c to oxygen|mitochondrial respiratory chain complex IV
FBgn0031831	COX5BL	electron	cytochrome-c oxidase activity|mitochondrial electron transport, cytochrome c to oxygen|mitochondrial respiratory chain complex IV|mitochondrial ATP synthesis coupled proton transport
FBgn0031830	COX5B	electron	cytochrome-c oxidase activity|mitochondrial electron transport, cytochrome c to oxygen|mitochondrial respiratory chain complex IV|mitochondrial ATP synthesis coupled proton transport
FBgn0037579	COX7AL	electron	cytochrome-c oxidase activity|mitochondrial respiratory chain supercomplex|regulation of oxidative phosphorylation|mitochondrial electron transport, cytochrome c to oxygen|mitochondrial respiratory chain supercomplex assembly|mitochondrial respiratory chain complex IV
FBgn0085201	CG34172	electron	cytochrome-c oxidase activity|mitochondrial respiratory chain|regulation of oxidative phosphorylation|mitochondrial respiratory chain supercomplex|mitochondrial respiratory chain supercomplex assembly
FBgn0050093	COX6AL	electron	cytochrome-c oxidase activity|mitochondrion|mitochondrial electron transport, cytochrome c to oxygen|aerobic respiration|mitochondrial respiratory chain complex IV|enzyme regulator activity
FBgn0015031	cype	electron	cytochrome-c oxidase activity|mitochondrion|mitochondrial electron transport, cytochrome c to oxygen|mitochondrial respiratory chain complex IV
FBgn0040773	COX7C	electron	cytochrome-c oxidase activity|negative regulation of neuroblast proliferation|mitochondrial electron transport, cytochrome c to oxygen|mitochondrial respiratory chain complex IV
FBgn0019624	COX5A	electron	cytochrome-c oxidase activity|negative regulation of neuroblast proliferation|mitochondrion|mitochondrial electron transport, cytochrome c to oxygen|positive regulation of cell cycle|mitochondrial respiratory chain complex IV
FBgn0034938	CG3803	electron	cytochrome-c oxidase activity|oxidoreductase activity, acting on the CH-CH group of donors|integral component of membrane|heme a biosynthetic process|oxidation-reduction process|oxidoreductase activity, acting on NAD(P)H, heme protein as acceptor|respiratory chain complex IV assembly|mitochondrial inner membrane
FBgn0013676	mt:CoIII	electron	cytochrome-c oxidase activity|oxidoreduction-driven active transmembrane transporter activity|electron transfer activity|membrane|mitochondrion|mitochondrial electron transport, cytochrome c to oxygen|aerobic respiration|mitochondrial respiratory chain complex IV|aerobic electron transport chain
FBgn0040529	COX7A	electron	cytochrome-c oxidase activity|regulation of oxidative phosphorylation|mitochondrial respiratory chain supercomplex|mitochondrion|mitochondrial electron transport, cytochrome c to oxygen|mitochondrial respiratory chain supercomplex assembly|mitochondrial respiratory chain complex IV
FBgn0013674	mt:CoI	electron	cytochrome-c oxidase activity|respiratory chain complex IV|electron transport coupled proton transport|integral component of membrane|mitochondrial electron transport, cytochrome c to oxygen|aerobic respiration|mitochondrial respiratory chain complex IV|heme binding
FBgn0039651	Cyt-c1L	electron	electron transporter, transferring electrons within CoQH2-cytochrome c reductase complex activity|mitochondrial respiratory chain complex III|mitochondrial electron transport, ubiquinol to cytochrome c|mitochondrial ATP synthesis coupled proton transport|heme binding

FBgn0035600	Cyt-c1	electron	electron transporter, transferring electrons within CoQH2-cytochrome c reductase complex activity|mitochondrion|mitochondrial respiratory chain complex III|mitochondrial electron transport, ubiquinol to cytochrome c|mitochondrial ATP synthesis coupled proton transport|heme binding
FBgn0044419	Pmi	electron	integral component of mitochondrial inner membrane|mitochondrion morphogenesis|inner mitochondrial membrane organization|mitochondrial ATP synthesis coupled electron transport|molecular_function|mitochondrial inner membrane|mitochondrion organization
FBgn0086907	Cyt-c-d	electron	mitochondrial intermembrane space|oxidative phosphorylation|sperm individualization|electron transfer activity|mitochondrion|mitochondrial electron transport, cytochrome c to oxygen|cytosol|activation of cysteine-type endopeptidase activity involved in apoptotic process|mitochondrial electron transport, ubiquinol to cytochrome c|mitochondrial inner membrane|heme binding|regulation of compound eye retinal cell programmed cell death
FBgn0030975	SdhBL	electron	mitochondrial membrane|electron transfer activity|respiratory electron transport chain|tricarboxylic acid cycle|mitochondrial electron transport, succinate to ubiquinone|aerobic respiration|2 iron, 2 sulfur cluster binding
FBgn0034251	ND-51L1	electron	mitochondrial respiratory chain complex I|FMN binding|NAD binding|mitochondrial electron transport, NADH to ubiquinone|NADH dehydrogenase (ubiquinone) activity|4 iron, 4 sulfur cluster binding
FBgn0031684	ND-13A	electron	mitochondrial respiratory chain complex I|mitochondrial electron transport, NADH to ubiquinone|mitochondrion|respiratory electron transport chain
FBgn0013680	mt:ND2	electron	mitochondrial respiratory chain complex I|mitochondrial electron transport, NADH to ubiquinone|NADH dehydrogenase (ubiquinone) activity
FBgn0037172	ND-B14.5AL	electron	mitochondrial respiratory chain complex I|mitochondrial electron transport, NADH to ubiquinone|NADH dehydrogenase (ubiquinone) activity
FBgn0034007	ND-51L2	electron	mitochondrial respiratory chain complex I|multicellular organism reproduction|extracellular space|NADH dehydrogenase activity|mitochondrial electron transport, NADH to ubiquinone|4 iron, 4 sulfur cluster binding
FBgn0031021	ND-18	electron	mitochondrial respiratory chain complex I|NADH dehydrogenase (ubiquinone) activity|electron transport chain|mitochondrial respiratory chain complex I assembly
FBgn0037001	ND-39	electron	mitochondrial respiratory chain complex I|NADH dehydrogenase activity|coenzyme binding|mitochondrial electron transport, NADH to ubiquinone|ubiquinone-6 biosynthetic process
FBgn0052230	ND-MLRQ	electron	mitochondrial respiratory chain complex I|NADH dehydrogenase activity|cytochrome-c oxidase activity|mitochondrial electron transport, NADH to ubiquinone|mitochondrial respiratory chain complex IV
FBgn0031771	ND-51	electron	mitochondrial respiratory chain complex I|NADH dehydrogenase activity|FMN binding|mitochondrial electron transport, NADH to ubiquinone|NAD binding|NADH dehydrogenase (ubiquinone) activity|4 iron, 4 sulfur cluster binding
FBgn0032511	ND-B22	electron	mitochondrial respiratory chain complex I|NADH dehydrogenase activity|mitochondrial electron transport, NADH to ubiquinone
FBgn0031228	ND-15	electron	mitochondrial respiratory chain complex I|NADH dehydrogenase activity|mitochondrial electron transport, NADH to ubiquinone
FBgn0029971	ND-MNLL	electron	mitochondrial respiratory chain complex I|NADH dehydrogenase activity|mitochondrial electron transport, NADH to ubiquinone
FBgn0047038	ND-13B	electron	mitochondrial respiratory chain complex I|NADH dehydrogenase activity|mitochondrial electron transport, NADH to ubiquinone
FBgn0035046	ND-19	electron	mitochondrial respiratory chain complex I|NADH dehydrogenase activity|mitochondrial electron transport, NADH to ubiquinone

FBgn0001989	ND-B17	electron	mitochondrial respiratory chain complex I|NADH dehydrogenase activity|mitochondrial electron transport, NADH to ubiquinone
FBgn0029868	ND-B16.6	electron	mitochondrial respiratory chain complex I|NADH dehydrogenase activity|mitochondrial electron transport, NADH to ubiquinone
FBgn0040705	ND-B8	electron	mitochondrial respiratory chain complex I|NADH dehydrogenase activity|mitochondrial electron transport, NADH to ubiquinone
FBgn0019957	ND-42	electron	mitochondrial respiratory chain complex I|NADH dehydrogenase activity|mitochondrial electron transport, NADH to ubiquinone|cytoplasm|mitochondrion|NADH dehydrogenase (ubiquinone) activity
FBgn0011455	ND-SGDH	electron	mitochondrial respiratory chain complex I|NADH dehydrogenase activity|mitochondrial electron transport, NADH to ubiquinone|determination of adult lifespan|mitochondrion|response to reactive oxygen species
FBgn0262952	mt:ND4	electron	mitochondrial respiratory chain complex I|NADH dehydrogenase activity|mitochondrial electron transport, NADH to ubiquinone|electron transport coupled proton transport|NADH dehydrogenase (ubiquinone) activity|ubiquinone binding|aerobic respiration
FBgn0034645	ND-B12	electron	mitochondrial respiratory chain complex I|NADH dehydrogenase activity|mitochondrial electron transport, NADH to ubiquinone|mitochondrial respiratory chain complex I assembly
FBgn0021967	ND-PDSW	electron	mitochondrial respiratory chain complex I|NADH dehydrogenase activity|mitochondrial electron transport, NADH to ubiquinone|mitochondrion
FBgn0033570	ND-B14	electron	mitochondrial respiratory chain complex I|NADH dehydrogenase activity|mitochondrial electron transport, NADH to ubiquinone|mitochondrion
FBgn0017567	ND-23	electron	mitochondrial respiratory chain complex I|NADH dehydrogenase activity|mitochondrial electron transport, NADH to ubiquinone|mitochondrion|4 iron, 4 sulfur cluster binding|mitochondrial respiratory chain complex I assembly|aerobic respiration
FBgn0030853	ND-24	electron	mitochondrial respiratory chain complex I|NADH dehydrogenase activity|mitochondrial electron transport, NADH to ubiquinone|mitochondrion|NADH dehydrogenase (ubiquinone) activity
FBgn0033961	ND-B15	electron	mitochondrial respiratory chain complex I|NADH dehydrogenase activity|mitochondrial electron transport, NADH to ubiquinone|mitochondrion|NADH dehydrogenase (ubiquinone) activity
FBgn0029888	ND-ASHI	electron	mitochondrial respiratory chain complex I|NADH dehydrogenase activity|mitochondrial electron transport, NADH to ubiquinone|NADH dehydrogenase (ubiquinone) activity
FBgn0030605	ND-B18	electron	mitochondrial respiratory chain complex I|NADH dehydrogenase activity|mitochondrial electron transport, NADH to ubiquinone|NADH dehydrogenase (ubiquinone) activity
FBgn0036706	ND-24L	electron	mitochondrial respiratory chain complex I|NADH dehydrogenase activity|mitochondrial electron transport, NADH to ubiquinone|NADH dehydrogenase (ubiquinone) activity
FBgn0025839	ND-B14.5A	electron	mitochondrial respiratory chain complex I|NADH dehydrogenase activity|mitochondrial electron transport, NADH to ubiquinone|NADH dehydrogenase (ubiquinone) activity
FBgn0031505	ND-B14.5B	electron	mitochondrial respiratory chain complex I|NADH dehydrogenase activity|mitochondrial electron transport, NADH to ubiquinone|NADH dehydrogenase (ubiquinone) activity
FBgn0030718	ND-20	electron	mitochondrial respiratory chain complex I|NADH dehydrogenase activity|quinone binding|mitochondrial electron transport, NADH to ubiquinone|electron transport coupled proton transport|determination of adult lifespan|NADH dehydrogenase (ubiquinone) activity|regulation of terminal button organization|4 iron, 4 sulfur cluster binding|mitochondrial respiratory chain complex I assembly|response to reactive oxygen species|aerobic respiration

<table>
<tr><td>FBgn0039669</td><td>ND-20L</td><td>electron</td><td>mitochondrial respiratory chain complex I|NADH dehydrogenase activity|quinone binding|mitochondrial electron transport, NADH to ubiquinone|electron transport coupled proton transport|NADH dehydrogenase (ubiquinone) activity|4 iron, 4 sulfur cluster binding|mitochondrial respiratory chain complex I assembly|inter-male aggressive behavior|aerobic respiration</td></tr>
<tr><td>FBgn0039331</td><td>ND-49L</td><td>electron</td><td>mitochondrial respiratory chain complex I|NADH dehydrogenase activity|quinone binding|mitochondrial electron transport, NADH to ubiquinone|NAD binding</td></tr>
<tr><td>FBgn0039909</td><td>ND-49</td><td>electron</td><td>mitochondrial respiratory chain complex I|NADH dehydrogenase activity|quinone binding|mitochondrial electron transport, NADH to ubiquinone|NAD binding|mitochondrion</td></tr>
<tr><td>FBgn0027785</td><td>NP15.6</td><td>electron</td><td>mitochondrial respiratory chain complex I|respiratory electron transport chain|molecular_function</td></tr>
<tr><td>FBgn0052649</td><td>Coq8</td><td>electron</td><td>mitochondrion|protein kinase activity|mitochondrial electron transport, ubiquinol to cytochrome c|extrinsic component of mitochondrial inner membrane|kinase activity|ubiquinone biosynthetic process</td></tr>
<tr><td>FBgn0013683</td><td>mt:ND4L</td><td>electron</td><td>NADH dehydrogenase complex|mitochondrial respiratory chain complex I|NADH dehydrogenase (ubiquinone) activity|ATP synthesis coupled electron transport</td></tr>
<tr><td>FBgn0030733</td><td>UQCR-14</td><td>electron</td><td>negative regulation of neuroblast proliferation|ubiquinol-cytochrome-c reductase activity|mitochondrial respiratory chain complex III assembly|mitochondrial respiratory chain complex III|cellular respiration|mitochondrial electron transport, ubiquinol to cytochrome c|aerobic respiration</td></tr>
<tr><td>FBgn0029502</td><td>COQ7</td><td>electron</td><td>negative regulation of transcription by RNA polymerase II|nucleus|2-octoprenyl-3-methyl-6-methoxy-1,4-benzoquinone hydroxylase activity|determination of adult lifespan|response to drug|regulation of reactive oxygen species metabolic process|oxidation-reduction process|positive regulation of transcription by RNA polymerase II|ubiquinone biosynthetic process|mitochondrial ATP synthesis coupled electron transport|mitochondrial inner membrane</td></tr>
<tr><td>FBgn0017566</td><td>ND-75</td><td>electron</td><td>plasma membrane respiratory chain complex I|reactive oxygen species metabolic process|mitochondrial respiratory chain complex I|NADH dehydrogenase activity|electron transfer activity|mitochondrion|NADH dehydrogenase (ubiquinone) activity|cellular respiration|ATP synthesis coupled electron transport|4 iron, 4 sulfur cluster binding</td></tr>
<tr><td>FBgn0261439</td><td>SdhA</td><td>electron</td><td>plasma membrane succinate dehydrogenase complex|anaerobic respiration|succinate dehydrogenase (ubiquinone) activity|mitochondrial respiratory chain complex II, succinate dehydrogenase complex (ubiquinone)|flavin adenine dinucleotide binding|electron transfer activity|mitochondrion|tricarboxylic acid cycle|mitochondrial electron transport, succinate to ubiquinone|electron transport chain|succinate dehydrogenase activity</td></tr>
<tr><td>FBgn0038271</td><td>UQCR-C1</td><td>electron</td><td>protein processing involved in protein targeting to mitochondrion|ubiquinol-cytochrome-c reductase activity|mitochondrial matrix|mitochondrial processing peptidase complex|mitochondrion|mitochondrial respiratory chain complex III|protein processing|mitochondrial electron transport, ubiquinol to cytochrome c|aerobic respiration|metalloendopeptidase activity</td></tr>
<tr><td>FBgn0250814</td><td>UQCR-C2</td><td>electron</td><td>protein processing involved in protein targeting to mitochondrion|ubiquinol-cytochrome-c reductase activity|mitochondrion|mitochondrial respiratory chain complex III|mitochondrial electron transport, ubiquinol to cytochrome c|metalloendopeptidase activity|mitochondrial inner membrane</td></tr>
<tr><td>FBgn0039689</td><td>CIA30</td><td>electron</td><td>response to hyperoxia|mitochondrial respiratory chain complex I|response to heat|oxidative phosphorylation|response to hypoxia|mitochondrial electron transport, NADH to ubiquinone|mitochondrion|response to starvation|unfolded protein binding|mitochondrial respiratory chain complex I assembly|mitochondrion organization</td></tr>
<tr><td>FBgn0031436</td><td>ND-B17.2</td><td>electron</td><td>response to oxidative stress|mitochondrial respiratory chain complex I|NADH dehydrogenase activity|mitochondrial electron transport, NADH to ubiquinone|electron transfer activity|NADH dehydrogenase (ubiquinone) activity</td></tr>
<tr><td>FBgn0037873</td><td>SdhC</td><td>electron</td><td>response to oxidative stress|succinate dehydrogenase (ubiquinone) activity|mitochondrial respiratory chain complex II, succinate dehydrogenase complex (ubiquinone)|electron transfer activity|determination of adult lifespan|tricarboxylic acid cycle|mitochondrial electron transport, succinate to ubiquinone|ubiquinone binding|heme binding</td></tr>
<tr><td>FBgn0037860</td><td>CG6629</td><td>electron</td><td>response to oxidative stress|succinate dehydrogenase (ubiquinone) activity|mitochondrial respiratory chain complex II, succinate dehydrogenase complex (ubiquinone)|electron transfer activity|tricarboxylic acid cycle|mitochondrial electron transport, succinate to ubiquinone|ubiquinone binding|succinate dehydrogenase activity|heme binding</td></tr>
</table>

FBgn0014028	SdhB	electron	succinate dehydrogenase (ubiquinone) activity|electron transfer activity|respiratory electron transport chain|tricarboxylic acid cycle|mitochondrial electron transport, succinate to ubiquinone|ubiquinone binding|mitochondrial inner membrane|mitochondrial membrane|mitochondrial respiratory chain complex II, succinate dehydrogenase complex (ubiquinone)|3 iron, 4 sulfur cluster binding|4 iron, 4 sulfur cluster binding|aerobic respiration|2 iron, 2 sulfur cluster binding
FBgn0039112	SdhD	electron	succinate dehydrogenase (ubiquinone) activity|mitochondrial respiratory chain complex II, succinate dehydrogenase complex (ubiquinone)|integral component of membrane|tricarboxylic acid cycle|mitochondrial electron transport, succinate to ubiquinone|ubiquinone binding|succinate dehydrogenase activity|mitochondrial inner membrane|heme binding
FBgn0039576	UQCR-14L	electron	ubiquinol-cytochrome-c reductase activity|mitochondrial respiratory chain complex III assembly|determination of adult lifespan|mitochondrial respiratory chain complex III|mitochondrial electron transport, ubiquinol to cytochrome c|response to reactive oxygen species|aerobic respiration
FBgn0011227	ox	electron	ubiquinol-cytochrome-c reductase activity|mitochondrial respiratory chain complex III assembly|mitochondrial respiratory chain complex III|mitochondrial electron transport, ubiquinol to cytochrome c|aerobic respiration
FBgn0034245	UQCR-6.4	electron	ubiquinol-cytochrome-c reductase activity|mitochondrial respiratory chain complex III|mitochondrial electron transport, ubiquinol to cytochrome c
FBgn0050354	UQCR-11L	electron	ubiquinol-cytochrome-c reductase activity|mitochondrial respiratory chain complex III|mitochondrial electron transport, ubiquinol to cytochrome c|aerobic respiration
FBgn0260008	UQCR-11	electron	ubiquinol-cytochrome-c reductase activity|mitochondrial respiratory chain complex III|mitochondrial electron transport, ubiquinol to cytochrome c|aerobic respiration
FBgn0036728	UQCR-Q	electron	ubiquinol-cytochrome-c reductase activity|mitochondrial respiratory chain complex III|mitochondrial electron transport, ubiquinol to cytochrome c|ubiquinone binding
FBgn0021906	RFeSP	electron	ubiquinol-cytochrome-c reductase activity|mitochondrion|mitochondrial respiratory chain complex III|mitochondrial electron transport, ubiquinol to cytochrome c|2 iron, 2 sulfur cluster binding
FBgn0029870	Marf	onal transport of	mitochondrial fusion|regulation of mitochondrial fission|adult locomotory behavior|endoplasmic reticulum organization|mitochondrial envelope|mitochondrion organization|ecdysone biosynthetic process|GTP binding|intrinsic component of mitochondrial outer membrane|mitochondrion morphogenesis|positive regulation of mitochondrial fusion|GTPase activity|lipid droplet organization|axonal transport of mitochondrion|mitochondrion localization|response to endoplasmic reticulum stress
FBgn0029131	Debcl		apoptotic process involved in morphogenesis|positive regulation of macroautophagy|ectopic germ cell programmed cell death|protein homodimerization activity|regulation of programmed cell death|intrinsic apoptotic signaling pathway in response to DNA damage|cellular response to starvation|extrinsic apoptotic signaling pathway in absence of ligand|mitochondrial outer membrane|mitochondrial envelope|regulation of mitochondrial membrane permeability|negative regulation of neuron apoptotic process|neuron cellular homeostasis|protein heterodimerization activity|negative regulation of apoptotic process|apoptotic process|mitochondrion|positive regulation of necrotic cell death|programmed cell death involved in cell development|response to ionizing radiation
FBgn0035039	Adck		ATP binding|lipid homeostasis|protein kinase activity|protein phosphorylation|mitochondrion organization|mitochondrial inner membrane
FBgn0036702	CG6512		ATP binding|zinc ion binding|cristae formation|proteolysis|mitochondrion|mitochondrial fusion|integral component of membrane|mitochondrial protein processing|metalloendopeptidase activity|mitochondrial inner membrane
FBgn0026761	Trap1		ATPase activity|protein kinase binding|unfolded protein binding|positive regulation of response to oxidative stress|protein folding|mitochondrial inner membrane|ATP binding|response to oxidative stress|nucleus|response to heat|cellular response to heat|RNA binding|extracellular exosome|mitochondrial matrix|mitochondrion|mitochondrial unfolded protein response

FBgn0032365	CG14929	biological_process|cristae formation|mitochondrial crista junction|MICOS complex|cellular_component|molecular_function
FBgn0263033	CG43328	biological_process|cristae formation|mitochondrial crista junction|MICOS complex|cellular_component|molecular_function
FBgn0030717	Slc25A46a	biological_process|mitochondrial membrane fission|mitochondrial outer membrane|cellular_component|molecular_function
FBgn0035299	CG11815	biological_process|mitochondrial respiratory chain complex I|cellular_component|molecular_function
FBgn0058002	ND-AGGG	biological_process|mitochondrial respiratory chain complex I|molecular_function
FBgn0085468	ND-MWFE	biological_process|mitochondrial respiratory chain complex I|molecular_function
FBgn0085736	CG40472	biological_process|mitochondrial respiratory chain complex I|molecular_function
FBgn0069923	CG41128	biological_process|mitochondrion|MICOS complex|molecular_function
FBgn0040871	CG12479	biological_process|mitochondrion|MICOS complex|molecular_function
FBgn0032664	Slc25A46b	biological_process|nucleus|mitochondrial membrane fission|cytoplasm|mitochondrial outer membrane|molecular_function|plasma membrane
FBgn0001122	Galphao	cell adhesion involved in heart morphogenesis|axon ensheathment in central nervous system|establishment of endothelial blood-brain barrier|G protein-coupled receptor signaling pathway|sensory perception of sweet taste|asymmetric cell division|behavioral response to starvation|negative regulation of synaptic growth at neuromuscular junction|establishment of glial blood-brain barrier|adenylate cyclase-modulating G protein-coupled receptor signaling pathway|plasma membrane|cortical actin cytoskeleton organization|GTP binding|heart development|ventral cord development|G protein-coupled receptor binding|heterotrimeric G-protein complex|protein binding|septate junction assembly|GTPase activity|establishment of imaginal disc-derived wing hair orientation|G-protein beta/gamma-subunit complex binding|calcium-mediated signaling|non-canonical Wnt signaling pathway
iProtKB:A0A0B4K	CG43327	cristae formation|mitochondrial crista junction|MICOS complex
FBgn0010808	Chchd3	cristae formation|mitochondrial fusion|mitochondrial inner membrane
UniProtKB:F3YDF1	YME1L	cristae formation|mitochondrial fusion|mitochondrial protein processing|mitochondrial inner membrane
FBgn0038400	CG5903	cristae formation|protein binding|MICOS complex|mitochondrial outer membrane
FBgn0036726	QIL1	cristae formation|regulation of cristae formation|mitochondrial crista junction|MICOS complex

FBgn0038925	Cchl	cytochrome c-heme linkage|holocytochrome-c synthase activity|mitochondrion|mitochondrial inner membrane
FBgn0037574	Coq2	defense response to Gram-negative bacterium|determination of adult lifespan|transcription by RNA polymerase I|4-hydroxybenzoate decaprenyltransferase activity|4-hydroxybenzoate octaprenyltransferase activity|ubiquinone biosynthetic process|mitochondrial inner membrane|RNA polymerase III complex|RNA polymerase I complex|integral component of mitochondrial inner membrane|DNA-directed 5'-3' RNA polymerase activity|mitochondrion|integral component of membrane|defense response to fungus|defense response to Gram-positive bacterium|transferase activity, transferring alkyl or aryl (other than methyl) groups
FBgn0031263	Tspo	determination of adult lifespan|regulation of oxidative phosphorylation|positive regulation of apoptotic process|integral component of membrane|mitochondrial outer membrane|mitochondrial envelope
FBgn0033690	EndoG	ectopic germ cell programmed cell death|spermatid development|DNA catabolic process, endonucleolytic|DNA-dependent DNA replication|endodeoxyribonuclease activity|single-stranded DNA endodeoxyribonuclease activity|mitochondrial inner membrane|endoribonuclease activity|nucleic acid binding|mitochondrion inheritance|nucleus|metal ion binding|apoptotic DNA fragmentation|endonuclease activity|mitochondrion|exodeoxyribonuclease activity
FBgn0029661	CG16781	endoplasmic reticulum membrane|ubiquitin-protein transferase activity|zinc ion binding|protein polyubiquitination|mitochondrial outer membrane
FBgn0037242	CG9855	endoplasmic reticulum membrane|ubiquitin-protein transferase activity|zinc ion binding|protein polyubiquitination|mitochondrial outer membrane
FBgn0039498	CG17991	endoplasmic reticulum membrane|ubiquitin-protein transferase activity|zinc ion binding|protein polyubiquitination|mitochondrial outer membrane
FBgn0030015	CG10761	endoplasmic reticulum membrane|ubiquitin-protein transferase activity|zinc ion binding|protein polyubiquitination|mitochondrial outer membrane
FBgn0000337	cn	FAD binding|quinolinate biosynthetic process|mitochondrial outer membrane|positive regulation of neuron death|kynurenine 3-monooxygenase activity|tryptophan catabolic process|kynurenine metabolic process|flavin adenine dinucleotide binding|ommochrome biosynthetic process|NAD(P)H oxidase activity|mitochondrion|NAD metabolic process|compound eye pigmentation
FBgn0033465	Etf-QO	fatty acid beta-oxidation|integral component of mitochondrial inner membrane|oxidative phosphorylation|electron transfer activity|mitochondrion|oxidoreductase activity, oxidizing metal ions with flavin as acceptor|electron-transferring-flavoprotein dehydrogenase activity|ubiquinone binding|4 iron, 4 sulfur cluster binding|mitochondrial inner membrane
FBgn0266268	FeCH	ferrochelatase activity|mitochondrion|heme biosynthetic process|protoporphyrinogen IX biosynthetic process|mitochondrial inner membrane
FBgn0053517	Dop2R	G protein-coupled receptor activity|integral component of plasma membrane|anesthesia-resistant memory|G protein-coupled receptor signaling pathway|adrenergic receptor activity|adenylate cyclase-activating adrenergic receptor signaling pathway|integral component of membrane|dopamine receptor signaling pathway|dopamine neurotransmitter receptor activity, coupled via Gi/Go|adenylate cyclase-modulating G protein-coupled receptor signaling pathway|G protein-coupled amine receptor activity
FBgn0037146	CG7470	glutamate 5-kinase activity|delta1-pyrroline-5-carboxylate synthetase activity|mitochondrion|glutamate-5-semialdehyde dehydrogenase activity|proline biosynthetic process|oxidation-reduction process|mitochondrial inner membrane
FBgn0022160	Gpo1	glycerol metabolic process|glycerol-3-phosphate dehydrogenase complex|glycerol-3-phosphate catabolic process|flight behavior|calcium ion binding|mitochondrion|glycerophosphate shuttle|mitochondrial inner membrane|glycerol-3-phosphate dehydrogenase (quinone) activity|glycerol-3-phosphate dehydrogenase [NAD+] activity
FBgn0027579	mino	glycerol-3-phosphate metabolic process|phospholipid biosynthetic process|endoplasmic reticulum|fusome|glycerol-3-phosphate O-acyltransferase activity|mitochondrial outer membrane|plasma membrane|fatty acid metabolic process|plasma membrane organization|mitochondrial membrane|mitochondrion|triglyceride biosynthetic process|piRNA metabolic process|female germline ring canal

FBgn0011596	fzo	GTP binding|intrinsic component of mitochondrial outer membrane|GTPase activity|spermatogenesis|mitochondrial fusion|sperm mitochondrion organization|integral component of membrane|Nebenkern assembly|mitochondrion localization|mitochondrial envelope
FBgn0020018	Ppox	heme biosynthetic process|oxygen-dependent protoporphyrinogen oxidase activity|oxidation-reduction process|mitochondrial inner membrane
FBgn0032222	CG5037	heme O biosynthetic process|mitochondrial membrane|cytochrome-c oxidase activity|protoheme IX farnesyltransferase activity|mitochondrion|heme biosynthetic process|integral component of membrane|cytochrome complex|cellular respiration|respiratory chain complex IV assembly
FBgn0032200	CG5676	integral component of mitochondrial outer membrane|autophagy of mitochondrion
FBgn0031729	CG12511	integral component of mitochondrial outer membrane|autophagy of mitochondrion
FBgn0035587	Gdap1	integral component of mitochondrial outer membrane|protein targeting to mitochondrion|mitochondrion|mitochondrial fusion|mitochondrion organization|mitochondrial fission
FBgn0035483	Mul1	integral component of mitochondrial outer membrane|ubiquitin-protein transferase activity|peroxisome|zinc ion binding|positive regulation of mitochondrial fission|protein ubiquitination
FBgn0025814	Mgstl	intracellular membrane-bounded organelle|prostaglandin-E synthase activity|prostaglandin biosynthetic process|glutathione transferase activity|oxidation-reduction process|mitochondrial outer membrane
FBgn0263987	spoon	intracellular mRNA localization|dorsal appendage formation|dorsal/ventral axis specification, ovarian follicular epithelium|border follicle cell migration|Golgi apparatus|mitochondrial outer membrane|centripetally migrating follicle cell migration|long-term memory|RNA binding|negative regulation of actin filament polymerization|chromosome organization|regulation of protein kinase A signaling|mitochondrion|protein kinase A regulatory subunit binding|thermosensory behavior|maternal determination of dorsal/ventral axis, ovarian follicular epithelium, germ-line encoded
FBgn0050493	CG30493	lipid binding|ubiquinone biosynthetic process|mitochondrial inner membrane
FBgn0036142	CG7616	lipid homeostasis|mitochondrion organization|mitochondrial inner membrane
FBgn0260960	Baldspot	long-chain fatty acid biosynthetic process|spermatogenesis|integral component of endoplasmic reticulum membrane|fatty acid elongation|very long-chain fatty acid biosynthetic process|fatty acid elongation, saturated fatty acid|mitochondrial outer membrane|fatty acid elongation, polyunsaturated fatty acid|fatty acid elongase activity|fatty acid elongation, monounsaturated fatty acid|sphingolipid biosynthetic process
FBgn0011207	pelo	male meiosis I|ribosome disassembly|meiotic spindle organization|G2/MI transition of meiotic cell cycle|nuclear-transcribed mRNA catabolic process, non-stop decay|female germ-line stem cell asymmetric division|meiotic cell cycle|spermatocyte division|Dom34-Hbs1 complex|compound eye morphogenesis|meiotic nuclear envelope disassembly|RNA surveillance|cytoplasm|nonfunctional rRNA decay|germ-line stem cell population maintenance|ribosome binding|posttranscriptional gene silencing|nuclear-transcribed mRNA catabolic process, no-go decay
FBgn0261276	Opa1	membrane fusion|mitochondrial fusion|negative regulation of endoplasmic reticulum stress-induced intrinsic apoptotic signaling pathway|dynamin family protein polymerization involved in mitochondrial fission|mitochondrion organization|mitochondrial fission|microtubule binding|GTP binding|mitochondrial membrane|mitochondrion morphogenesis|compound eye morphogenesis|positive regulation of mitochondrial fusion|cytoplasm|GTPase activity|mitochondrion|membrane
FBgn0019886	Letm1	mitochondrial inner membrane

FBgn0000447	Dhod	mitochondrial intermembrane space|'de novo' pyrimidine nucleobase biosynthetic process|pyrimidine ribonucleotide biosynthetic process|mitochondrion|dihydroorotate dehydrogenase activity|oxidation-reduction process|mitochondrial inner membrane|plasma membrane
FBgn0011476	l(3)neo43	mitochondrial membrane
FBgn0039749	CG11498	mitochondrial protein catabolic process|mitophagy by induced vacuole formation|cellular response to stress|mitochondrial outer membrane
FBgn0033861	CG12464	mitochondrial respiratory chain complex I
FBgn0030292	CG11752	mitochondrial respiratory chain complex I
FBgn0034919	CG5569	mitochondrial respiratory chain complex I assembly|mitochondrial inner membrane
FBgn0034576	ND-B14.7	mitochondrial respiratory chain complex I|mitochondrial respiratory chain complex I assembly|molecular_function
FBgn0002021	l(2)37Bb	mitochondrial respiratory chain complex I|oxidoreductase activity|cytoplasm|oxidation-reduction process|mitochondrial respiratory chain complex I assembly
FBgn0033093	CG3270	mitochondrial respiratory chain complex I|oxidoreductase activity|cytoplasm|oxidation-reduction process|mitochondrial respiratory chain complex I assembly
FBgn0032744	Ttc19	mitochondrial respiratory chain complex III assembly|mitochondrion|jump response|optomotor response|mitochondrial inner membrane
FBgn0031066	COX6B	mitochondrial respiratory chain complex IV assembly|cytochrome-c oxidase activity|protein binding|mitochondrion|mitochondrial respiratory chain complex IV
FBgn0085271	CG34242	mitochondrial respiratory chain complex IV assembly|integral component of membrane|mitochondrial inner membrane
FBgn0034248	CG14483	mitochondrial respiratory chain complex IV assembly|integral component of mitochondrial inner membrane|unfolded protein binding
FBgn0002354	l(3)87Df	mitochondrial respiratory chain complex IV assembly|mitochondrion|aerobic respiration|mitochondrial inner membrane
FBgn0029117	Surf1	mitochondrial respiratory chain complex IV assembly|phototaxis|mitochondrial inner membrane|respiratory chain complex IV assembly|visual behavior|instar larval development
FBgn0019960	Mitofilin	mitochondrion morphogenesis|mitochondrion|molecular_function|mitochondrial inner membrane
FBgn0033086	CG9410	mitochondrion|cellular respiration|ubiquinone binding|ubiquinone biosynthetic process|mitochondrial inner membrane
FBgn0034973	CG13564	mitochondrion|MICOS complex|defense response to bacterium|molecular_function

<table>
<tr><td>FBgn0030883</td><td>CG7772</td><td>mitochondrion|molecular_function|mitochondrial inner membrane|mitochondrial fission</td></tr>
<tr><td>FBgn0052174</td><td>CG32174</td><td>mitochondrion|ubiquinone biosynthetic process|molecular_function|mitochondrial inner membrane</td></tr>
<tr><td>FBgn0034087</td><td>clu</td><td>mitotic spindle|outer mitochondrial membrane protein complex|intracellular distribution of mitochondria|cytoplasm|ribosome binding|mitochondrion|mRNA binding|asymmetric neuroblast division|endoplasmic reticulum|Golgi apparatus|mitochondrion localization|extrinsic component of mitochondrial outer membrane</td></tr>
<tr><td>FBgn0013681</td><td>mt:ND3</td><td>NADH dehydrogenase complex|mitochondrial respiratory chain complex I|NADH dehydrogenase (ubiquinone) activity</td></tr>
<tr><td>FBgn0285943</td><td>knon</td><td>Nebenkern assembly|mitochondrial proton-transporting ATP synthase complex</td></tr>
<tr><td>FBgn0036831</td><td>CG6839</td><td>nucleic acid binding|metal ion binding|apoptotic DNA fragmentation|DNA catabolic process, endonucleolytic|endonuclease activity|exodeoxyribonuclease activity|mitochondrion|mitochondrial inner membrane|single-stranded DNA endodeoxyribonuclease activity|hydrolase activity|endoribonuclease activity</td></tr>
<tr><td>FBgn0039592</td><td>CG14062</td><td>nucleic acid binding|metal ion binding|apoptotic DNA fragmentation|DNA catabolic process, endonucleolytic|endonuclease activity|mitochondrion|exodeoxyribonuclease activity|mitochondrial inner membrane|single-stranded DNA endodeoxyribonuclease activity|hydrolase activity|endoribonuclease activity</td></tr>
<tr><td>FBgn0036321</td><td>CG14120</td><td>nucleic acid binding|metal ion binding|apoptotic DNA fragmentation|endonuclease activity|DNA catabolic process, endonucleolytic|mitochondrion|exodeoxyribonuclease activity|mitochondrial inner membrane|single-stranded DNA endodeoxyribonuclease activity|hydrolase activity|endoribonuclease activity</td></tr>
<tr><td>FBgn0033490</td><td>CG12917</td><td>nucleic acid binding|metal ion binding|apoptotic DNA fragmentation|endonuclease activity|DNA catabolic process, endonucleolytic|mitochondrion|exodeoxyribonuclease activity|single-stranded DNA endodeoxyribonuclease activity|mitochondrial inner membrane|hydrolase activity|endoribonuclease activity</td></tr>
<tr><td>FBgn0036323</td><td>CG14118</td><td>nucleic acid binding|metal ion binding|DNA catabolic process, endonucleolytic|endonuclease activity|apoptotic DNA fragmentation|mitochondrion|exodeoxyribonuclease activity|mitochondrial inner membrane|single-stranded DNA endodeoxyribonuclease activity|hydrolase activity|endoribonuclease activity</td></tr>
<tr><td>FBgn0036833</td><td>CG3819</td><td>nucleic acid binding|metal ion binding|endonuclease activity|apoptotic DNA fragmentation|DNA catabolic process, endonucleolytic|exodeoxyribonuclease activity|mitochondrion|single-stranded DNA endodeoxyribonuclease activity|mitochondrial inner membrane|hydrolase activity|endoribonuclease activity</td></tr>
<tr><td>FBgn0053346</td><td>CG33346</td><td>nucleic acid binding|metal ion binding|endonuclease activity|DNA catabolic process, endonucleolytic|apoptotic DNA fragmentation|mitochondrion|exodeoxyribonuclease activity|mitochondrial inner membrane|single-stranded DNA endodeoxyribonuclease activity|hydrolase activity|endoribonuclease activity</td></tr>
<tr><td>FBgn0051679</td><td>Tengl3</td><td>nucleic acid binding|nucleus|metal ion binding|apoptotic DNA fragmentation|DNA catabolic process, endonucleolytic|endonuclease activity|mitochondrion|exodeoxyribonuclease activity|mitochondrial inner membrane|single-stranded DNA endodeoxyribonuclease activity|hydrolase activity|endoribonuclease activity</td></tr>
<tr><td>FBgn0052463</td><td>Tengl2</td><td>nucleic acid binding|nucleus|metal ion binding|apoptotic DNA fragmentation|DNA catabolic process, endonucleolytic|endonuclease activity|mitochondrion|exodeoxyribonuclease activity|mitochondrial inner membrane|single-stranded DNA endodeoxyribonuclease activity|hydrolase activity|endoribonuclease activity</td></tr>
<tr><td>FBgn0051682</td><td>Tengl1</td><td>nucleic acid binding|nucleus|metal ion binding|DNA catabolic process, endonucleolytic|apoptotic DNA fragmentation|endonuclease activity|mitochondrion|exodeoxyribonuclease activity|single-stranded DNA endodeoxyribonuclease activity|mitochondrial inner membrane|hydrolase activity|endoribonuclease activity</td></tr>
<tr><td>FBgn0037857</td><td>Tengl4</td><td>nucleic acid binding|nucleus|metal ion binding|endonuclease activity|apoptotic DNA fragmentation|DNA catabolic process, endonucleolytic|mitochondrion|exodeoxyribonuclease activity|single-stranded DNA endodeoxyribonuclease activity|mitochondrial inner membrane|hydrolase activity|endoribonuclease activity</td></tr>
<tr><td>FBgn0039593</td><td>Sid</td><td>nucleic acid phosphodiester bond hydrolysis|DNA catabolic process, endonucleolytic|response to paraquat|ribonuclease activity|mitochondrial inner membrane|single-stranded DNA endodeoxyribonuclease activity|endoribonuclease activity|nucleic acid binding|response to oxidative stress|response to bacterium|deoxyribonuclease activity|metal ion binding|cytoplasm|apoptotic DNA fragmentation|endonuclease activity|membrane|mitochondrion|exodeoxyribonuclease activity</td></tr>
</table>

FBgn0033918	CG8531	nucleus|cristae formation|protein import into mitochondrial matrix|mitochondrion|MICOS complex|ATPase activator activity
FBgn0037007	CG5059	nucleus|mitochondrial outer membrane permeabilization|positive regulation of apoptotic process|integral component of membrane|mitochondrial outer membrane
FBgn0284248	Cyt-c-p	oxidative phosphorylation|electron transfer activity|mitochondrion|cytosol|oxidation-reduction process|mitochondrial inner membrane|heme binding
FBgn0001112	Gld	oxidoreductase activity, acting on CH-OH group of donors|pupal chitin-based cuticle development|flavin adenine dinucleotide binding|sperm storage|oxidation-reduction process|glucose metabolic process
FBgn0039930	CG11077	peroxisomal membrane|cytoplasm|homeostatic process|integral component of membrane|mitochondrial inner membrane|mitochondrial genome maintenance
FBgn0039969	Fis1	peroxisomal membrane|integral component of mitochondrial outer membrane|integral component of peroxisomal membrane|apoptotic process|mitochondrial fragmentation involved in apoptotic process|positive regulation of mitochondrial fission|mitochondrial outer membrane|autophagy of mitochondrion|mitochondrion organization|mitochondrial fission
ProtKB:A0A0B4K	Dhap-at	peroxisomal membrane|mitochondrial membrane|phospholipid biosynthetic process|glycerone-phosphate O-acyltransferase activity|fatty acid metabolic process|ether lipid biosynthetic process
FBgn0038486	CG5265	peroxisome|carnitine O-acetyltransferase activity|carnitine metabolic process, CoA-linked|endoplasmic reticulum|mitochondrial inner membrane|fatty acid metabolic process|carnitine metabolic process
FBgn0067628	CG33331	phosphatidate cytidylyltransferase activity|extrinsic component of mitochondrial inner membrane|cardiolipin biosynthetic process
FBgn0264694	mgr	polysome|establishment or maintenance of neuroblast polarity|tubulin binding|centrosome cycle|tubulin complex assembly|cytoplasm|beta-tubulin binding|prefoldin complex|protein folding|spindle assembly involved in meiosis|microtubule-based process|mitotic spindle assembly
FBgn0011706	rpr	positive regulation of cysteine-type endopeptidase activity involved in execution phase of apoptosis|positive regulation of ubiquitin-dependent protein catabolic process|regulation of protein catabolic process|apoptotic signaling pathway|negative regulation of neuron apoptotic process|cell death|apoptotic process|cellular response to ionizing radiation|positive regulation of protein ubiquitination|protein homodimerization activity|larval midgut cell programmed cell death|salivary gland cell autophagic cell death|intrinsic apoptotic signaling pathway in response to DNA damage|ecdysone-mediated induction of salivary gland cell autophagic cell death|larval central nervous system remodeling|phospholipid binding|mitochondrial outer membrane|imaginal disc-derived male genitalia morphogenesis|intrinsic apoptotic signaling pathway in response to osmotic stress|ubiquitin conjugating enzyme binding|cellular response to gamma radiation|ubiquitin protein ligase binding|cytoplasm|mitochondrion|positive regulation of cysteine-type endopeptidase activity|programmed cell death
FBgn0040491	Buffy	positive regulation of macroautophagy|ectopic germ cell programmed cell death|protein homodimerization activity|positive regulation of programmed cell death|regulation of apoptotic process|endoplasmic reticulum|intrinsic apoptotic signaling pathway in response to DNA damage|cellular response to starvation|extrinsic apoptotic signaling pathway in absence of ligand|mitochondrial outer membrane|protein heterodimerization activity|negative regulation of apoptotic process|apoptotic process|programmed cell death
FBgn0029665	CG14270	protein import into mitochondrial inner membrane|TIM22 mitochondrial import inner membrane insertion complex
FBgn0035088	CG3776	protein insertion into mitochondrial inner membrane from matrix side|protein binding|ribosome binding|mitochondrion|inner mitochondrial membrane organization|mitochondrial inner membrane
FBgn0050412	CG30412	protein insertion into mitochondrial inner membrane from matrix side|ribosome binding|inner mitochondrial membrane organization|mitochondrial inner membrane

FBgn0034846	CG9863	protein insertion into mitochondrial inner membrane from matrix side|ribosome binding|inner mitochondrial membrane organization|mitochondrial inner membrane
FBgn0034835	CG3092	protein insertion into mitochondrial inner membrane from matrix side|ribosome binding|inner mitochondrial membrane organization|mitochondrial inner membrane
FBgn0033235	CG8728	protein processing involved in protein targeting to mitochondrion|mitochondrial matrix|protein processing|metalloendopeptidase activity|mitochondrial inner membrane
FBgn0030669	CG9240	protein processing involved in protein targeting to mitochondrion|serine-type peptidase activity|integral component of membrane|mitochondrial inner membrane peptidase complex
FBgn0034535	CG11110	protein processing involved in protein targeting to mitochondrion|serine-type peptidase activity|mitochondrial respiratory chain complex assembly|mitochondrial inner membrane peptidase complex
FBgn0250874	ttm50	protein serine/threonine phosphatase activity|TIM23 mitochondrial import inner membrane translocase complex|phosphoprotein phosphatase activity|protein import into mitochondrial matrix|protein tyrosine phosphatase activity|mitochondrion|protein dephosphorylation|mitochondrion organization|mitochondrial inner membrane|mitochondrial membrane organization
FBgn0032971	ttm3	protein serine/threonine phosphatase activity|TIM23 mitochondrial import inner membrane translocase complex|phosphoprotein phosphatase activity|protein import into mitochondrial matrix|protein tyrosine phosphatase activity|mitochondrion|protein dephosphorylation|mitochondrion organization|mitochondrial inner membrane|mitochondrial membrane organization
FBgn0035124	ttm2	protein serine/threonine phosphatase activity|TIM23 mitochondrial import inner membrane translocase complex|phosphoprotein phosphatase activity|protein import into mitochondrial matrix|protein tyrosine phosphatase activity|nuclear speck|mitochondrion|ribonucleoprotein complex binding|protein dephosphorylation|mitochondrion organization|mitochondrial inner membrane|mitochondrial membrane organization
FBgn0030620	CG5662	protein targeting to mitochondrion|mitochondrial outer membrane|mitochondrial sorting and assembly machinery complex
FBgn0036920	CG8004	protein targeting to mitochondrion|mitochondrial outer membrane|mitochondrial sorting and assembly machinery complex
FBgn0037710	CG9393	protein targeting to mitochondrion|mitochondrial outer membrane|mitochondrial sorting and assembly machinery complex
FBgn0039463	CG18472	protein targeting to mitochondrion|nucleus|heat shock protein binding|mitochondrial outer membrane
FBgn0014877	Roe1	protein targeting to mitochondrion|protein homodimerization activity|protein import into mitochondrial matrix|mitochondrial matrix|chaperone binding|mitochondrion|PAM complex, Tim23 associated import motor|unfolded protein binding|protein folding|adenyl-nucleotide exchange factor activity
FBgn0266582	ND-30	reactive oxygen species metabolic process|mitochondrial respiratory chain complex I|NADH dehydrogenase activity|mitochondrion
FBgn0017429	CG5989	ribosome binding|mitochondrial inner membrane
FBgn0261266	zuc	RNA phosphodiester bond hydrolysis, endonucleolytic|oogenesis|oocyte karyosome formation|P granule|mitochondrion|dorsal appendage formation|gene silencing by RNA|endoribonuclease activity, producing 5'-phosphomonoesters|piRNA metabolic process|mitochondrial outer membrane|cardiolipin hydrolase activity
FBgn0039835	mRpL32	structural constituent of ribosome|mitochondrial translation|mitochondrial large ribosomal subunit|mitochondrial inner membrane|translation
FBgn0031971	Sirup	succinate dehydrogenase (ubiquinone) activity|mitochondrial respiratory chain complex II, succinate dehydrogenase complex (ubiquinone)|neural retina development|cellular respiration|mitochondrial respiratory chain complex II assembly|cellular response to reactive oxygen species

FBgn0039827	CG1544	thiamine pyrophosphate binding|generation of precursor metabolites and energy|mitochondrial membrane|oxoglutarate dehydrogenase (succinyl-transferring) activity|oxoglutarate dehydrogenase complex|cytosol|tricarboxylic acid cycle
FBgn0038387	blp	TIM23 mitochondrial import inner membrane translocase complex|embryonic development via the syncytial blastoderm|protein import into mitochondrial matrix|instar larval development
FBgn0031708	CG7382	TIM23 mitochondrial import inner membrane translocase complex|mitochondrial respiratory chain complex IV assembly|protein import into mitochondrial matrix|mitochondrial respiratory chain complex I assembly
FBgn0029964	CG1409	TIM23 mitochondrial import inner membrane translocase complex|protein import into mitochondrial matrix
FBgn0036488	CG6878	TIM23 mitochondrial import inner membrane translocase complex|regulation of autophagy of mitochondrion|protein import into mitochondrial matrix|mitochondrion|protein import into mitochondrial inner membrane
FBgn0014018	Rel	Toll signaling pathway|peptidoglycan recognition protein signaling pathway|positive regulation of nitric oxide biosynthetic process|cellular response to amino acid starvation|sequence-specific DNA binding|positive regulation of antibacterial peptide biosynthetic process|positive regulation of transcription by RNA polymerase II|positive regulation of biosynthetic process of antibacterial peptides active against Gram-negative bacteria|peripheral nervous system neuron development|dendrite morphogenesis|DNA-binding transcription factor activity|proximal promoter DNA-binding transcription activator activity, RNA polymerase II-specific|immune response|defense response to virus|defense response to Gram-negative bacterium|signal transduction|positive regulation of defense response to virus by host|cellular response to DNA damage stimulus|DNA-binding transcription factor activity, RNA polymerase II-specific|positive regulation of antifungal peptide biosynthetic process|nucleus|DNA binding|response to bacterium|protein binding|positive regulation of innate immune response|cytoplasm|negative regulation of stem cell proliferation|innate immune response|positive regulation of gene expression|regulation of innate immune response|nuclear euchromatin
FBgn0036479	mel\CG13458	translation regulator activity|positive regulation of mitochondrial translation|extrinsic component of mitochondrial inner membrane
FBgn0015245	Hsp60A	unfolded protein binding|protein refolding|'de novo' protein folding|mitochondrion organization|mitochondrial inner membrane|protein targeting to mitochondrion|protein import into mitochondrial intermembrane space|ATP binding|cellular response to heat|apoptotic mitochondrial changes|mitochondrial matrix|mitochondrion|cytosol
FBgn0031893	MICU1	uniplex complex|anesthesia-resistant memory|calcium import into the mitochondrion|positive regulation of mitochondrial calcium ion concentration|calcium ion binding|medium-term memory
FBgn0026479	Drp1	ventral furrow formation|regulation of autophagy of mitochondrion|dynamin family protein polymerization involved in mitochondrial fission|microtubule associated complex|GTP binding|apoptotic mitochondrial changes|mitotic cytokinesis|GTPase activity|mitochondrion localization|peroxisome fission|membrane fusion|sperm mitochondrion organization|regulation of mitochondrial fission|mitochondrial fragmentation involved in apoptotic process|positive regulation of mitochondrial fission|mitochondrion organization|mitochondrial fission|microtubule binding|mitochondrial membrane|cytoplasm|intracellular distribution of mitochondria|synaptic vesicle budding from presynaptic endocytic zone membrane|mitochondrion|membrane|regulation of mitochondrion organization
FBgn0003462	Sod1	zinc ion binding|protein homodimerization activity|antioxidant activity|regulation of autophagy of mitochondrion|determination of adult lifespan|age-dependent response to oxidative stress|superoxide dismutase activity|aging|response to oxidative stress|peroxisome|extracellular space|superoxide metabolic process|copper ion binding|cytoplasm|removal of superoxide radicals|oxidation-reduction process|regulation of terminal button organization|superoxide dismutase copper chaperone activity

Figure S1

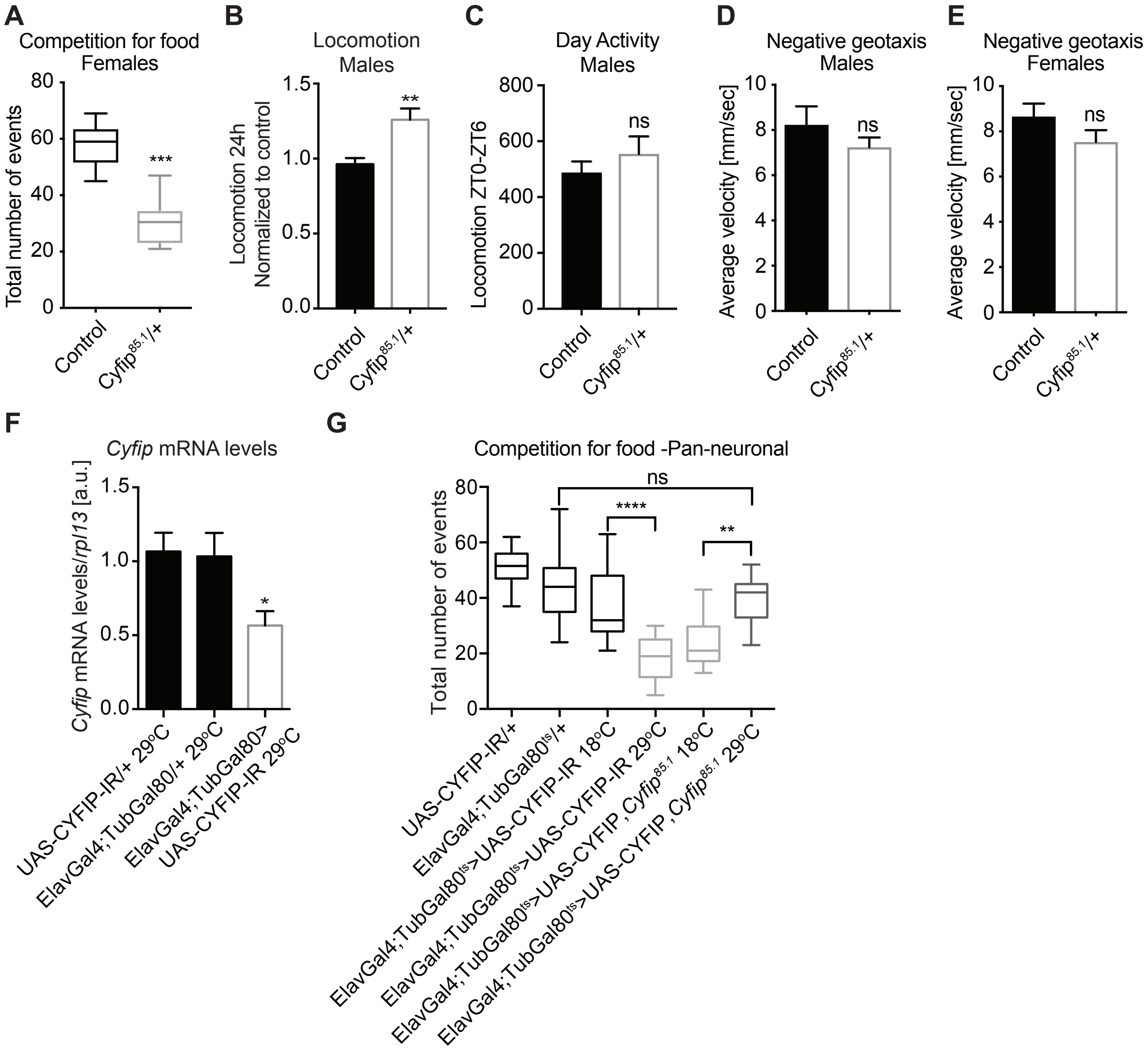
A
Competition for food
Females
Total number of events
80
60
40
20
0
***
Control
Cyfip$^{85.1}$/+
B
Locomotion
Males
Locomotion 24h
Normalized to control
1.5
1.0
0.5
0.0
**
Control
Cyfip$^{85.1}$/+
C
Day Activity
Males
Locomotion ZT0-ZT6
800
600
400
200
0
ns
Control
Cyfip$^{85.1}$/+
D
Negative geotaxis
Males
Average velocity [mm/sec]
10
8
6
4
2
0
ns
Control
Cyfip$^{85.1}$/+
E
Negative geotaxis
Females
Average velocity [mm/sec]
10
8
6
4
2
0
ns
Control
Cyfip$^{85.1}$/+
F
Cyfip mRNA levels
Cyfip mRNA levels/*rpl13* [a.u.]
1.5
1.0
0.5
0.0
*
UAS-CYFIP-IR/+ 29°C
ElavGal4;TubGal80/+ 29°C
ElavGal4;TubGal80>
UAS-CYFIP-IR 29°C
G
Competition for food -Pan-neuronal
Total number of events
80
60
40
20
0
ns
****
**
UAS-CYFIP-IR/+
ElavGal4;TubGal80^{ts}/+
ElavGal4;TubGal80^{ts}>UAS-CYFIP-IR 18°C
ElavGal4;TubGal80^{ts}>UAS-CYFIP-IR 29°C
ElavGal4;TubGal80^{ts}>UAS-CYFIP,Cyfip$^{85.1}$ 18°C
ElavGal4;TubGal80^{ts}>UAS-CYFIP,Cyfip$^{85.1}$ 29°C

Figure S2

A

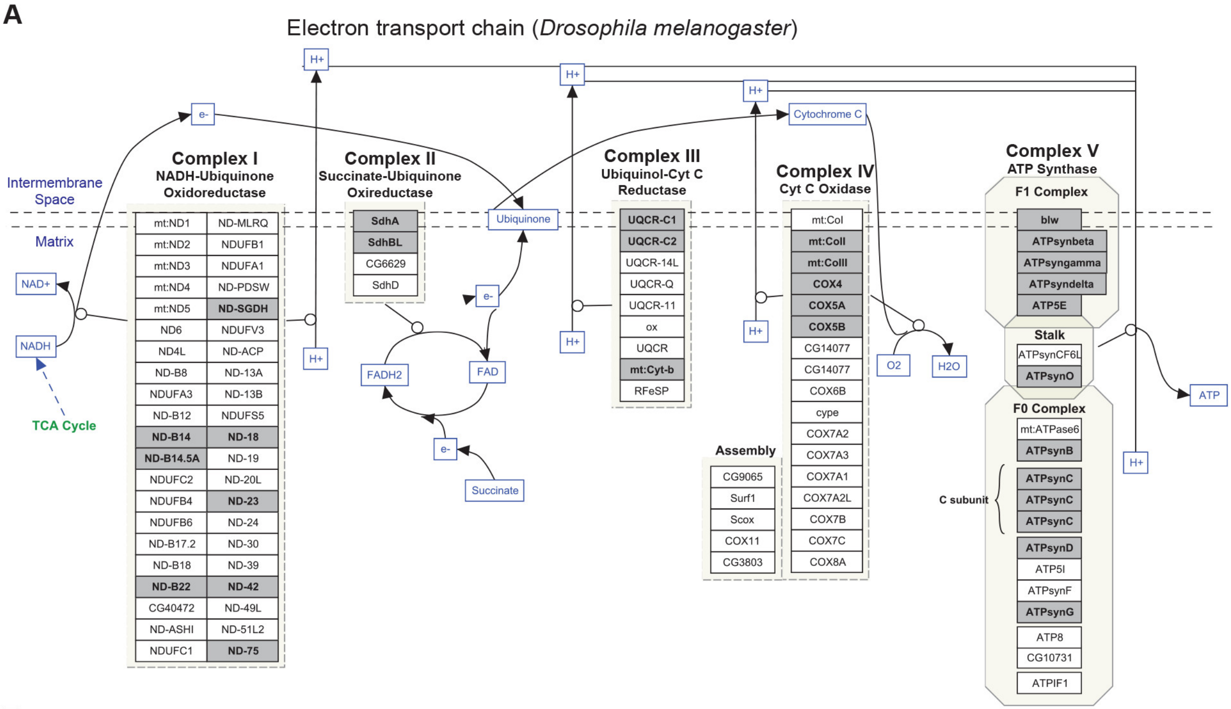
Electron transport chain (Drosophila melanogaster)
H+
H+
H+
e-
Cytochrome C
Intermembrane Space
Matrix
Complex I
NADH-Ubiquinone Oxidoreductase
mt:ND1
ND-MLRQ
mt:ND2
NDUFB1
mt:ND3
NDUFA1
mt:ND4
ND-PDSW
mt:ND5
ND-SGDH
ND6
NDUFV3
ND4L
ND-ACP
ND-B8
ND-13A
NDUFA3
ND-13B
ND-B12
NDUFS5
ND-B14
ND-18
ND-B14.5A
ND-19
NDUFC2
ND-20L
NDUFB4
ND-23
NDUFB6
ND-24
ND-B17.2
ND-30
ND-B18
ND-39
ND-B22
ND-42
CG40472
ND-49L
ND-ASHI
ND-51L2
NDUFC1
ND-75
NAD+
NADH
TCA Cycle
Complex II
Succinate-Ubiquinone Oxireductase
SdhA
SdhBL
CG6629
SdhD
Ubiquinone
e-
FADH2
FAD
e-
Succinate
H+
Complex III
Ubiquinol-Cyt C Reductase
UQCR-C1
UQCR-C2
UQCR-14L
UQCR-Q
UQCR-11
ox
UQCR
mt:Cyt-b
RFeSP
H+
Complex IV
Cyt C Oxidase
mt:CoI
mt:CoII
mt:CoIII
COX4
COX5A
COX5B
CG14077
CG14077
COX6B
cype
COX7A2
COX7A3
COX7A1
COX7A2L
COX7B
COX7C
COX8A
Assembly
CG9065
Surf1
Scox
COX11
CG3803
H+
O2
H2O
Complex V
ATP Synthase
F1 Complex
blw
ATPsynbeta
ATPsyngamma
ATPsyndelta
ATP5E
Stalk
ATPsynCF6L
ATPsynO
F0 Complex
mt:ATPase6
ATPsynB
C subunit
ATPsynC
ATPsynC
ATPsynC
ATPsynD
ATP5I
ATPsynF
ATPsynG
ATP8
CG10731
ATPIF1
H+
ATP

B

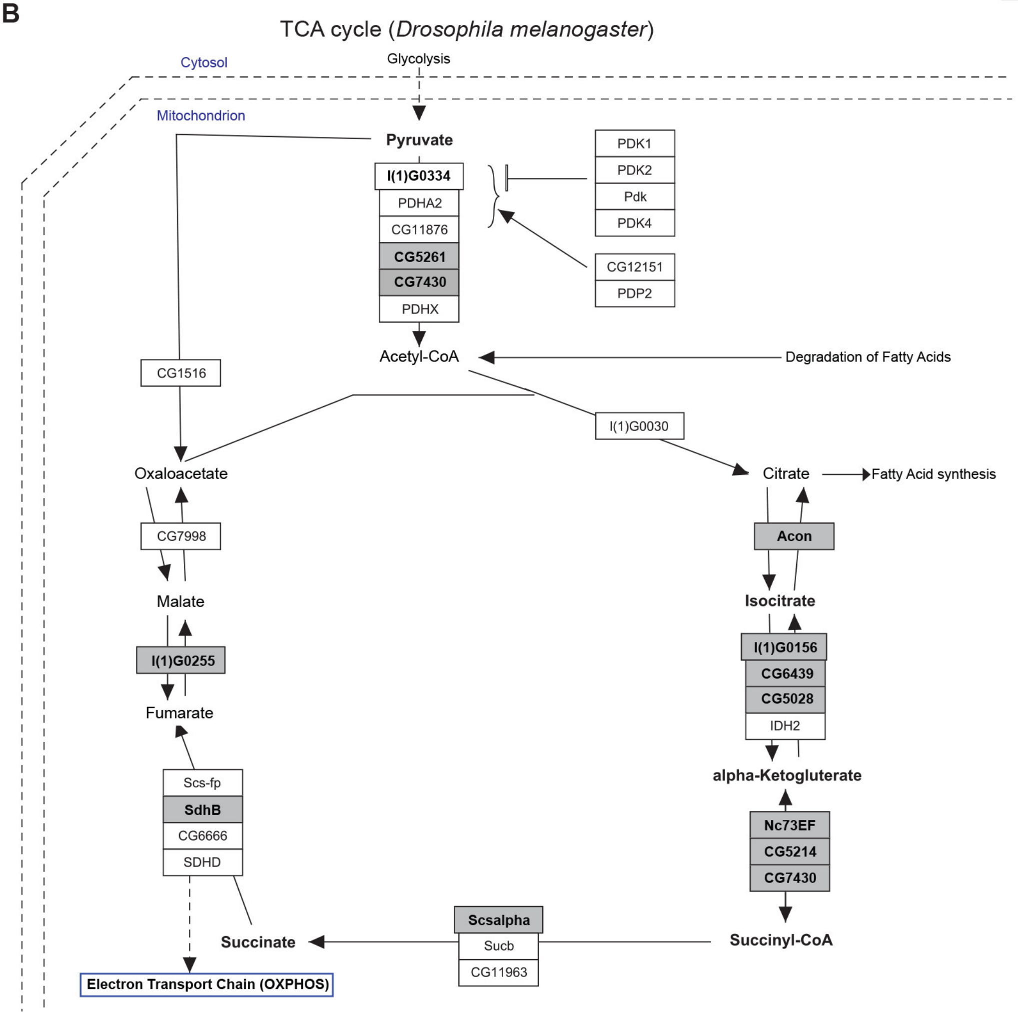
TCA cycle (Drosophila melanogaster)
Cytosol
Glycolysis
Mitochondrion
Pyruvate
l(1)G0334
PDHA2
CG11876
CG5261
CG7430
PDHX
PDK1
PDK2
Pdk
PDK4
CG12151
PDP2
Acetyl-CoA
Degradation of Fatty Acids
CG1516
l(1)G0030
Oxaloacetate
Citrate
Fatty Acid synthesis
CG7998
Acon
Malate
Isocitrate
l(1)G0255
l(1)G0156
CG6439
CG5028
IDH2
Fumarate
alpha-Ketogluterate
Scs-fp
SdhB
CG6666
SDHD
Nc73EF
CG5214
CG7430
Scsalpha
Sucb
CG11963
Succinate
Succinyl-CoA
Electron Transport Chain (OXPHOS)

Figure S3

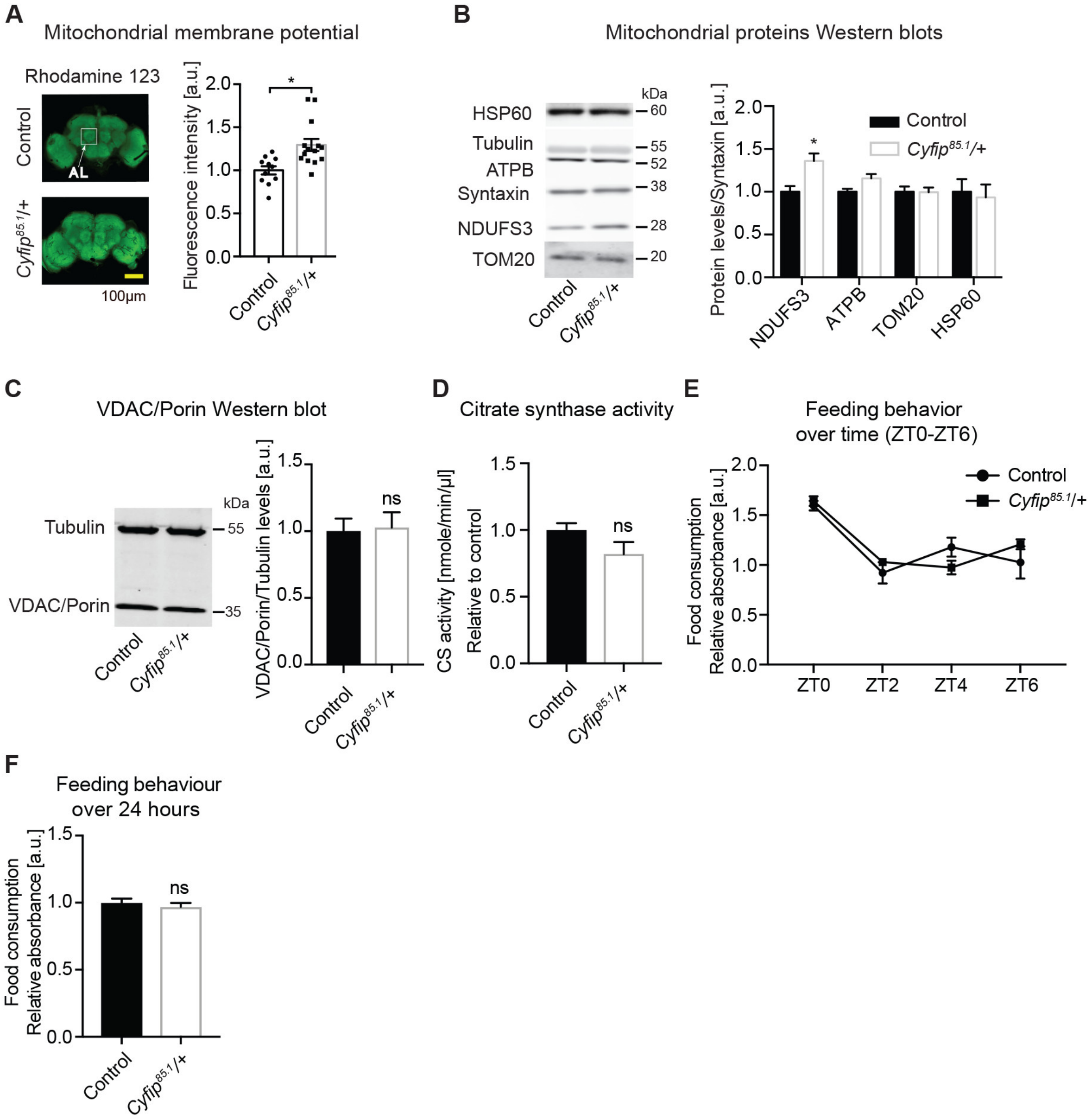
A
Mitochondrial membrane potential
Rhodamine 123
Control
AL
Cyfip85.1/+
100µm
Fluorescence intensity [a.u.]
2.0
1.5
1.0
0.5
0.0
*
Control
Cyfip85.1/+
B
Mitochondrial proteins Western blots
HSP60
Tubulin
ATPB
Syntaxin
NDUFS3
TOM20
kDa
60
55
52
38
28
20
Control
Cyfip85.1/+
Protein levels/Syntaxin [a.u.]
2.0
1.5
1.0
0.5
0.0
*
Control
Cyfip85.1/+
NDUFS3
ATPB
TOM20
HSP60
C
VDAC/Porin Western blot
Tubulin
VDAC/Porin
kDa
55
35
Control
Cyfip85.1/+
VDAC/Porin/Tubulin levels [a.u.]
1.5
1.0
0.5
0.0
ns
Control
Cyfip85.1/+
D
Citrate synthase activity
CS activity [nmole/min/µl]
Relative to control
1.5
1.0
0.5
0.0
ns
Control
Cyfip85.1/+
E
Feeding behavior
over time (ZT0-ZT6)
Food consumption
Relative absorbance [a.u.]
2.0
1.5
1.0
0.5
0.0
Control
Cyfip85.1/+
ZT0
ZT2
ZT4
ZT6
F
Feeding behaviour
over 24 hours
Food consumption
Relative absorbance [a.u.]
1.5
1.0
0.5
0.0
ns
Control
Cyfip85.1/+

Figure S4

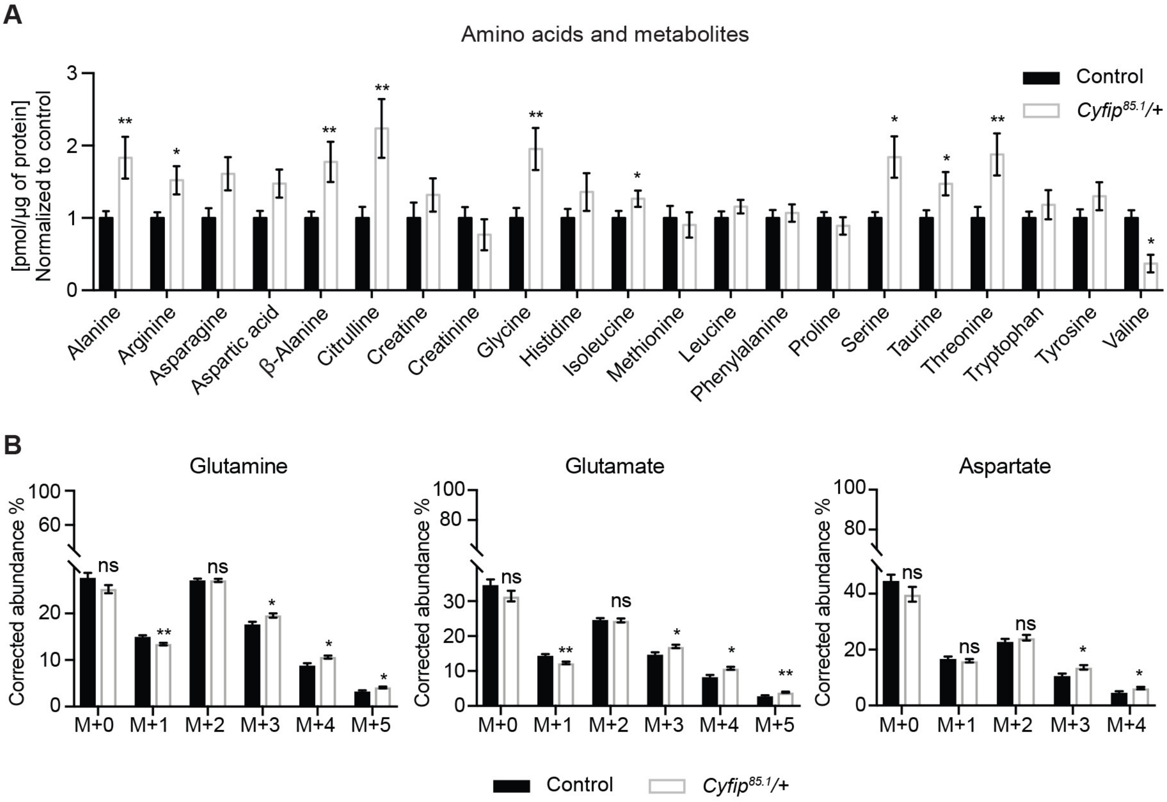
A
Amino acids and metabolites
[pmol/µg of protein]
Normalized to control
0
1
2
3
Control
Cyfip^85.1/+
Alanine
Arginine
Asparagine
Aspartic acid
β-Alanine
Citrulline
Creatine
Creatinine
Glycine
Histidine
Isoleucine
Methionine
Leucine
Phenylalanine
Proline
Serine
Taurine
Threonine
Tryptophan
Tyrosine
Valine
**
*
**
**
**
*
*
*
**
*
B
Glutamine
Glutamate
Aspartate
Corrected abundance %
0
10
20
60
100
30
80
40
ns
**
ns
*
*
*
M+0
M+1
M+2
M+3
M+4
M+5
ns
**
ns
*
*
**
ns
ns
ns
*
*
Control
Cyfip^85.1/+

Figure S5

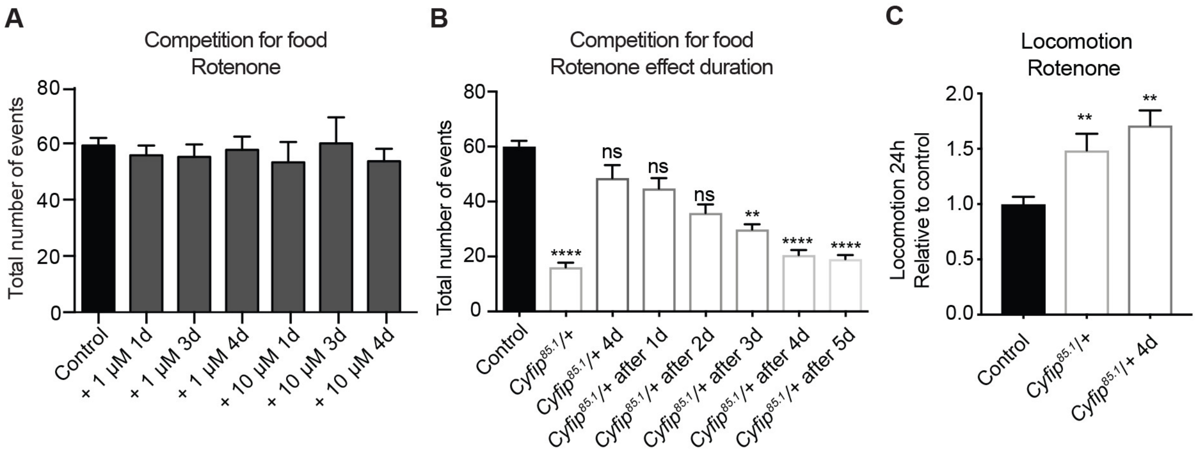
A
Competition for food
Rotenone
Total number of events
80
60
40
20
0
Control
+ 1 µM 1d
+ 1 µM 3d
+ 1 µM 4d
+ 10 µM 1d
+ 10 µM 3d
+ 10 µM 4d
B
Competition for food
Rotenone effect duration
Total number of events
80
60
40
20
0
****
ns
ns
ns
**
****
****
Control
Cyfip$^{85.1}$/+
Cyfip$^{85.1}$/+ 4d
Cyfip$^{85.1}$/+ after 1d
Cyfip$^{85.1}$/+ after 2d
Cyfip$^{85.1}$/+ after 3d
Cyfip$^{85.1}$/+ after 4d
Cyfip$^{85.1}$/+ after 5d
C
Locomotion
Rotenone
Locomotion 24h
Relative to control
2.0
1.5
1.0
0.5
0.0
**
**
Control
Cyfip$^{85.1}$/+
Cyfip$^{85.1}$/+ 4d

Figure S6

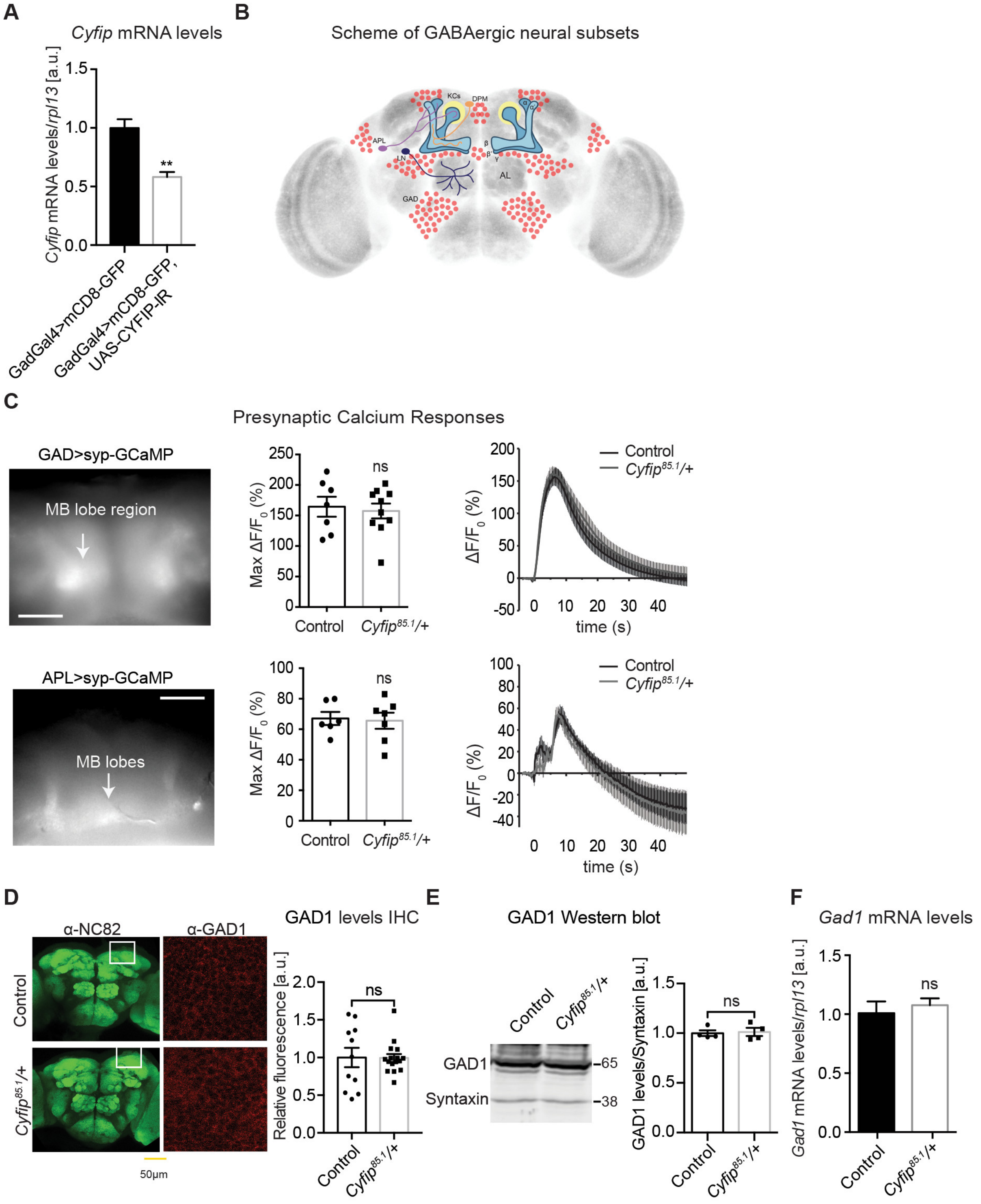
A
Cyfip mRNA levels
Cyfip mRNA levels/rpl13 [a.u.]
1.5
1.0
0.5
0.0
**
GadGal4>mCD8-GFP
GadGal4>mCD8-GFP, UAS-CYFIP-IR
B
Scheme of GABAergic neural subsets
KCs
DPM
APL
LN
GAD
AL
α
α'
β
β'
γ
C
Presynaptic Calcium Responses
GAD>syp-GCaMP
MB lobe region
Max ΔF/F0 (%)
250
200
150
100
50
0
ns
Control
Cyfip85.1/+
ΔF/F0 (%)
200
150
100
50
0
-50
0
10
20
30
40
time (s)
Control
Cyfip85.1/+
APL>syp-GCaMP
MB lobes
Max ΔF/F0 (%)
100
80
60
40
20
0
ns
Control
Cyfip85.1/+
ΔF/F0 (%)
100
80
60
40
20
0
-20
-40
0
10
20
30
40
time (s)
Control
Cyfip85.1/+
D
α-NC82
α-GAD1
Control
Cyfip85.1/+
50µm
GAD1 levels IHC
Relative fluorescence [a.u.]
2.0
1.5
1.0
0.5
0.0
ns
Control
Cyfip85.1/+
E
GAD1 Western blot
Control
Cyfip85.1/+
GAD1
Syntaxin
-65
-38
GAD1 levels/Syntaxin [a.u.]
1.5
1.0
0.5
0.0
ns
Control
Cyfip85.1/+
F
Gad1 mRNA levels
Gad1 mRNA levels/rpl13 [a.u.]
1.5
1.0
0.5
0.0
ns
Control
Cyfip85.1/+

Figure S7

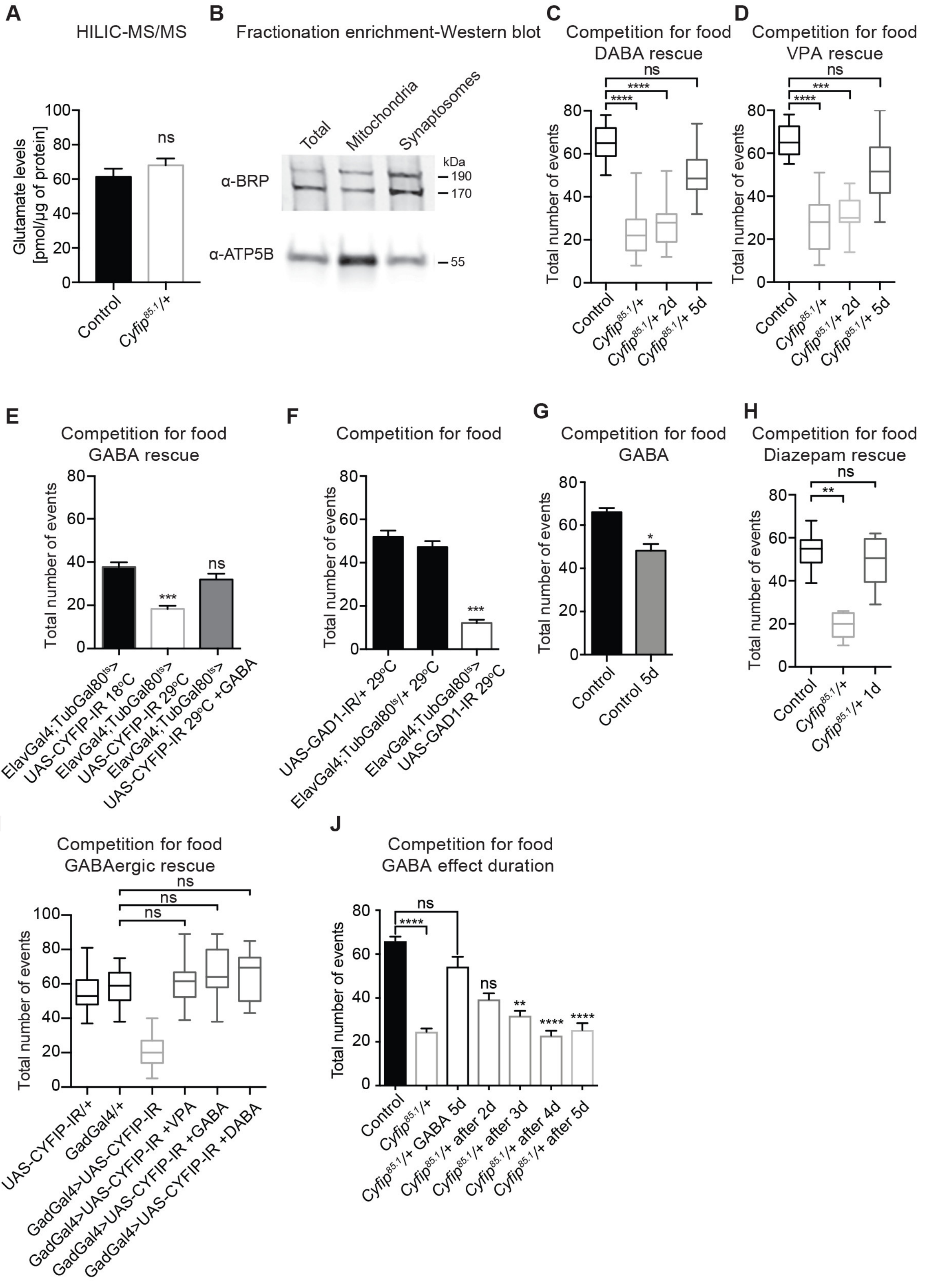
A
HILIC-MS/MS
Glutamate levels [pmol/µg of protein]
100
80
60
40
20
0
ns
Control
Cyfip^85.1/+
B
Fractionation enrichment-Western blot
Total
Mitochondria
Synaptosomes
α-BRP
α-ATP5B
kDa
190
170
55
C
Competition for food
DABA rescue
ns
****
****
Total number of events
80
60
40
20
0
Control
Cyfip^85.1/+
Cyfip^85.1/+ 2d
Cyfip^85.1/+ 5d
D
Competition for food
VPA rescue
ns
***
****
Total number of events
80
60
40
20
0
Control
Cyfip^85.1/+
Cyfip^85.1/+ 2d
Cyfip^85.1/+ 5d
E
Competition for food
GABA rescue
Total number of events
80
60
40
20
0
***
ns
ElavGal4;TubGal80ts> UAS-CYFIP-IR 18°C
ElavGal4;TubGal80ts> UAS-CYFIP-IR 29°C
ElavGal4;TubGal80ts> UAS-CYFIP-IR 29°C +GABA
F
Competition for food
Total number of events
80
60
40
20
0
***
UAS-GAD1-IR/+ 29°C
ElavGal4;TubGal80ts/+ 29°C
ElavGal4;TubGal80ts> UAS-GAD1-IR 29°C
G
Competition for food
GABA
Total number of events
80
60
40
20
0
*
Control
Control 5d
H
Competition for food
Diazepam rescue
ns
**
Total number of events
80
60
40
20
0
Control
Cyfip^85.1/+
Cyfip^85.1/+ 1d
I
Competition for food
GABAergic rescue
ns
ns
ns
Total number of events
100
80
60
40
20
0
UAS-CYFIP-IR/+
GadGal4/+
GadGal4>UAS-CYFIP-IR
GadGal4>UAS-CYFIP-IR +VPA
GadGal4>UAS-CYFIP-IR +GABA
GadGal4>UAS-CYFIP-IR +DABA
J
Competition for food
GABA effect duration
ns
****
ns
**
****
****
Total number of events
80
60
40
20
0
Control
Cyfip^85.1/+
Cyfip^85.1/+ GABA 5d
Cyfip^85.1/+ after 2d
Cyfip^85.1/+ after 3d
Cyfip^85.1/+ after 4d
Cyfip^85.1/+ after 5d

Figure S8

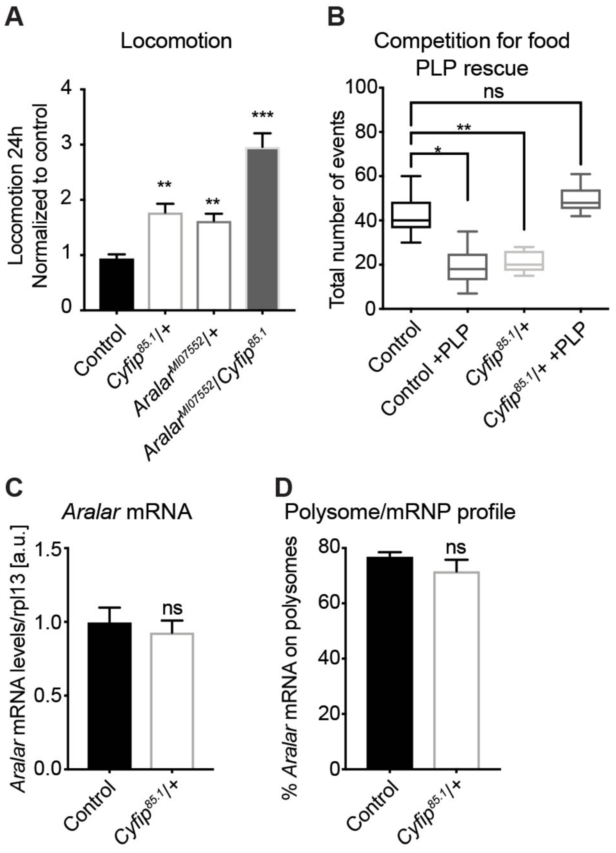
A
Locomotion
Locomotion 24h Normalized to control
4
3
2
1
0
**
**
***
Control
Cyfip85.1/+
AralarMI07552/+
AralarMI07552/Cyfip85.1
B
Competition for food PLP rescue
Total number of events
100
80
60
40
20
0
ns
**
*
Control
Control +PLP
Cyfip85.1/+
Cyfip85.1/+ +PLP
C
Aralar mRNA
Aralar mRNA levels/rpl13 [a.u.]
1.5
1.0
0.5
0.0
ns
Control
Cyfip85.1/+
D
Polysome/mRNP profile
% Aralar mRNA on polysomes
80
60
40
20
0
ns
Control
Cyfip85.1/+

Social event CTR

Click here to access/download

Supplemental Videos and Spreadsheets

Video 1 - Social events CTR.m4v

Social event Cyfip1 het

Supplemental Videos and Spreadsheets

Video 2 - Social event Cyfip het.m4v

Courtship CTR

Click here to access/download
Supplemental Videos and Spreadsheets
Video 3 - Courtship CTR.m4v

Courtship Cyfip het

Supplemental Videos and Spreadsheets

Video 4 - Courtship Cyfip het.m4v

Grooming CTR

Grooming Cyfip het

Click here to access/download
Supplemental Videos and Spreadsheets
Video 6 - Grooming Cyfip het.m4v